Analysis of the glutamine dependent transaminases as possible therapeutic targets in colon cancer cells

Inaugural-Dissertation

to obtain the academic degree

Doctor rerum naturalium (Dr. rer. nat.)

submitted to the

Department of Biology, Chemistry, Pharmacy

of

Freie Universität Berlin

by

Şafak Bayram, M. Sc.

Berlin, 2023

This thesis was carried out under the supervision of Dr. Stefan Kempa from April 2018 until December 2022 at the Max Delbrück Centrum für Molekulare Medizin, Berlin, Germany.

1st Reviewer: Dr. Stefan Kempa

2nd Reviewer: Prof. Dr. Petra Knaus

Date of Disputation: 27.11.2023

Hiermit erkläre ich, dass die vorliegende Dissertation selbstständig von mir verfasst und angefertigt wurde. Es wurden außerdem keine anderen als die angegebenen Quellen und Hilfsmittel verwendet. Geistiges Eigentum anderer Autoren wurde entsprechend gekennzeichnet. Ebenso versichere ich, dass ich an keiner anderen Stelle ein Prüfungsverfahren beantragt bzw. die Dissertation in dieser oder anderer Form keiner anderen Fakultät als Dissertation vorgelegt habe.

Acknowledgements

First of all, I want to thank Dr. Stefan Kempa for giving me the chance to be a part of his team as well as introducing me to the world of science. Thank you for the impressive lecture you gave at the university that inspired me to start my journey at your lab. Thank you for teaching me that biology is hard to predict and time will help to understand even the most confusing data results. Furthermore, thank you for always playing good music! I also would like to thank Jenny Grobe without whom I couldn't have finished any pSIRM experiments. Thank you for your support and your patience, when I asked again and again for "nur noch ein kleines Experiment", which usually ended up with 400 plates and a night shift. Thank you for keeping the lab going, you made lab-life easier. Many thanks to Dr. Martin Forbes, my lab partner in crime, for introducing to and teaching me about the world of codes. Thank you for your support at every stage during my doctoral studies and especially for your friendship. Furthermore thanks go to Dr. Guido Mastrobuoni for sharing his proteomics know how and overall skills, creating good-mood and of course for the best Tiramisu recipe. I want to thank Dr. Sabrina Geisberger for her unconditional support from day one on.

Thanks go also to former lab members Susi, Matthias, Nadine, Christin, and Fardad who all made a lasting impression on me.

I would like to acknowledge my Doctoral Committee members: Prof. Dr. Claus Scheidereit and Prof. Dr. Matthias Selbach for providing crucial input and expertise. Furthermore, I would also like to thank Prof. Dr. Petra Knaus for her impressive lectures during my biochemistry studies, our discussions and her supervision on my work. To me she is a true inspiration as a woman in science.

Last but not least, I also want to thank Fouad El-Haj, Navid Afkhami, and Sabrina Deter, who always steadily provided the necessities of logistics, IT and administration to keep my Doctoral studies running.

Thank you all! I will always cherish this special and unique time in my life!

Summary

The project's objective is to gain knowledge about the interconnection between cell growth and metabolism in the colon cancer cells HCT116 and RKO that rely on glutamine's nitrogen. The non-cancerous HEK293 cells were tested in parallel to understand the specific metabolic settings and differences in glutamine-independent proliferation. A proteome analysis via liquid chromatography coupled to mass spectrometry (MS) was performed and revealed compartment specific protein expression in HCT116 and RKO cells. Interestingly, the enzyme glutamine synthetase (GLUL) was highly expressed in HEK293 cells under normal growth conditions. We wanted to know if HCT116 and RKO cells can grow independently from glutamine and starved the cells upon glutamine for a longer period. Surprisingly, HCT116 cells survived and persisted, while RKO cells did not. We suspected small molecules or residual glutamine in the growth medium and replaced the cell culture medium composition by dialyzed fetal bovine serum (FBS). Interestingly, in this case neither HCT116 nor HEK293 cells were able to proliferate when glutamine was deprived. Thus, glutamine was also essential for these cells when using dialyzed FBS. Based on these results, we assumed that HCT116 and HEK293 cells synthesize glutamine in the absence of external glutamine. Therefore, a supplementation growth experiment with substrates of the glutamine-centric metabolic network was performed. HCT116 and HEK293 cells showed highest proliferation rates in Glu + NH_4^+, while RKO cells revealed an irreplaceable dependence on glutamine supplemented medium. Treatment with a competitive inhibitor of glutamine synthetase, methionine sulfoximine (MSO), blocked proliferation. Thus, glutamine synthetase was confirmed to be the survival factor in glutamine-depleted conditions, if substrates are provided. In order to examine the metabolic fate of glutamine, newly synthesized via GLUL, we have developed an isotope tracing technique using ultra high resolution MS, which allows us to distinguish between simultaneous labeling of carbon-13 and nitrogen-15 isotopic patterns and that allows new insights into biological reactions in glutamine-deprived HCT116, RKO and HEK293 cells. With this new technique we were able to observe ^{13}C and ^{15}N incorporation in purine nucleotides. Additionally, we investigated the glutamine-analogue 6-Diazo-5-oxo-l-norleucine (DON) as it inhibits all glutamine-utilizing enzymes with focus on amidotransferases. An inital DON-inhibition experiment was performed to examine the interconnection of nucleotide synthesis and glutamine. We revealed an accumulation of nucleotide intermediates in HCT116 and HEK293 cells. To gain a clearer understanding, we traced glutamine's nitrogen flow in *de novo* nucleotide biosynthesis and where it is interfered by DON. Therefore, in the Kempa laboratory a new technique and method based on direct-infusion MS was developed that facilitates dynamic tracing of nitrogen with applied drugs on nucleotide substrates (Rayman (2022)). Finally, we observed decreased nitrogen incorporation into FGAR and the nucleotides of the purine pathway upon DON treatment in

HCT116 cells. In conclusion, we demonstrated the inability of RKO cells to synthesize glutamine or to compensate glutamine-deficiency perhaps because of missing functionality of the enzyme GLUL. However, HCT116 and HEK293 cells have proven survivability. Furthermore, we were able to show DON targets in the purine nucleotide biosynthesis.

Zusammenfassung

Ziel des Projekts ist es, Kenntnisse über die Verbindungen zwischen Zellwachstum und Metabolismus in Kolonkrebszellen zu erlangen, die vom Nitrogen des Glutamins abhängig sind. Die nicht-karzenomen HEK293-Zellen waren Gegenstand von Parallelversuchen, deren Zielsetzung das Verständnis von spezifischen metabolischen Grundanlagen und Unterschieden bei Glutamin-unabhängiger Proliferation waren. Eine Proteomen-Analyse via Flüssigchromatographie verbunden mit Massenspektrometrie offenbarte Kompartiment spezifische Protein-Expressionen in HCT116- und RKO-Zellen. Bemerkenswerterweise war die Glutamin-Synthetase (GLUL) in HEK293-Zellen bereits unter normalen Bedingungen hochgradig exprimiert. Wir wollten nun wissen, ob HCT116- und RKO-Zellen von Glutamin unabhängig wachsen können, und enthielten ihnen zunächst für eine längere Zeit Glutamin gänzlich vor. Überraschenderweise überlebten die HCT116-Zellen und blieben bestehen, während dies den RKO-Zellen nicht gelang. Wir führten dies auf kleine Moleküle oder restliches Glutamin im Wachstumsmedium zurück und ersetzten die Zellkulturmediumskomposition durch dialysiertes Rinderfötalserum (FBS). Interessanterweise gelang es in diesem Falle weder den HCT116- noch den HEK293-Zellen, sich unter Glutamin-Abwesenheit zu vermehren. Damit erwies sich Glutamin also auch für HEK293-Zellen bei Nutzung dialysierten FBS' als essentiell. Basierend auf diesen Ergebnissen kamen wir zu dem Schluss, dass HEK293-Zellen in Abwesenheit externen Glutamins das fehlende Glutamin selbst synthetisieren. Deshalb wurde ein Supplementierungs-Wachstumsexperiment mit Substraten aus dem Glutamin zentrischen metabolischen Netzwerk durchgeführt. HCT116- und HEK293-Zellen zeigten die höchsten Vermehrungsraten in Glu + NH_4^+, während RKO-Zellen eine unersetzbare Abhängigkeit von Glutamin supplementiertem Medium zeigten. Die Behandlung mit einem konkurrierenden Inhibitor der Glutamin-Synthetase, Methionin-Sulfoximin (MSO), blockierte die Vermehrung, wodurch sich die Glutamin-Synthetase als der entscheidende Überlebensfaktor unter Glutamin entzogenen Bedingungen erwies, wenn Substrate zur Verfügung gestellt werden. Um das metabolische Schicksal des via GLUL neu synthetisierten Glutamins zu untersuchen, haben wir eine Isotopen-Tracing-Technik auf dem ultrahoch auflösenden Massenspektrometer entwickelt, die uns ermöglicht, isotopische Muster der simultan gelabelten ^{13}C und ^{15}N voneinander zu unterscheiden, was neue Einblicke in biologische Reaktionen in des Glutamins beraubten HCT116-, RKO- und HEK293-Zellen ermöglicht. Wir beobachteten Carbon-13- und Nitrogen-15-Inkorporation bei Purin-Nucleotiden. Darüberhinaus untersuchten wir das Glutamin-Analog DON, da es alle Glutamin verwendenden Enzyme inhibiert, wobei wir den Schwerpunkt auf die Amidotransferasen legten. Ein einleitendes DON-Inhibitionsexperiment wurde durchgeführt, um die Zusammenschaltung von Nucleotid-Synthese und Glutamin zu untersuchen. Dies legte die Akkumulation von Nucleotid-Intermediaten in HCT116- und HEK293-Zellen offen. Um dies

besser zu verstehen, verfolgten wir den Nitrogen-Fluss des Glutamin in der ***de novo*** Nucleotid-Biosynthese und wo dieser von DON gestört wird. Hierfür wurde in der Kempa-Gruppe eine neue Technik und Methode entwickelt, basierend auf der Direktinfusion MS, die eine dynamische Untersuchung des Nitrogens mittels Drogen hinsichtlich der Nucleotid-Substrate ermöglicht (Rayman (2022)). Schließlich beobachteten wir abnehmende Nitrogen-Einbindung in FGAR und in die Nucleotide des Purin-Weges bei DON-Behandlung in HCT116-Zellen. Abschließend demonstrierten wir die Unfähigkeit der RKO-Zellen, Glutamin zu synthetisieren oder Glutamin-Defizienz durch andere Substrate zu kompensieren, was womöglich auf die fehlende Funktionalität des Enzyms GLUL zurückzuführen ist. Demgegenüber erwiesen sich HCT116- und HEK293-Zellen als überlebensfähig. Des Weiteren konnten wir DON-Targets in der Purine Nukleotidbiosynthese zeigen.

Contents

List of Figures

List of Tables

List of Abbreviations

General abbreviations

ACN	Acetonitrile
BPTES	Bis-2-(5-phenylacetamido-1,2,4-thiadiazol-2-yl)ethyl sulfide
BSA	Bovine serum albumin
CBMP	Carbamoylphosphate
CCM	Central carbon metabolism
C968	Compound968
DMEM	Dulbecco's Modified Eagle's Medium
DON	6-Diazo-5-oxo-l-norleucine
DTT	Dithiothreitol
EI	Electron Impact
ESI	Electrospray Ionization
FBS	Fetal bovine serum
F6P	Fructose-6-phosphate
GlcN6P	Glucosamine 6-phosphate
GC	Gas chromatography
IAA	Iodoacetamide
LC	Liquid chromatography
LFQ	Label free quantification
MeOH	Methanol
MeOX	Methoxamine hydrochloride
MCW	Methanol-Chloroform-Water
MS	Mass spectrometry
MSO	Methionine sulfoximine
MTBSTFA	N-(tert-Butyldimethylsilyl)-N-methyltrifluoracetamide
OXPHOS	Oxidative phosphorylation
PBS	Phosphate-buffered saline
pSIRM	Pulsed stable isotope-resolved metabolomics
PPP	Pentose phosphate pathway
PVDF	Polyvinylidene difluoride
RT	Retention time
TCA cycle	Tricarboxylic acid cylce
tSIRM	targeted stable isotope-resolved metabolomics

Enzymes

ABAT	4-Aminobutyrate aminotransferase
ALDA	aldolase A
ASNS	Asparagine synthetase
ASRGL1	Asparaginase
ACO	Aconitase
ACYL	ATP-Citrate lyase

CAD	Carbamoyl-phosphate synthetase 2, aspartate transcarbamylase, and dihydroorotase
CCBL1	Cysteine-S-conjugate beta-lyase
CPS	Glutamine-dependent carbamoyl-phosphate synthase
CS	Citrate Synthase
CTPS	Cytidine triphosphate synthase
FH	Fumarate Hydratase
GAPDH	Glyceraldehyde-3-phosphate Dehydrogenase
GCLC	Glutamate-cysteine ligase catalytic subunit
GFPT	Glutamine-fructose-6-phosphate transaminase
GLS	Glutaminase
GLUD	Glutamate dehydrogenase
GLUL	Glutamine synthase
GMPS	GMP synthase
GOT	Glutamate oxaloacetate transaminase
GPT	Glutamate pyruvate transaminase
HK	Hexokinase
IDH	Isocitrate Dehydrogenase
KGA	Kidney-glutaminase
KGA	Liver-type glutaminase (LGA)
LDH	Lactate dehydrogenase
MDH	Malate dehydrogenase
NADSYN	Glutamine-dependent NAD(+) synthetase
OGDC	oxoglutarate dehydrogenase complex
PAICS	Phosphoribosylaminoimidazole carboxylase
PDH	Pyruvate Dehydrogenase
PGI	Phosphoglucose isomerase
PGK	Phosphoglycerate kinase
PGM	Phosphoglycerate mutase
PFAS	Phosphoribosylformylglycinamidine synthase
PFK1	Phosphofructokinase 1
PK	Pyruvate Kinase
PPAT	Phosphoribosyl pyrophosphate amidotransferase
PSAT	Phosphoserine aminotransferase
SCS	Succinyl-CoA Synthetase
SDH	Succinate Dehydrogenase

Metabolites

α-KG	α-Ketoglutarate
Acetyl-CoA	Acetyl coenzyme A
ADP	Adenosine diphosphate
AICAR	5-Aminoimidazole-4-carboxamide ribonucleotide
AIR	5-Aminoimidazole ribonucleotide
Ala	Alanine
Asn	Asparagine
Asp	Aspartate
AMP	Adenosine monophosphate
ATP	Adenosine triphosphate
1,3BPG	1,3-Bisphosphoglyceric acid
CAIR	4-carboxy-5-aminoimidazole ribonucleotide
Cys	Cysteine
Cit	Citrate
DHAP	Dihydroxyacetone phosphate

diORO	Dihydroorotate
dTDP	Deoxythymidine diphosphate
dTMP	Deoxythymidine monophosphate
dTTP	Deoxythymidine triphosphate
dUDP	Deoxyuridine diphosphate
dUMP	Deoxyuridine monophosphate
dUTP	Deoxyuridine triphosphate
F6P	Fructose-6-phosphate
FBP	Fructose-1,6-bisphosphate
FAICAR	N-Formylaminoimidazole 4-carboxamide ribonucleotide
FGAM	Formylglycineamidine ribonucleotide
FGAR	Formylglycineamide ribonucleotide
Fum	Fumarate
G3P	Glyceraldehyde-3-phosphate
G6P	Glucose-6-phosphate
Gamma-EC	Gamma-l-glutamyl-l-cysteine
GABA	4-aminobutyrate
GAR	Glycineamide ribonucleotide
GCLC	Glutamate–cysteine ligase catalytic subunit
GDP	Guanosine diphosphate
Glc	Glucose
Gln	Glutamine
Glu	Glutamate
Gly	Glycine
GMP	Guanosine monophosphate
GTP	Guanosine triphosphate
IMP	Inosine monophosphate
Isocit	Isocitrate
KYAT	Kynurenine-oxoglutarate transaminase
Lac	Lactate
Mal	Malate
NaAD	Nicotinic acid adenine dinucleotide
OAA	Oxaloacetate
OMP	Orotidine 5-monophosphate
ORO	Orotic acid
PEP	Phosphoenolpyruvic acid
3-PGA	3-Phosphoglyceric acid
2-PGA	2-Phosphoglyceric acid
3-PHP	3-phosphohydroxypyruvate
5-PRA	5-phosphoribosylamine
PRPP	Phosphoribosyl pyrophosphate
Pyr	Pyruvate
R5P	Ribose-5-phosphate
SAICAR	N-succinylo-5-aminoimidazole-4-carboxamide ribonucleotide
SEP	Phosphoserine
Ser	Serine
Suc	Succinate
SucCOA	Succinyl-coenzyme A
UMP	Uridine monophosphate

Chapter 1

Introduction

1.1 Cancer and Metabolism

Cancer is a complex disease that undergoes specific metabolic reprogramming to sustain cell growth and proliferation (Vander Heiden et al. (2009), Amelio et al. (2014), Cairns et al. (2011)). Nearly a century ago, the pioneering work of Otto Warburg linked metabolism and tumor cells by revealing enhanced aerobic glycolysis compared to normal cells (Warburg (1956), Dang (2012a)). Nowadays it is known that crucial characteristics of cancer disease and metabolism are multifaceted, spanning from activation of oncogenes to loss of tumor suppressors resulting in changed signaling pathways due to mutated enzymes (Coller (2014)). The re-engineered metabolism effectively contributes to cancer development providing energy, macromolecules and production of antioxidants to counteract detrimental effects of reactive oxygen species (ROS) (Cairns et al. (2011)). Moreover, the complex deregulation enables cancer cells to evade immune cells and circumvent drug treatment through resistance. Cancer metabolism alterations in intracellular and extracellular metabolites also have profound effects on the tumor microenvironment (Pavlova and Thompson (2016)). In sum, the continuous progress in deciphering cancer cell biology demonstrates how intricate and heterogeneous cancer is and why no single model of cancer metabolism can cover this diversity (Cantor and Sabatini (2012)). One most intensively studied cell transformation is the glucose metabolism as well as glutamine as an additional source of carbon and nitrogen to satisfy the cancer cells‘ demands (Amoêdo et al. (2013)).

1.1.1 Glucose metabolism

Glucose is a sugar with six carbon and six oxygen atoms and is an anaerobic energy source for normal cells. Glucose metabolism comprises the glycolysis pathway as well as the hexosamine pathway, the pentose phosphate pathway (PPP) and the one-carbon metabolism that requires glucose. Together, these pathways contribute to anabolic processes producing nucleic acids, proteins and membranes via the generation of nucleotides, amino acids and fatty acids (Hay (2016)). Glycolysis is divided into two stages and is the first part of cell respiration. In the "investment phase" energy is required to convert one molecule glucose to two glyceraldehyde 3-phosphate via 4 steps, including phosphorylation by two ATP molecules. Followed by the "energy-releasing phase", where the phosphates are converted to pyruvate, and where two molecules of ATP and two molecules of NADH are produced (Berg et al. (2013)). Finally

pyruvate is transported from the cytosol to the mitochondria to enter the tricarboxylic acid (TCA) cycle. In the second part of cell respiration, the glucose derivate is further processed in eight enzymatic steps under aerobic conditions. Before entering into the TCA cycle pyruvate is decarboxylated to acetyl-CoA via pyruvate dehydrogenase. Followed by the condensation of acetyl-CoA and oxaloacetate (OAA) to the metabolite citrate via the enzyme citrate synthase (CS). In the upcoming steps isomerisation, oxidative decarboxylation and hydration of the six-carbon generates two molecules CO_2, three molecules of NADH, and one molecule of GTP and $FADH_2$ (Berg et al. (2013)). The third and final part of cellular respiration is the electron transport chain (ETC). Here, four protein complexes (complex I-IV) are involved to oxidize NADH and $FADH_2$ (Berg et al. (2013)). Thereby, electrons are transported from donors to acceptors by pumping protons from the mitochondrial matrix to the intermembrane space, generating a potential. The ATP synthase complex (complex V) generates ATP from ADP and inorganic phosphate (Pi) to equalize the membrane potential. Overall, the end products from one molecule glucose of the oxidative phosphorylation (OXPHOS) chain are 34 molecules ATP (Berg et al. (2013)).

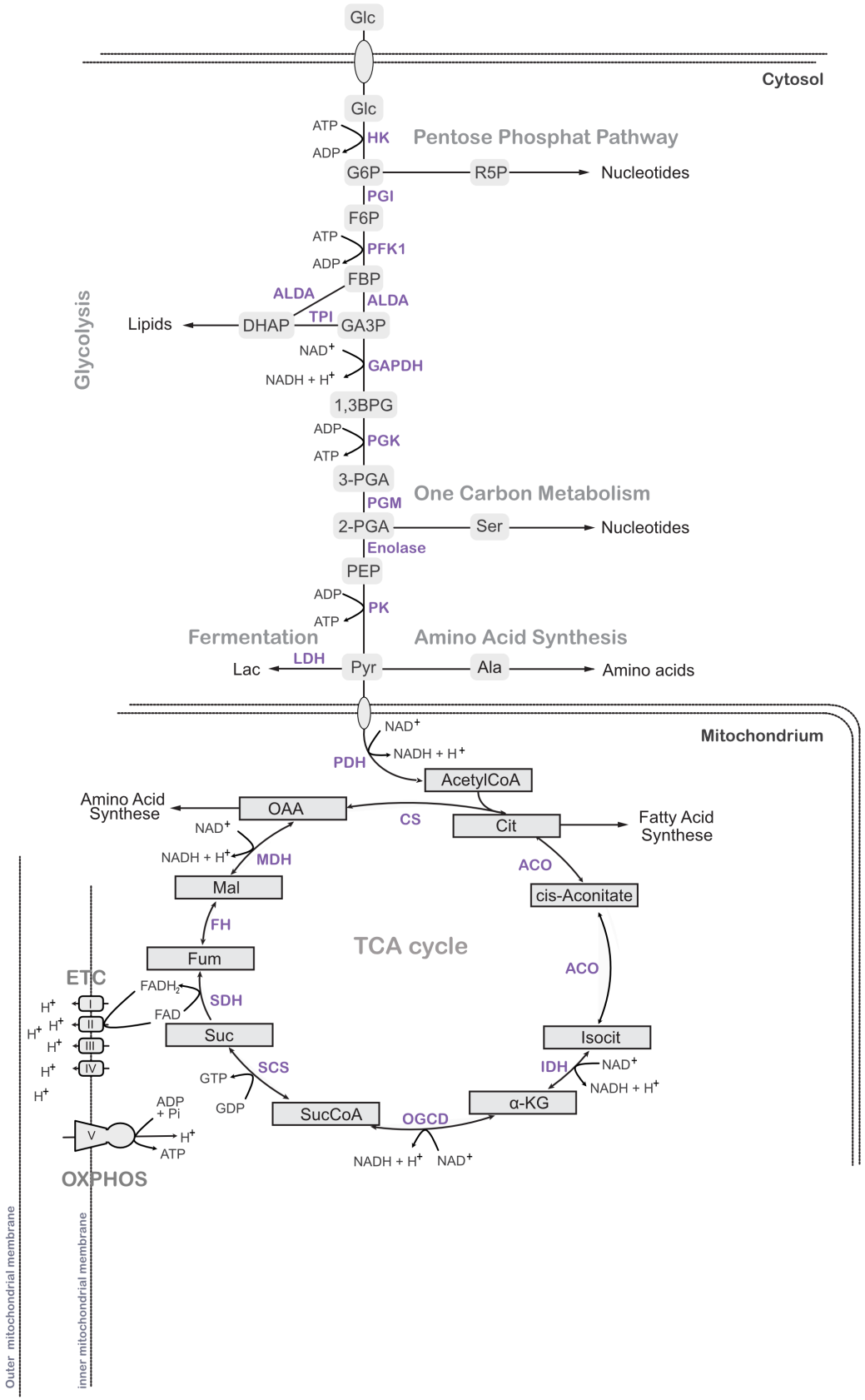

Figure 1.1: Central carbon metabolism - Glycolysis and TCA cycle. One molecule glucose is transported into the cytosol. Followed by 10 enzymatic reactions of the glycolysis 2 moles of pyruvate, ATP and NADH are generated. Pyruvate is transported to the mitochondria and is condensed to acetyl-CoA via PDH. In the TCA cycle acetyl-CoA is oxidized into CO_2 and 3 moles of NADH, 1 mole of GTP and 1 mole of $FADH_2$ are generated at once. Subsequently, NADH and $FADH_2$ are used for ATP generation via electron transport chain (ETC) and oxidative phosphorylation (OXPHOS). Beside ATP generation glycolysis and TCA cycle contributes to the production of nucleotides, amino acids and fatty acids. Essential abbreviations provided in the list of abbreviations.

1.1.2 Glutamine metabolism

Glutamine is the most abundant amino acid in the blood plasma with concentrations varying between 0.6 and 0.8 mM (Scalise et al. (2017), Cruzat et al. (2018)). The human body endogenously synthesizes glutamine from glucose, which is provided to the blood stream by adipose tissue, lung and skeletal muscle. Exogenous glutamine is absorbed via the gut and liver. Under particular conditions, such as injury or sepsis, glutamine request is increased and it becomes an essential amino acid, while in physiological conditions it is nutritionally classified as a non-essential amino acid (Altman et al. (2016), Oehler and Roth (2003), Bergström et al. (1974), Cruzat et al. (2018)). Glutamine plays a central role in several cellular processes including maintenance of mitochondrial membrane potential and integrity, supporting redox homestasis, macromolecule synthesis, essential amino acid uptake and maintaining activation of Target of Rapamycin kinase (Wise and Thompson (2011), Nicklin et al. (2009), Bott et al. (2019)). Glutamine is an universal precursor as it provides its carbon skeleton as well as its nitrogen for several cellular processes and purposes. Considering the carbon flow: As an anaplerotic substrate, glutamine fuels the TCA cycle to produce TCA cycle intermediates and other amino acids (e.g. aspartate). Furthermore, this routing of glutamine, termed as glutaminolysis, contributes to the generation of ATP, precursors for fatty acids, and the maintenance of the redox equilibrium (Amoêdo et al. (2013)). The glutaminolysis takes place in the mitochondria. For a long time, it was not clear how glutamine enters mitochondria. Recent studies by Yoo et al. (2020) showed that a variant of the glutamine plasma transporter SLC1A5 has a mitochondrial targeting signal for mitochondrial localization caused by HIF-2a. The versatile amino acid is converted to glutamate either by deamination through the enzyme glutaminase (GLS), which in addition releases a free ammonium, or by aminotransamination by the enzymes asparagine synthetase (ASNS), glutamate oxaloacetate transaminase (GOT) and glutamate pyruvate transaminase (GPT) (Altman et al. (2016)).

Fig.1.2 presents the multiplicity of glutamine's nitrogen. Transaminases are involved in the nitrogen flow of glutamine as they transfer the γ-nitrogen of glutamine to another acceptor molecule. Asparagine synthetase (ASNS), for instance, converts asparatate and glutamine to asparagine and glutamate (Zhang et al. (2017)). Since transaminases are the majority of glutamine-converting enzymes and have bilateral functions, they link glutamine metabolism to a multitude of other pathways, e.g., NAD synthesis or glucosamine 6-phosphate synthesis. In particular, glutamine-dependent transaminases are involved in the *de novo* nucleotide biosynthesis. However, intracellular glutamine-derived glutamate is surmised to be produced mainly from the enzyme GLS (Zhang et al. (2017), Yang et al. (2017)).

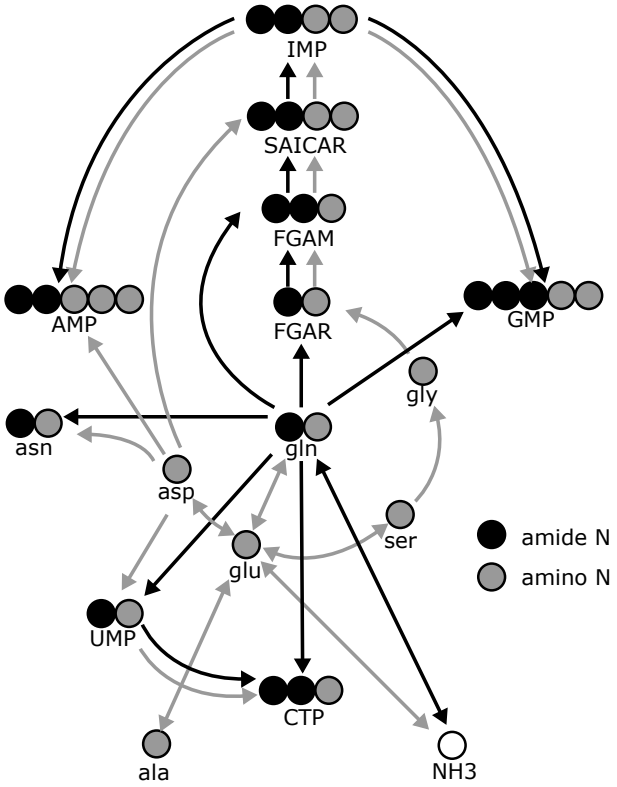

Figure 1.2: Glutamine-centric nitrogen metabolism with focus on amino acids and nucleotides. Glutamine-centric nitrogen metabolism with focus on amino acids and nucleotides. Abbreviations: inosine-monophosphate (IMP), guanosine-monophosphate (GMP), adenosine monophosphate (AMP), cytidin triphosphate (CTP), uridine monophosphate (UMP), glutamine (gln), asparagine (asn), aspartate (asp), glutamate (glu), serine (ser), glycine (gly), alanine (ala), formyl-glycine-amide-ribonucleotide (FGAR), formyl-glycine-amidine-ribonucleotide (FGAM), 5amino-imidazol-4-N-succino-carboxamid-ribonucleotide (SAICAR). Figure was published in figure 1 in Bayram et al. (2020).

Glutamine's carbon bone fuels TCA cycle

Glutamate produced from glutamine can be further deaminized to α-ketoglutarate by either glutamate dehydrogenase (GLUD), which releases a free ammonium, or again by aminotransaminases (fig. 1.4). Aminotransaminases, such as GOT, GPT, or phosphoserine aminotransferase (PSAT), transfer the α-nitrogen from glutamate in order to produce other amino acids, e.g., alanine, cysteine or aspartate. Just as in glutamine-dependent transaminases deamination of glutamate via GLUD to α-ketoglutarate is the main contributor, despite a greater amount of transaminases (Yang et al. (2017)). The glutamine-derived carbon back bone of α-ketoglutarate is further proceeded in the TCA cycle to generate bioenergetic NADH and $FADH_2$ equivalents, followed by the usage of the coenzymes to generate ATP via the ETC coupled to OXPHOS or for cellular redox homeostasis maintenance. Furthermore, the reductive carboxylation produces acetyl-CoA from α-ketoglutarate, that is carboxylated into citrate and exported to the cytosol, followed by cleavage to oxaloacetate and acetyl-CoA via ATP-Citrate lyase (ACLY). Acetyl-CoA serves as an acetylation precursor and is also used for fatty acid synthesis (Ku et al. (2020)). Besides, glutamine-derived α-ketoglutarate generates diverse biosynthetic precursors, e.g., citrate and aspartate, supporting nucleotide as well as amino acid synthesis (Icard et al. (2021), Berg et al. (2013), Zhang et al. (2017).

1.1.3 Introduction to nucleotide metabolism

Steadily proliferating cells rely on access to DNA replication as well as RNA production, hence cells increase nucleotide synthesis. A nucleotide is built of three subunit molecules: a 5-carbon sugar, a nitrogen base and one to three phosphates. The energy demanding nucleotide biosynthesis consumes a number of carbon and nitrogen sources, that are provided through several metabolic pathways in varied cell compartments (Lane and Fan (2015)). Ribose 5-phosphate (R5P) is the main precursor for purine and pyrimidine nucleotide biosynthesis and derives from glycolysis, which is branched twice and feeds into the pentose phosphate pathway (PPP). The oxidative as well as the non-oxidative PPP use different glycolysis intermediates for R5P production, glucose-6-phosphate (G6P) and fructose-6-phosphate (F6P), and glyceraldehyde-3-phosphate (G3P), respectively. By activating R5P to phosphoribosyl pyrophosphate (PRPP) via phosphorylation nucleotide biosynthesis pathway is initiated. One obligate nitrogen donor for *de novo* nucleotide biosynthesis is glutamine (Fig. 1.4). Besides, one-carbon pathway, aspartate-transaminase, and glutaminolysis also contribute to the synthesis of the building blocks of DNA and RNA (Lane and Fan (2015)).

De novo purine nucleotide biosynthesis

Once PRPP is produced it is further converted to inosine monophosphate (IMP), which is proceeded to generate adenosine and guanosine derivates (Fig. 1.4). First, PRPP is transformed to 5-phosphoribosylamine (5-PRA) by condensation with glutamine via the enzyme glutamine phosphoribosyl pyrophosphate aminotransferase. Glutamine's nitrogen links the purine base with the ribose. Producing 5-PRA is the rate-limiting step of the purine biosynthesis, that is allostericaly inhibited by IMP, AMP and GMP. Next, two carbon atoms and one nitrogen atom of glycine are used to build the purine ring. In addition, 1 mole of ATP is used to catalyse the synthesis of glycinamide ribonucleotide (GAR) by the enzyme glycinamide kinosynthase. The folate cycle contributes a formyl group from N10-formyltetrahydrofolate (10-formyl THF) for the synthesis of formylglycinamide ribonucleotide (FGAR). Again, glutamine's nitrogen is incorporated which consumes 1 mole of ATP. In five enzymatic steps formylglycineamidine ribonucleotide (FGAM) is converted to N-formylaminoimidazole 4-carboxamide ribonucleotide (FAICAR) through the usage of ATP, aspartate, and 10-formyl THF. Via a hydrolysation step the purine base hypoxanthine is formed. Together with linked R5P the intermediate inosine monophosphate (IMP) is synthesized. Subsequently, aspartate and NAD+, glutamine and ATP are used to synthesize AMP and GMP, respectively (Lane and Fan (2015)).

De novo pyrimidine nucleotide biosynthesis

The first three steps of the pyrimidine biosynthesis are performed by the protein CAD (fig. 1.4). The trifunctional enzyme comprises carbamoyl phosphate synthetase, aspartate carbamoyltransferase and dihydroorotase. Thereby, glutamine, aspartate, and CO_2 are used, while glutamine is donating a nitrogen group in a rate-limiting step. The generated dihydroorotate (diORO) is further proceeded to orotic acid (ORO) in an NAD+-dependent reaction, followed by a condensation with PRPP to orotidine-5-phosphate (OMP). A decarboxylation forms uridine monophosphate (UMP), which is phosphorylated by 2 moles of ATP to UTP. Subsequently,

glutamine donates a nitrogen to generate CTP from UTP via the enzyme CTP synthetase (CTPS) (fig. 1.4) (Lane and Fan (2015)).

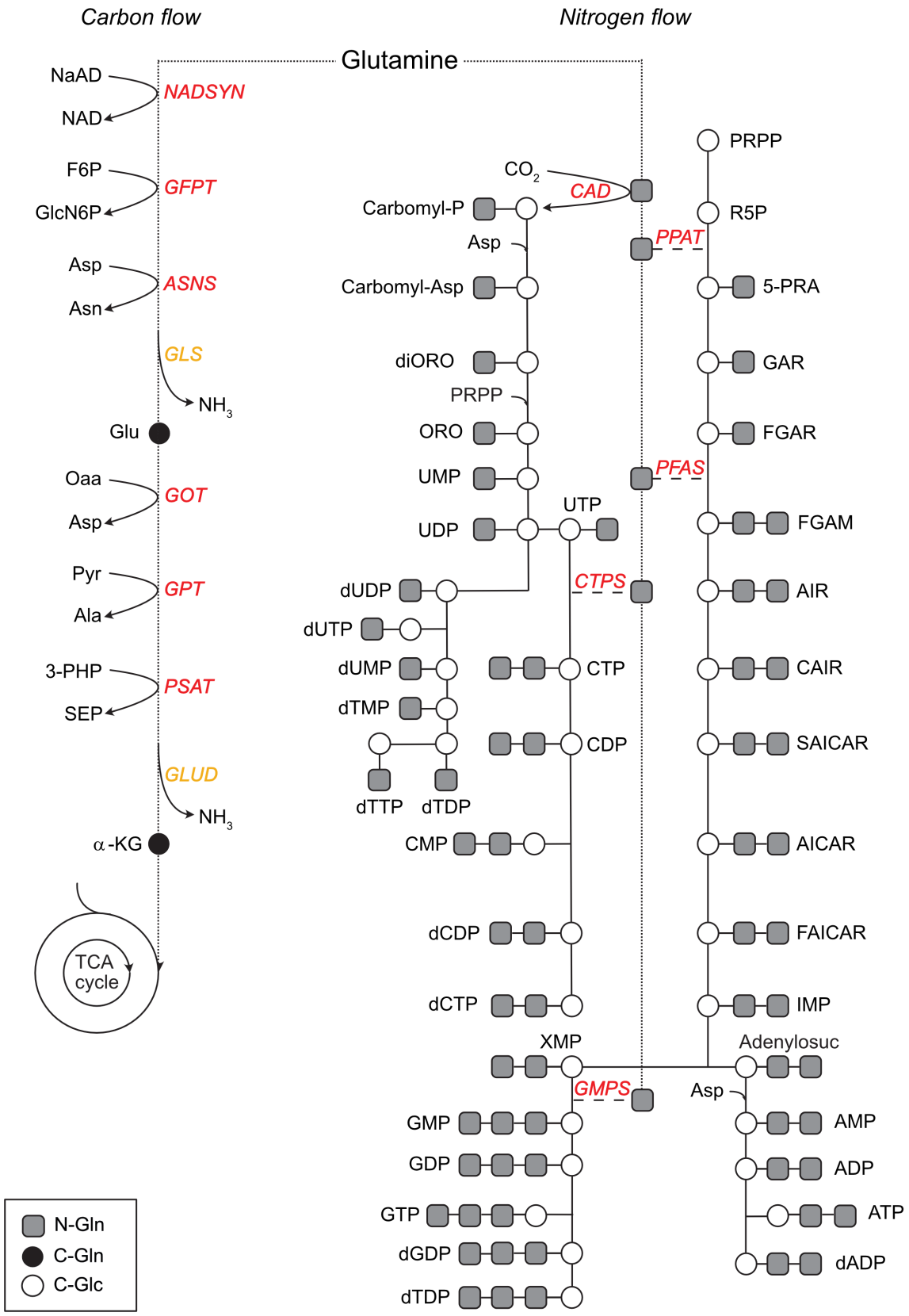

Figure 1.3: Glutamine centric carbon and nitrogen pathway in TCA cycle anaplerosis and *de novo* nucleotide biosynthesis. Glutamine's carbon backbone (black circle) is converted to glutamate by either transaminases (red) that transfer glutamine's nitrogen to an acceptor molecule or by glutaminase (GLS (yellow)) accompanied by the release of free ammonia (NH_3). Glutamate is further converted to α-ketoglutarate by deamination by glutamate-dehydrogenase (GLUD (yellow)) or by transamination (red). α-ketoglutarate introduces the carbon backbone of glutamine in the TCA cycle. Glutamine contributes its nitrogen (grey box) in three reactions in the *de novo* purine biosynthesis and in two reactions in the *de novo* pyrimidine biosynthesis. All reactions were carried out by transamination enzymes (red). Essential abbreviations provided in the list of abbreviations.).

1.2 Reprogrammed glutamine metabolism in cancer cells

The proto-oncogene *c-MYC* (*MYC*) is a major regulator of cellular processes such as proliferation, cell growth, differentiation, metabolism as well as apoptosis (Poole and van Riggelen (2017), Royla (2018)). It plays a pivotal role in cancer developement as 60–70 % of all cancers show upregulated levels of *MYC* protein and is a hallmark of those cells (Poole and van Riggelen (2017)). Deregulated *MYC* expression leads to changes in glucose and glutamine metabolism, which causes a higher consumption of these substrates to meet the needs of affected cells (Wise et al. (2008), Dang (2012b), Gao et al. (2009), Dang (2013)). To increase the import of glutamine *MYC* positively regulates the upregulation of the plasma glutamine transporters Amino acid transporter/ Solute carrier family 1 member 5 (ASCT2/SLC1A5) and System N transporter 2/ Solute carrier family 38 member 5 (SN2/SLC38A5) (Pavlova et al. (2022), Wise et al. (2008)). Besides, *MYC* also has an impact on the enzyme Glutaminase 1 (GLS1), that enhances the activity and finally maintains the TCA cycle with carbons from glutamine via α-ketoglutarate (Gao et al. (2009)). Furthermore, microRNAs-23a/b, respressors of GLS transcription, were suppressed by *MYC* to increase its expression (Li et al. (2021)). As well amidotransferases involved in the nucleotide pathway e.g. Phosphoribosylpyrophosphate (PRPP), CTP synthase (CTPS) and carbomyl phosphate synthetase II (CAD protein) were transcriptionally regulated by *MYC* (Bush et al. (1998), Li et al. (2021)). However, *in vivo* studies with ^{13}C-glucose labeling have demonstrated that tumor-dependent different anaplerotic routes were preferred. For example: pancreatic and lung tumors prefer TCA cycle replenishment via oxaloacetate, which is generated due to the carboxylation of pyruvate by pyruvate carboxylase (PC) (Pavlova et al. (2022), Lau et al. (2020), Sellers et al. (2015)). Zhao et al. (2019) could show in *in vivo* studies by applied $^{13}C_5$-glutamine that colorectal originated xenografts depend on glutamine for anaplerosis. *In vitro* studies by Eagle in 1955 revealed that glutamine requirements were significantly greater than for any other amino acid and the depletion of glutamine causes cell death in mammalian cells (Zielke et al. (1984), Yuneva et al. (2007), Wise and Thompson (2011)). Over the decades further investigation pointed out the crucial role of altered glutamine metabolism in tumorigenesis and tumor development and its interconnection to *MYC*, which heightened the interest (Deberardinis and Cheng (2010), Yuneva et al. (2007), Wise and Thompson (2011), Le et al. (2012), Nieminen et al. (2013)). The latter was shown to be not one-side influenced by Dejure et al. (2017) as the depletion of the amino acid glutamine suppresses translation of endogenous MYC via the 3'-UTR of the MYC mRNA (Royla (2018)). Furthermore, it was observed that proliferation was stopped under glutamine deprivation in the tested colon cancer cell lines. Increased protein expression of enzymes involved in glutamine metabolism was also revealed in KRAS-transformed cells due to the oncogenic KRAS (Gaglio et al. (2011), Yang et al. (2017)). Besides, some cancers with deregulated phosphatidylinositol 3-kinase/AKT/mammalien target of rapamycin (PI3K/AKT/mTOR) pathway show changed glutamine metabolism (Yang et al. (2017)).

Based on the knowledge of glutamine's potential role as the second major nutrient in cancer it has been examined extensively in order to elucidate novel therapeutic approaches that are based on the concept of glutamine dependency.

1.2.1 Targeting glutamine metabolism in cancer therapy

Several therapeutic strategies utilizing the regulation of glutamine have been developed: Transporter inhibition to reduce glutamine uptake, reduction of glutamine pools in the blood stream, inhibition of key enzymes involved in glutaminolysis, and glutamine mimetics to restrain all glutamine-utilizing enzymes (Li et al. (2021), Chen et al. (2016), Cluntun et al. (2017)). Based on the pivotal role of glutamine in *MYC*-driven cancer cells the enzyme glutaminase has been proposed as a biomarker. Therefore, investigations have been focused on the inhibition of this enzyme as promising therapeutic target (Cluntun et al. (2017), Chen and Cui (2015)). In mammals glutaminase occurs in two isoforms: GLS and GLS2, also known as kidney-glutaminase isoform (KGA) and liver-type glutaminase (LGA), respectively. GLS has a truncated version termed GAC by alternative splicing. KGA and GAC are broadly expressed with highest expression in kidney cells, whereas liver cells have mainly the GLS2 isoform. GLS and GLS2 differ in their regulation. The product glutamate inhibits GLS, while GLS2 is not inhibited. *Vice versa* ammonia inhibits GLS2 but not GLS. Both GLS isoforms require inorganic phosphate as an activator (Altman et al. (2016)). *MYC*-driven cancer cells show upregulated KGA and GAC expression, while the tumor suppressor p53 regulates the transcription of GLS2 (Delabarre et al. (2011)). Many cancer cells show a lack of p53 positively function and thus GLS2 expression is reduced (Lane (1994), Saha et al. (2019)). Accordingly, investigations focused on the development of therapeutic targets against GLS (Cluntun et al. (2017), Chen and Cui (2015), Katt and Cerione (2014)). The inhibitor Bis-2-(5-phenylacetamido-1,2,4-thiadiazol-2-yl)ethyl sulfide (BPTES) was identified by a compound library screening and selectively inhibits GLS (Newcomb (2001), Delabarre et al. (2011), Robinson et al. (2007)). It is a non-competitive inhibitor regarding the substrate glutamine and phosphate. BPTES causes a change in the conformation of GLS, associated with reduced affinity for phosphate. Thus, the latter cannot allosterically activate GLS. Structurally BPTES has no similarity to glutamine or glutamate and binds glutaminase to a site distinct from the substrate-binding site (Robinson et al. (2007)). Moreover, it binds glutaminase without as well as with glutamine (Robinson et al. (2007)). Despite promising results in preclinical studies, BPTES was not examined in clinical trails because of low solubility, poor metabolic stability and moderate potency (Li and Simon (2013), Chen et al. (2016), Elgogary et al. (2016)). Compound-968 (C968) is a specific, non-competitive and allosteric inhibitor of GLS (fig. 5.3) (Katt and Cerione (2014)). It binds to a hydrophobic pocket within the monomer, which is a different allosteric site than BPTES. Here, C968 impedes the formation of a tetramer by inorganic phosphates and prevents GLS activation (Lukey et al. (2013), Ramachandran et al. (2016)). Even though C968 was demonstrated to block glutaminase activation and suppress cell growth, it is largely ineffective at inhibiting once the enzyme has been activated by phosphate (Wang (2010), Katt and Cerione (2014), Chen and Cui (2015)). The low potency and poor aqueous solubility made C968 an unsatisfactory drug candidate for clinical trails (Li and Simon (2013)). The inhibitor CB839 is a selective, non-competitive and more potent GLS inhibitor than BPTES (fig. 5.3). It has shown to decrease proliferation in various cancer cell lines (Parlati et al. (2014), Chen and Cui (2015)). Currently, CB839 undergoes a clinical trial phase II in combination trials as this single agent showed minimal antitumor activity conducted by Calithera Biosciences (Parlati et al. (2014), Motzer et al. (2019), Emberley et al. (2021), Lemberg

et al. (2018)). Another strategy to target the glutamine pathway is the usage of a glutamine antagonist. 6-diazo-5-oxo-L-norleucine (DON) has been studied for decades. In early 1956 Ehrlich and Coffey isolated and characterized the biological effects of DON (Ehrlich et al. (1956)). In the same year DON was examined and further characterized by Dion et al. (1956). DON is produced by an undefined Streptomycin strain, which inhibits glutamine-utilizing enzymes in a two-step mechanism (Lemberg et al. (2018), Ahluwalia et al. (1990)). On one hand, it is a competitive inhibitor that binds covalently the catalytic pocket, resulting in an irreversible inhibition of the active site (Thangavelu et al. (2015), Thomas et al. (2013)). DON acts as a reactive electrophile that attacks nucleophile, which leads to the release of the diazo group and thereby to the formation of an enzyme-inhibitor complex (Lemberg et al. (2018), Thangavelu et al. (2015)). It is a non-selective inhibitor, which targets all glutamine metabolizing enzymes including glutaminase, glutamine aminotransferases involved in *de novo* purine and pyrimidine synthesis, amino acid synthesis, hexosamine production and coenzyme synthesis (fig. 5.3) (Lemberg et al. (2018), Cervantes-Madrid et al. (2015), Hartman (1963), Kaufman (1985), Levenberg et al. (1957), Levitzki et al. (1971), Laronde-Leblanc et al. (2009)). Preclinical studies showed promising results of DON in various tested cancer cell lines (Thangavelu et al. (2015)). However, in clinical trials DON demonstrated cytotoxic activity like nausea, vomiting, mucositis, leukopenia and thrombocytopenia (Cervantes-Madrid et al. (2015)). Therefore, DON never entered clinical phase III because of its dose-limiting toxicity (Kovach et al. (1981)). Meanwhile, Hanaford et al. (2019) have investigated a modification of DON and expounded preclinical results of increased oral bioavailability, which have to be further examined.

The glutamine synthesizing enzyme: Glutamate ammonia ligase

Glutamate ammonia ligase (GLUL) is a cataplerotic enzyme that uses in an ATP-dependent reaction glutamate and ammonia to synthesize glutamine (fig. 5.3). It supports nucleotide biosynthesis and mitochondrial bioenergetics and is mostly located in the cytosol. Studies have revealed that some cancer cells have overexpressed GLUL induced by *MYC* (Wang et al. (2019), Chiodi et al. (2021), Yuneva et al. (2012)). The function of high GLUL expression differs in each cancer type, e.g. breast cancer cells show high GLUL expression and glutamine independence, while lung cancer cells show high GLUL expression with glutamine accumulation despite of activated glutamine catabolism (Kim et al. (2021)). Besides, GLUL plays a key role in the tumor microenvironment. Among others, it supplies glutamine, modulates inflammatory responses and supports vascularization and metastasis of cancer cells (Kim et al. (2021)). Methionine sulfoximine (MSO) is an organosulfur analogue of glutamate and an irreversible competitive inhibitor of GLUL (fig. 5.3) (Berlicki (2008), Eisenberg et al. (2000)). Despite of effective inhibition of GLUL activity it is not applicable in clinical practice because of side effects such as convulsion.

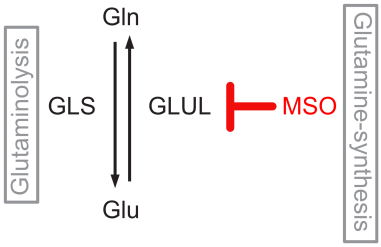

Figure 1.4: Glutamine-synthesizing and glutaminolysis. Glutaminolysis: Glutamine is converted to glutamate via GLS. Glutamine-synthesis: Glutamine is synthesized via GLUL. MSO is inhibiting GLUL. Essential abbreviations provided in the list of abbreviations.).

1.3 Medical Systems Biology in Cancer Research

Hanahan and Weinberg (2011) defined hallmarks to characterize the tremendous impact of altered cells to become tumor cells: Sustaining proliferative signaling, evading growth suppressors, activating invasion and metastasis, enabling replicative immortality, inducing angiogenesis, resisting cell death, deregulating cellular energetics, avoiding immune destruction, tumor-promoting inflammation, and genome instability and mutation. The rewired metabolic program of tumors affects the cell at the levels of the genome, transcriptome, proteome, metabolome and signaling, which in turn is in exchange with the environment and affects it *vice versa*. The traditional linear thinking of a restricted one-way-flow as it was stated by Francis Crick has been proven to be too limited to understand the multifaceted network of these molecular interactions (Crick (1970), Wagener et al. (2016)). For the characterization and analysis of the entire interactive and dynamic network of a cancer cell, an approach providing an overall systemic perspective is needed. In this regard, technological progress and innovation in high-throughput methods prompted the field of systems biology. Studies in systems biology are applied in order to gain an understanding of the biological and physiological complexity of a disease. In this framework, methods such as next generation genome sequencing, microarrays, nuclear magnetic resonance (NMR), gas chromatography (GC) coupled with mass spectrometry (MS), and others provide comprehensive data on genomics, epigenomics, transkriptomics, proteomics and metabolomics that can be integrated based on the combination of empirical, mathematical and computational techniques (Wang (2010)). Systems biology in cancer research could provide new insights into novel pathway interactions that allow to elude therapeutic targets. This would help to develop anti-cancer drugs and optimize treatment strategies - especially in personalized medicine (Wang (2010)).

1.3.1 The vital role of metabolomics

An essential component of systems biology is the field of metabolomics, which comprises the qualitative and quantitative study of small molecular weight molecules (Tolstikov (2016)). In the systems biology hierarchy metabolomics reveals the downstream products of gene and proteinexpression that can provide regulatory feedback to upstream processes (fig. 1.5) (Baharum and Azizan (2018), Zhang et al. (2013)).

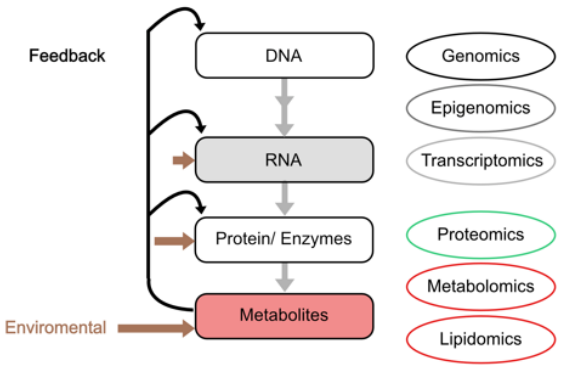

Figure 1.5: Metabolomics systems biology. Regulation of omics levels (grey arrows) via metabolites beyond the central dogma of molecular biology. Adapted and modified from Tolstikov (2016).).

The interaction between the regimes and metabolites can occur in form of, e.g. enzyme regulation via allosterical control or providing macromolecules to build DNA or RNA (Buescher and Driggers (2016)). Thus, metabolites are involved in cell cycle regulation, proliferation, and apoptosis (Zhang et al. (2013), Hsu and Sabatini (2008)). Ferrara et al. (2008) demonstrated a specific causal network that links gene expression and metabolic changes in liver cancer cells. Furthermore, an investigation on interaction of metabolomics and transcriptomics in prostate cancer cells revealed, *inter alia*, a potential biomarker (Ren et al. (2016)). In particular, investigation on metabolites to discover biomarkers for cancer and thus identify potential novel therapeutic targets has been increased over the last decade (Nam et al. (2009), Griffiths et al. (2010)).

1.3.2 Metabolomics studies

As stated in 1.1 cancer cell metabolism is a highly dynamic and complex network. The central carbon metabolism (CCM) has an essential role as it supplies energy and building blocks for cell growth and proliferation (Pietzke and Kempa (2014)). Metabolic flux analysis can show the effect of cellular interactions directly and provide an understanding of the metabolic changes that occur during carcinogenesis (Bruntz et al. (2017)). For this purpose gas chromatography coupled to Time-of-Flight mass spectrometry (GC-ToF-MS) has become a powerful platform. In particular, monitoring the conversion of stable isotope-labeled metabolites in a dynamic manner enables profound insights into an altered metabolism by tracking individual atomic routes within the CCM, e.g. glutamine (Pietzke and Kempa (2014)). The GC-ToF-MS technique is sensitive, robust and allows easy metabolite identification, because of standard libraries, which are based on the retention time and the specific fragmentation pattern of the equivalent compound. The metabolic flux displays the activity of enzymatic reactions, which are regulated by post-translational modifications such as phosphorylations (Pietzke and Kempa (2014)). The cellular metabolism adapts within seconds to environmental changes. Signal-transduction adaptations take minutes and transcription and translation take minutes to hours (Royla (2018)). In previous studies stable isotopes were applied to trace the carbon flow throughout the metabolic network in a dynamic manner. Due to long labeling times only stationary incorporation was observed. A method called pulsed Stable Isotope Resolved Metabolomics (pSIRM), established by the Kempa group in 2014, enables the measurement of the instationary metabolic turnover by applying heavy atom-labelled nutrients (fig. 1.6) (Pietzke and Kempa (2014)).

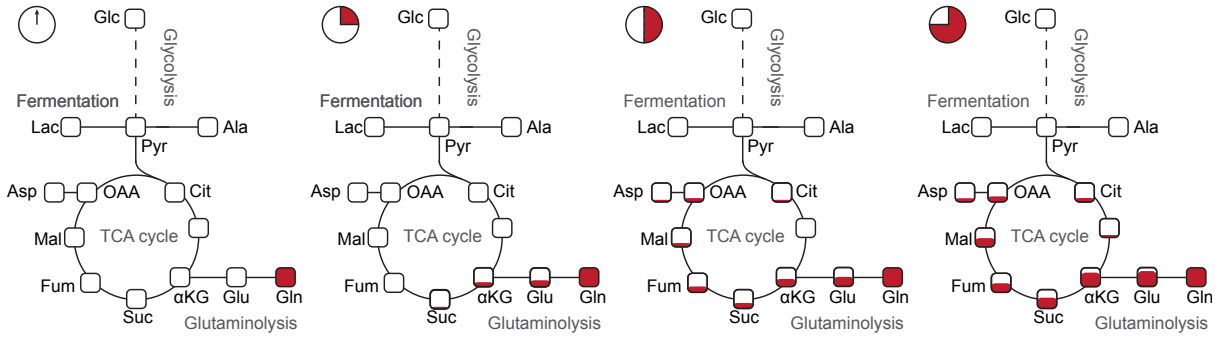

Figure 1.6: Pulsed stable isotope-resolved metabolomics (pSIRM). Dynamic incorporation of u-^{13}C-glutamine (red) allows to monitor the turnover-dependent replacement of carbon-12. By using time-resolved pulsed labeling the routing of applied substrates with or without inhibitor enables the assessment of preferated pathways (Royla (2018)).

1.3.3 Proteomics studies

In order to gain comprehensive data to understand cellular processes proteome analysis will also be required. Enzymes and proteins are an integral part of the metabolic network and thus of particular importance for the breakdown of cancer cell metabolism. The aim of proteomics is part of the larger network system by studying the multi protein systems in an organism (Karpievitch et al. (2011)). Liquid chromatography coupled to mass spectrometry (LC-MS) has become increasingly popular over the past decade as the tool of choice for identifying and quantifying the proteome (Xie et al. (2011)). For the characterization and analysis of proteins, mass spectrometry has been proven an effective tool. Combined with LC this high-throughput approach allows the separation and relative quantification of complex samples, e.g. cell culture samples. In the general workflow for proteomics by LC-MS cells first are lysed and proteins are converted to peptides by proteolytic digestion. Peptides are separated by LC, in which the samples are pushed with the polar mobile phase through the column with a non-polar, hydrophobic stationary phase. Depending on interactions of hydrophobic segments of the peptides, hydrophilic peptides will elute faster than hydrophobic peptides. Followed by ionization via electrospray ionization (ESI), peptides are then introduced into the mass spectrometer. To determine the mass to-charge ratio (m/z) the ionized samples get assigned via ion source and measured by mass analyzer. Subsequently, the ion detector measures the intensity of each ion species (Karpievitch et al. (2011)). The retention time (RT) is captured by a detector. Peptides are identified by the comparison of observed fragmentation spectra with the once generated *in silico* from a chosen database. The advantage of LC-MS technique is no limitation in the molecular weight of the analyses, more sensitivity than GC-MS, easy sample preparation and analyzation of thermolabile molecules (Lubes and Goodarzi (2018))

1.3.4 Nucleotide analysis via direct infusion MS-MS

The exploitation of multidisciplinary omic networks also includes the determination of nucleotides as well as intermediates of the nucleotide biosynthesis pathway. LC-MS was shown to be the method of choice to measure nucleosides rather than the former used GC-MS method (Esmans et al. (1985), Dudley and Bond (2014)). However, the phosphate groups of nucleotides hinder chromatographic seperation. Thus, a further possibility is direct infusion of MS-MS,

especially suitable for pure samples. For this, samples must be purified from contaminants that might interfere with mass spectrometric measurements. Before direct injection, cell extracts with enriched nucleotides are dissolved in methanol. MS-MS allows to obtain readily recognizable fragmentation patterns and to quantify the amount of the nucleotide (Quinn et al. (2013)). Characterization of nucleotide based either by monitoring the nucleotides end points or by using radioactive labelling to trace nucleotide intermediates (Mádrová et al. (2018), Sant et al. (1989)). The lack of an appropriate method for a detailed analysis of all intermediates is due to restricted sensitivity, the commercial unavailability of the compounds and the abscence of experimental fragmentation spectra (Mádrová et al. (2018)). The developement of a dedicated method would allow cancer research, enzyme studies as well as inhibition studies. In particular, an approach with applied labeling of relevant substrates for *de novo* nucleotide biosynthesis would provide a detailed insight of altered mechanisms in cancer.

1.4 Previous work of Kempa group

Previous investigations of Kempa Lab (BIMSB/MDC, Berlin-Germany) focused on the validation of glutaminase inhibitors in HCT116 and RKO cells (Royla (2018)). The application of ^{13}C-glutamine to glutaminase-inhibited cells revealed that several GLS inhibitors do not impair glutamine to glutamate conversion in the presence of glutamine. Contrarily, GLS inhibitor treated cells that have been deprived of glutamine prior to the ^{13}C-glutamine application showed a decelerated ^{13}C-incorporation into glutamate. Additionally, cell growth of HCT116 and RKO cells was affected upon inhibitor treatment, but not completely suppressed. We believe that other glutamine to glutamate converting reactions catalyzed by aminotransferases compensate for the inhibition of glutaminase. In particular, those involved in the nucleotide biosynthesis. Consequently, HCT116 and RKO cells may maintain glutamine requirements for bioenergetic and anabolic demands as well as for cell growth.

Chapter 2

Aims of the Thesis

MYC-driven cancer cells show enhanced glutaminolysis, which causes glutamine dependency for growth and survival. Besides glutamine being an anaplerotic substrate in providing its carbon skeleton to produce TCA cycle intermediates, it also plays a key role as a nitrogen donor in the synthesis of amino acids or nucleotides. Initial experiments revealed that HEK293 cells can grow independently from glutamine availability in FBS. It was demonstrated, that DON, a glutamine analoque, reduced cell proliferation, that was not due to restrictions of the glutaminolysis (Royla (2018)). The aim of the thesis is to gain knowledge about the interconnection of cell growth and metabolism in cancer cells that rely on glutamine's nitrogen as a substrate of transaminases involved in nucleotide biosynthesis. Consequently, this study will test for correlations between glutamine dependency and the survival in the absence of glutamine. In addition, DON was examined in interrupting glutamine's nitrogen flow. Firstly, we examined the glutamine dependency in two colon cancer cell lines, HCT116 and RKO, and in the non-cancerous cell line HEK293 in FBS and dialyzed FBS mediums. In addition, we analyzed, the capability of the cells to adapt in glutamine depleted and supplemented dialyzed FBS medium. The application of quantitative mass spectrometry approaches aimed at the identification of critical metabolic pathways, that may mediate for the adaptation. Identified pathways were validated for their involvement via rescue or inhibition experiments in the tested cell lines. Secondly, to enable simultaneous measuring of carbon and nitrogen, we have developed isotope tracing techniques using ultra high-resolution mass spectrometry. With these techniques we analyzed the incorporation of different stable isotopes within cellular metabolic intermediates. We wanted to determine metabolic dynamics at the crossroads of carbon and nitrogen, especially at nucleotide level. The integrative data analysis of cell growth, proteome and metabolic conversion data may provide a comprehensive insight into metabolic alteration that occur in glutamine-addicted cancer cells. Thirdly, we retraced glutamine's nitrogen donation to the nucleotide biosynthesis to expose DON's effect on involved transaminases and how purine synthesis pathway may be disrupted. Therefore, a new technique was developed based on direct-infusion MS to study dynamic nitrogen flow by using pSIRM and inhibition-treatment in parallel.

Chapter 3

Materials

3.1 Cell biology methods

3.1.1 Cell culture

HCT116, HEK293 and RKO cells were maintained in Dulbeccos modified Eagle Medium (DMEM/ without glutamine, glucose, phenol red and sodium pyruvate) supplemented with 2.5 g/ L glucose, 2mM glutamine and 10 % fetal bovine serum (FBS, v/v) or with 10 % dialysed fetal bovine serum (dFBS, v/v) at 37 °C, 21 % O_2 and 5 % CO_2 for routine cell cultivation. Cells have been passaged in appropriate split ratio every 2-3 days to avoid contact inhibition. When a confluence of at least 70 % was reached cells were washed once with 1x phosphate buffered saline (PBS) and detached from the plate by using TrypLE. To cease trypsinization fresh medium was added. Collected cell suspension was centrifuged (300 xg, 2 min), arised supernatant was removed and remaining cell pellet was resuspended in fresh pre-warmed media. Appropriate cell suspensions depending on cell line specific doubling time was transferred into a new dish.

3.1.2 Cell number determination

Cells were washed, trypsinized and harvested as descriped in 3.1.1. Resuspended cell pellet were mixed in a 1:2 ratio with trypan blue solution and subsequently 10 µL were loaded twice onto a cell counting slide. Cell number and viability was measured in technical duplicates using the automated cell counter TC20 (Biorad).

3.1.3 Cell defrosting

Cryovials were directly placed in a 37 °C water bath after removal from liquid nitrogen. Once cells started to thaw, cell suspension was transferred into a 15 mL falcon tube containing fresh media. Afterwards cells were centrifuged at 300 xg for 2 min. Supernatant was discarded and remaining cell pellet was resuspended in fresh media. Generated cell suspension was transferred into a new dish and cultivated. After 24 h media was replaced to remove residual DMSO.

3.1.4 Cell harvest

After discarding media from the plate, cells were gently washed with 1x PBS and subsequently scratched and transferred to a reaction tube. Cells were centrifugated for 2 min at 300 xg and 4 °C. Supernatant was removed and remaining cell pellet was snap-frozen in liquid nitrogen. Pellet was stored at -20 °C until further processing e.g. protein extraction.

3.1.5 Glutamine starvation experiment

HCT116 cells were seeded at 2.5 e+6 cells and HEK293 and RKO cells at 2.0 e+6 cells per well and cultivated in standard cell culture media with normal or dialzyed FBS for at least 24 h. To starve cells from glutamine, cells were washed once with 1x PBS and fresh media without glutamine was added.

3.1.6 Glutamine starvation experiment for 2 weeks 0, 0.1 and 2 mM Glutamine

Cells were cultivated in standard cell culture media with normal FBS and 2 mM glutamine for 24 h. The following day cells were washed once with 1x PBS and glutamine was added to the media in different concentrations of 2 mM, 0.1 mM or 0 mM. Cells were cultivated for at least 2 weeks. When reaching a confluency of at least 70% cells were passaged. Otherwise, media was replaced every 2-3 days to avoid limiting nutrients.

3.1.7 Readdition experiment

Cells were treated in normal FBS-supplemented standard medium as described above. Additional to glutamine starvation, cells were treated with 10 µM of an intended inhibitor or analogue for 16 h. Afterwards, fresh media with 2 mM glutamine was re-added for 30 min, 60 min, 120 min and 240 min. Table 3.1 lists inhibitors and analogues with their targets and the applied concentrations.

Table 3.1: Inhibitors applied in in vitro experiments.

Component	$[c]_{final}$	Target	Reference
Acivizin*	10 µM	Glutaminase	Dringen et al. (1997)
Azaserine*	10 µM	Glutaminase	Yanagida et al. (2014)
DON*	10 µM	Glutaminase	Chen and Cui (2015)
BPTES	10 µM	Glutaminase	Chen and Cui (2015)
CB839	10 µM	Glutaminase	Chen and Cui (2015)
C968	10 µM	Glutaminase	Chen and Cui (2015)
* glutamine analogue, inhibition of glutamine-utilizing enzymes			

3.1.8 Supplementation experiment

Cells were cultivated in dialyzed FBS-supplemented medium with glutamine as described in section 3.1.6. After 24 h viable cell count was measured for the 0 h time point. Afterwards, media was changed to dialyzed FBS-supplemented medium containing the following substances (corresponding abbrevations and concentrations are shown in brackets) instead of glutamine

in separate experiments: Asparagine (N, 1 mM), Aspartate (D, 1 mM), Aspartate (D, 1 mM) + NH_4^+ (0.8 mM), Glutamate (E, 1 mM), Glutamate (E, 1 mM) + NH_4^+ (0.8 mM), Glutamine (Q, 2 mM), NH_4^+ (0.8 mM). When reaching a confluency of at least 60%, cell count was determined and cells were passaged as described in section 3.1.1. Media was replaced every 2-3 days to avoid nutrient limitation.

Doubling time was calculated using the equation:

$$T2 = \frac{\Delta t}{log_2(\frac{\Delta N}{N_0} + 1)} \quad (1)$$

In the equation (1) N_0 is the number of cells at day 0 and ΔN is the increase in the number of cells during the period of time of the length Δt.

3.1.9 Proliferation inhibition assay with MSO-treatment

In a 6-well plate 3e+5 and 12e+5 cells/well of HCT116 and HEK293 cells, respsectively were plated in dialyzed FBS-supplemented cell culture media. The following day medium was replaced with medium containing either Methionine Sulfoximine (MSO) or sterile H_2O (solvent control). To avoid nutrient limitations, media containing respective treatment was replaced every 24 h. Viable cell count was determined at 24, 48, 72 and 96 hours post-treatment.

3.1.10 Inhibition assay with DON-treatment without glutamine labeling

HCT116 and HEK293 cells were plated in standard cell culture media with normal FBS as described above (3.1.1). After two weeks of glutamine starvation medium was replaced with medium containing the glutamine-analogue DON or the solvent control PBS for maximal 24 hours. Cells were harvested (section 3.1.4) at 2, 8 and 24 hours and analysed via direct-infusion MS (section 3.5).

3.1.11 Inhibition assay with DON-treatment and glutamine labeling

HCT116 cells were plated in standard cell culture media with normal FBS as described above (3.1.1). After two weeks of glutamine starvation medium was replaced with medium containing the glutamine-analogue DON or the solvent control PBS in 4 different conditions: i.) Cells were simultaneously treated with DON or the solvent control PBS and labelled glutamine. Afterwards, cells were incubated for 24 hours.
ii.) Cells were simultaneously treated with DON or the solvent control PBS and labelled glutamine. Afterwards, cells were incubated for 6 hours.
iii.) Cells were treated with DON or PBS for 6 hours. After 2 hours of treatment labelled glutamine was added for 4 hours.
iv.) Cells were treated with DON or the solvent control PBS for 6 hours. After 5 hours of treatment labelled glutamine was added for 1 hour.
In addition to each condition 2 counting plates were added. For the determination of natural

abundance 3 plates were left untreated and unlabelled. In total, HCT116 cells were harvested after 0 h, 1 h, 4 h, 6 h and 24 h of ^{15}N-glutamine labelling for nucleotide measurements.

3.2 Biochemical methods

3.2.1 Cell lysation

After thawing cell pellets on ice, RIPA buffer (1 mM ETDA, 140 mM NaCl, 1 % Triton x-100 (v/v), 0.1 % sodium deoxycholate (v/v), 0.1 % sodium dodecyl sulfate (SDS, w/v), 50 mM TrisHCl (pH 7.9)) supplemented with protease and phosphatase inhibitors was added to the samples, accordingly to pellet size. Cells were resuspended, followed by chilling on ice for 10 min and sonification for 25 s (Bandelin Sonorex Digitec DT 100). Afterwards, cells were vortexed for 10 s. In total these steps were repeated three times. Subsequently, cell lysates were centrifuged at 14000 xg speed for 5 min at 4 °C to remove cell debris and protein concentration was determined as described in section 3.2.2. Overall 40 µg of protein were diluted in 2x SDS sample buffer (10 g/L bromphenol blue, 100 mM dithiothreitol (DTT), 2 % SDS (w/v), 10 % glycerol (v/v), 50 mM TrisBase (pH 6.8), diluted in H2O) and snap-frozen in liquid nitrogen. Cell lysates were stored at -20 °C for subsequent sodium dodecyl sulfate polyacrylamide gel electrophoresis (SDS-PAGE).

3.2.2 Protein quantification

To determine protein concentration colorimetric Pierce BCA Protein Assay Kit from Thermo Scientific was used. According to the manufacturer's instructions, 2 µL of cell lysate, a negative control (1x PBS) and a standard dilution series of bovine serum albumin (BSA) (50-10000 µg/mL diluted in 1x PBS) were each mixed with 100 µL of working solution and incubated for 30 minutes at room temperature. Colorimetric absorbance was detected via a plate reader at a wavelength of λ = 562 nm (Infinite2000, Tecan). Each sample was measured in technical duplicates. Negative control was used to correct for the background signal.

3.2.3 SDS PAGE

As given by Laemmli (Laemmli (1970)), 40 µg of protein were diluted in 2x SDS sampling buffer, denatured under constant agitation for 5 min at 95 °C and afterwards chilled on ice. Samples were spun down and subsequently loaded onto a suitable self-casted SDS polyacrylamide gel (for exact composition see 7.3) to separate proteins of interest. Biorad Mini Protean system filled with 1x SDS running buffer (190 mM glycine, 0.1 % SDS (w/v), 25 mM TrisBase, diluted in H_2O, pH 8.3) was used to carry out discontinuous electrophoresis at 60-135 V. A PageRuler pre-stained protein ladder from Thermo Scientific was used as a molecular weight marker.

3.2.4 Western Blot

Subsequent to separation proteins were transferred onto a polyvinylidene difluoride (PVDF) membrane. For that purpose the Biorad Trans-Blot Turbo Transfer semi-dry blotting system was used and carried out for 30 min at 25 V and 1 A. Transfer time was prolonged to 60 min for

proteins with higher molecular weight ($\geq$ 150 kDa). First, PVDF membrane was activated in Methanol (MeOH) and washed in H_2O. Membrane, filter papers and gel was then equilibrated in blotting buffer (40 mM glycine, 20 % MeOH (v/v), 0.075 % SDS (w/v), 48 mM TrisBase, diluted in H_2O) and assembled for western blotting. Subsequently, membrane was blocked for 30-60 min at room temperature with 1-5 % BSA (w/v) or 5 % milk (w/v) in TBS-T (1x TBS (137 mM NaCl, 20 mM TrisBase), 0.1 % Tween-20 (v/v)). Membrane was probed with a primary antibody under constant agitation overnight at 4 °C. The following day membrane was washed three times for 10 min in TBS-T before and after probing with a HRP-coupled secondary antibody for 1 hour at room temperature. To expose antibodies Amersham ECL Western Blotting detection solution (GE Healthcare) was used according to the manufacturer's protocol and performed on the ImageQuant LAS4000 system (GE Healthcare). The image processing program ImageJ was used for relative quantification of protein expression (Schneider et al. (2012)). According to the experimental setting, expression levels were normalized to a loading control.

3.3 Proteomics

3.3.1 Whole cell lysis

According to cell pellet size urea buffer (8 M Urea, 100 mM Tris (pH 8.2)) was added. Cells were lysed followed by sonification and centrifugation for 3 min at 14.000 xg at 4 °C. Supernatant were transferred into new reaction tubes and protein concentration was determined as described before (3.2.2).

3.3.2 Protein digestion

For further processing maximal 100 µg of protein were first denaturated and alkylated by treating samples with 2 mM Dithiothreitol (DTT) for 30 min at 25 °C and afterwards with 11 mM iodoacetamide (IAA) for 20 min at room temperature in the dark. Subsequently, proteins were digested by incubation with Lys-C (Wako, 1:40 w/w) overnight at 30 °C under gentle shaking (750 rpm). The next day Lys-C digestion products were diluted 1:4 (v/v) with 50 mM ammonium bicarbonate (AmBic), followed by incubation with trypsin beads (Applied Biosystems, 1:80 w/w, 4 h, 30 °C under rotation). After samples were spun down (10 min, 14.000 xg at room temperature), 5 µL of trifluoroacetic acid was added to stop tryptic digestion. Subsequently, samples were desalted on Stage Tips as described below in 3.3.3 (Rappsilber et al. (2007)).

3.3.3 Stage Tip desalting

For shotgun proteome analysis desalting of 15 µg of protein was performed with self-made STAGE Tips. The C18 matrix was activated by the addition of 50 µL buffer A (0.5 % acetic acid) followed by 50 µL buffer B (80 % acetonitrile, 0.5 % acetic acid) to wash out the MeOH. Again 50 µL buffer A was added to equilibrate the matrix. 15 µg of protein sample were loaded on a STAGE Tip. By adding 50 µL buffer A salts were washed out. To elute peptides in low-binding

tubes 50 µL of buffer B were put on the STAGE Tips. Samples were dried and finally resuspended in 15 µL of buffer A. Subsequently samples were measured on Liquid chromatography coupled to mass spectrometry (LC-MS) (section 3.3.4) (Rappsilber et al. (2007)).

3.3.4 LC-MS measurements

Five microliters of each peptide digest were injected in two technical replicates to a liquid chromatography coupled to tandem mass spectrometry system (LC-MS/MS; NanoLC 400 (Eksigent) coupled to Q Exactive Plus (Thermo Scientific)), using a 240 min gradient ranging from 5 % to 40 % of solvent B (80% acetonitrile, 0.1 % formic acid) in solvent A (5 % acetonitrile, 0.1 % formic acid). For the chromatographic separation 100 cm long MonoCap C18 HighResolution 2000 column (GL Sciences) was used. The nanospray source was operated with spray voltage of 2.4 kV and ion transfer line temperature of 260 °C. Data were acquired in data dependent mode, with a top10 method (one survey MS scan with a resolution of 70.000 at m/z 200, followed by up to 10 MS/MS scans on the most intense ions, intensity threshold 5.000). Once selected for fragmentation, ions were excluded from further selection for 45 s, in order to increase the identification rate of lower abundant peptides (Royla (2018), Bayram (2018)).

3.3.5 LC-MS data analyis

Raw data were analyzed using the MaxQuant proteomics pipeline (version 1.5.3.30) and the built in Andromeda search engine with the human Uniprot database (Cox et al. (2011), Tyanova et al. (2016)). Carbamidomethylation was set as a fixed modification, oxidation of methionine as well as acetylation of N-terminus as variable modifications. FDR was set at 1% to filter peptide assignments. Peptides with a minimum length of seven amino acids and a maximum of two miscleavages were further processed. For shotgun analysis peptides were matched between runs. All samples were quantified using label-free quantification (LFQ). Assigned razor peptides involves peptide groups with the largest matches and were used for calculation. To collate LFQ data the software Perseus (version 1.5.6.0) was used. Data were further analyzed via custom R script

3.4 Metabolomics

Targeted Stable Isotope Resolved Metabolomics (tSIRM) is a method that enables the direct measurement of a specific biological reaction by using dual isotope tracing. It allows the detection of relative contribution of extracellular carbon and nitrogen for a specific reaction and its downstream contribution. It was developed by the group of Dr. Stefan Kempa (Bayram et al. (2022)).

Pulse stable isotope resolved metabolomics (pSIRM) is a method that enables the direct measurement of the dynamic metabolic activity of the CCM by using stable isotopes. It allows time-resolved studies and was developed by the group of Dr. Stefan Kempa (Pietzke et al., 2014).

3.4.1 Targeted stable isotope resolved metabolomics (tSIRM)

HCT116 and HEK293 cells were plated on 10 cm plates in cell culture media with dialyzed FBS and supplemented with 1 mM Glu + 96 µM NH_4^+. Cells were cultivated in this condition for at least 1 month for cell growth assays. RKO cells were pre-cultivated in Gln-supplemented medium as RKO cells were unable to proliferate in Glu + NH_4^+. Therefore, medium was changed 3 days prior to targeted stable isotope resolved metabolomics (tSIRM) study to medium containing Glu + NH_4^+. HCT116 and HEK293 cells were seeded at 2 e+6 cells dish for tSIRM study. All three cell lines were labelled with ^{13}C-glutamate and ^{15}N-NH_4^+ and treated with either 500 µM MSO or sterile H_2O (control) for 24 hours. Subsequently, media was removed, cells were shortly flushed with labeling buffer (140 mM NaCl, 5 mM HEPES, 2.5 g/mL Glc, pH 7.4) to remove extracellular metabolites. Labeling buffer was removed and ice-cold methanol (MeOH, 50 % v$\check{}$), containing 2 µg/ µL cinnamic acid as an internal extraction standard, was immediately added in order to quench metabolism. Cells were scratched and transferred into a 15 mL Falcon tube and stored at -20 °C until further processing.

3.4.2 pulse Stable Isotope Resolved Metabolomics (pSIRM)

HCT116, RKO and HEK293 cells were cultivated as described in 3.4.1. All three were pre-treated for 6 hours with either 1 mM MSO or sterile H_2O (control), in fresh Glu + NH_4^+-supplemented dialyzed FBS medium. Afterwards, cells were labeled for 15 min, 30 min, 1 hour, and 3 hours with ^{13}C-glutamate and ^{15}N-NH_4^+ with or without 1 mM MSO treatment. Cells were harvested as described in 3.4.1.

3.4.3 Extraction of Polar Metabolites

1 mL Chloroform was added to methanolic cell extracts (section 3.4.1 and 3.4.2), followed by 1 h shaking at 4 °C and a centrifugation for 15 min at 4.000 xg at 4 °C. Polar phases were collected, transferred to a new 15 mL Falcon tube and vacuum dried overnight. The next day 600 µL 20 % MeOH were added to dried polar phases, shaken for 30 min at 4 °C and subsequently centrifuged (5 min, 4.000 xg at 4 °C). Polar phases were fractionated to generate two technical replicates. Twice 290 µL were transferred to new tubes and once more vacuum dried over night. Samples were stored at -20 °C until preparation for Gas chromatography coupled to mass spectrometry (GC-MS) measurements

3.4.4 Sample Preparation for GC-MS

In order to obtain volatility and stability for GC-MS measurements, dried cell extracts were resuspended in 25 µL of N-(tert-Butyldimethylsilyl)-N-methyltrifluoracetamide (MTBSTFA), 25 µL of Acetonitrile (ACN) and and 0.5 µL alkane mix. Afterwards, cells were incubated for 60 min at 80 °C under constant shaking. Subsequently, samples were centrifuged for 15 min at 14.000 xg to remove insoluble parts. Aliquots of 40 µL were transferred into glass vials for GC-MS measurements. Identification and quantification standards were treated in parallel.

3.4.5 GC-MS Settings

Metabolite profiling analysis (pSIRM) was performed on a GC-ToF-MS and tSIRM on a Q Exactive Orbitrap system (Thermo Fisher). 1 µL of quantification standards and samples were injected in a temperature-controlled injector (TriPlus RSH auto-sampler, Thermo Fisher) with a baffled glass liner in a 1:5 split mode. A temperature gradient program (80 °C for 15 s, 7 °C/s until 260 °C, hold for 3 min) was used for distinct seperation of metabolites and a flow rate of 1.2 mL/ min helium, as carrier gas, was adjusted. Gas chromatographic separation was carried out on a Trace 1,300 GC (Thermo Fisher) equipped with a TG-5SILMS column (30 m length, 250 µm inner diameter, 0.25 µm film thickness (Thermo Fisher). Gas chromatography was performed with an initial temperature of 68 °C for 2 min, followed by an increase of 5 °C/min up to 120 °C, followed by an increase of 7 °C/min up to 200 °C, followed by an increase of 12 °C/ min up to 320 °C which is held for 6 min. The spectra were recorded in a mass range of m/z = 60—600 with resolution at 200 m/z set at 120,000 (Bayram et al. (2022)). First idents and quants were determined, followed by measuring biological replicate (Opialla et al. (2020)). Wash steps (consisting of alkanmix and MTBSTFA) were integrated between different cell lines and within a cell line. Quant dilution series was treated in parallel.

3.4.6 Data Analysis

For the calculation the exact mass of elemental composition of different glutamine fragments were compared with known literature-values. An in-house made compound library including the mass shifts induced by ^{13}C and ^{15}N was used to extract the intensities for the different isotopic masses. A custom R-script that based on the known masses for the fragments and the number of potentially incorporated carbon and nitrogen atoms were used for mass shift calculations. Each incorporated ^{13}C or ^{15}N increased the target mass by 1.0033548 or 0.99693689, respectively. For the analysis of the SIRM experiment, this newly developed target list was imported as a Tracefinder Compound database (Tracefinder 5.0 (Thermo Fisher)). Subsequently, SIRM samples were then processed and peaks were integrated by extracting the extracted ion chromatograms (EIC) within a 5 ppm window. For the analysis of the pSIRM experiment Xcalibur Quanbrowser (Thermo Fisher) was used. Samples were processed and peaks integrated by extracting EIC with a mass tolerance of 2.5 ppm. For both, peak integration quality was visually checked and finally all peak areas were exported (Bayram et al. (2022)).

3.5 Nucleotides

3.5.1 Sample preparation

For direct-infusion MS nucleotide measurements samples (section 3.1.10 and 3.1.11) were prepared to an established protocol (Lorkiewicz et al. (2012)). Dried samples (polar metabolites (3.4.3)) were resuspended with required volume of 5 mM hexylamine buffer A (5 mM hexylamine, pH adjusted to 6.3 with acetic acid) to get 3 e+5 cells in 10 µL. Followed by centrifugation (at 4 °C at 14.000 xg for 5 min) of samples and nucleotide calibration standards (10 µM - 20 nM in 5 mM hexylamine buffer, pH 6.3). In the upcoming preparation steps samples were kept on ice. ZipTips (Millipore) were equilibrated by aspirating 5x 10 µL of 100 % MeOH followed

by 5x 10 µL of buffer A. Afterwards, samples were loaded onto the C18 solid phase of the ZipTip by 8x 10 µL aspirating and dispensing. Followed by a wash step by aspirating buffer A (4x 10 µL) to flush out unbound residuals. Finally, nucleotides were eluted by 12 cycles aspirating and dispensing with 10 µL of elution buffer (70 % buffer A, 30 % buffer B (90 % MeOH, 10 % ammonium acetate (NH_4AC), pH adjusted to 8.5 with NH_4OH)). Elution was diluted with 20 µL of MeOH before direct-infusion MS measurements.

3.5.2 Direct-infusion MS measurements

Nucleotide analysis of the samples in section 3.1.10 were performed on a TSQ Quantiva triple quadrupole mass spectrometer (Thermo Scientific) coupled to a Triversa Nanomate (Advion) nanoESI ion source (1.5 kV spray voltage, 0.5 psi head gas pressure). Argon was used as the collision gas (1.5 mTorr pressure). Data acquisition for the sum of the two transitions for each of the 40 nucleotides was carried out in negative mode. In total, for three minutes per sample with a cycle time of 3.3 seconds, resulting in 55 SRM scans per nucleotide. The full width half maximum (FWHM) resolution was set at 0.7 for both Q1 and Q3. Transitions and unique fragment sizes are documented in 7.1.1.

3.5.3 Direct-infusion MS measurements with labelling

The following nucleotide measurement and analysis protocol was established by Dr. Martin Forbes (Research scientist in the Kempa-Lab, BIMSB/MDC, Berlin-Germany) and Liam Rayman (Master student in the Kempa-Lab, BIMSB/MDC, Berlin-Germany) (Rayman (2022)).

For the preparation of a target list: The elemental composition of various fragments for each coumpound was calculated based on the exact mass and compared with known literature-values (7.1.1). The nucleotides AMP and dGMP, ADP and dGDP, and ATP and dGTP were grouped and measured together as these compounds have identical masses. Each sample was added with 15 µl to a well on a 96 well plate and subsequently placed on a TriVersa NanoMate® nanoESI ion source (spray voltage: 1.5 kV, head gas pressure: 0.5 psi) coupled to a Q Exactive HF, Thermo Fisher Scientific. Each sample was run in triplicate. Data acquisition was performed in negative mode over three minutes. Full scans were performed from 140 m/z to 850 m/z before switching to 10 multiplexed targeted Single Ion Monitoring (tSIM) scans, each of five nucleotide masses taken from a target list of 48. In total scans were repeated for 10 cycles over 3 minutes. Targeted scans went from -1 m/z to +5 m/z of the intermediate or nucleotide m/z for the detection of isotopes and for accounting of mass errors. Scan resolution at 200 m/z was set to 240,000. A constructed compound library including the mass shifts induced by ^{13}C and ^{15}N were used as comparision to extract intensities of different isotopic masses. A custom R-script that based on the known masses for the fragments and the number of potentially incorporated carbon and nitrogen atoms was used for mass shift calculations. Each incorporated ^{13}C or ^{15}N increased the target mass by 1.0033548 or 0.99693689, respectively. To calculate the M-H fragment of the uncharged molecule 1.00728 was subtracted from the exact mass. Transitions and unique fragment sizes are documented in 7.1.1.

3.5.4 Direct-infusion MS analysis

The quality of each measurement was checked manually by using Xcalibur (Software, Thermo Fisher Scientific). Scans with poor signal or stalling in scanning were not taken into account. OpenMS package and in-house developed R-scripts were used for further data processing and statistical analysis RStudio Desktop software (version 1.2.5019.0.).

Chapter 4

Results

Parts of this chapter present data that was published under the title "Investigating the role of GLUL as a survival factor in cellular adaptation to glutamine depletion via targeted stable isotope resolved metabolomics" in the Frontiers Journal in 2022 (Bayram et al. (2022)).

4.1 Glutamine and cMYC interaction

Royla (2018) demonstrated that glutamine starvation suppressed MYC expression and cell growth in several cell lines via a fine-tune feedback in response to external glutamine supply. In all cell lines, except for HEK293, Gln starvation inhibited and Gln re-addition induced MYC protein expression. HEK293 cells sustained MYC protein expression in the absence of glutamine and maintained proliferation. How this effect might be mediated and whether there is a candidate mediating alterations in glutamine supply is still to be elucidated.

To examine if the GLS inhibitors BPTES, CB839 and C968 as well as the glutamine analogues Acivizine, Azaserine and DON have an effect on MYC-levels by targeting glutamine metabolism a time-course experiment was performed. Here, after the respective treatment glutamine was re-added for maximal 4 hours and MYC protein expression was monitored (fig. 4.1, fig. 4.2, fig. 4.3). In order to evaluate the inhibitory effects, solvent controls were treated in parallel.

The investigated two colon cancer cell lines HCT116 and RKO and the non-cancerous cell line HEK293 were plated and starved for glutamine in standard cell culture media with normal FBS and treated with an inhibitor or analogue for 16 h. Subsequently, the amino acid was re-added for 30 min, 60 min, 120 min and 240 min Substrates were either solved in DMSO or H_2O. Both solvents were used as control. MYC protein expression was analyzed by Western Blotting. The depletion of glutamine distinctly suppressed MYC levels in HCT116 and RKO cells. The non-cancerous kidney cell line HEK293 showed a moderate repression and overall sustained MYC protein expression. All three cell lines restored MYC protein levels with a cell line-specific kinetic (fig. 7.1, fig. 7.2, 7.3). A dynamic recovery is observable in the glutaminase specific inhibitors BPTES, CB839 and, C968 as well as the glutamine-analogue Acivizine and Azaserine in HEK293, HCT116 and RKO cells. The recovering upon glutamine re-addition in DON treated conditions is strongest delayed and interrupts the dynamic, especially at glutamine re-addition for 30 min in HCT116 and RKO cells. Therefore, in fig. 4.1, fig. 4.2 and fig.

4.3 the ratio of 30 min solvent control and treatment with 30 min re-added glutamine after 16 h of starvation is calculated for HCT116, RKO and HEK293 cells.

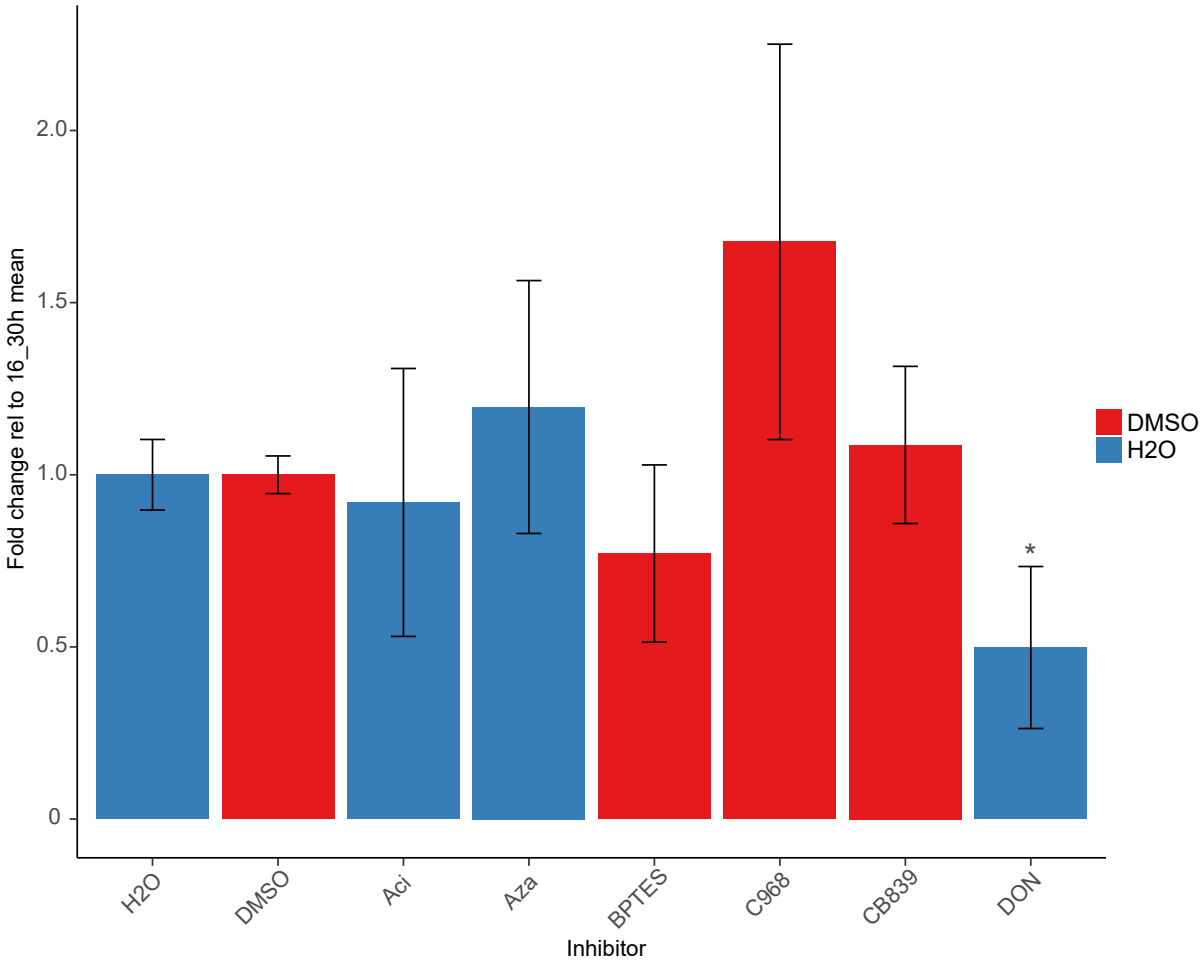

Figure 4.1: Calculated ratio of MYC protein expression upon glutamine starvation and re-addition in normal FBS in HCT116 cells. Relative quantification of MYC protein expression after glutamine re-addition for 30 min of at least three independent experiments. Each value was normalized to solvent control re-addition for 30 min. Asterisk indicates statistically significant differences.

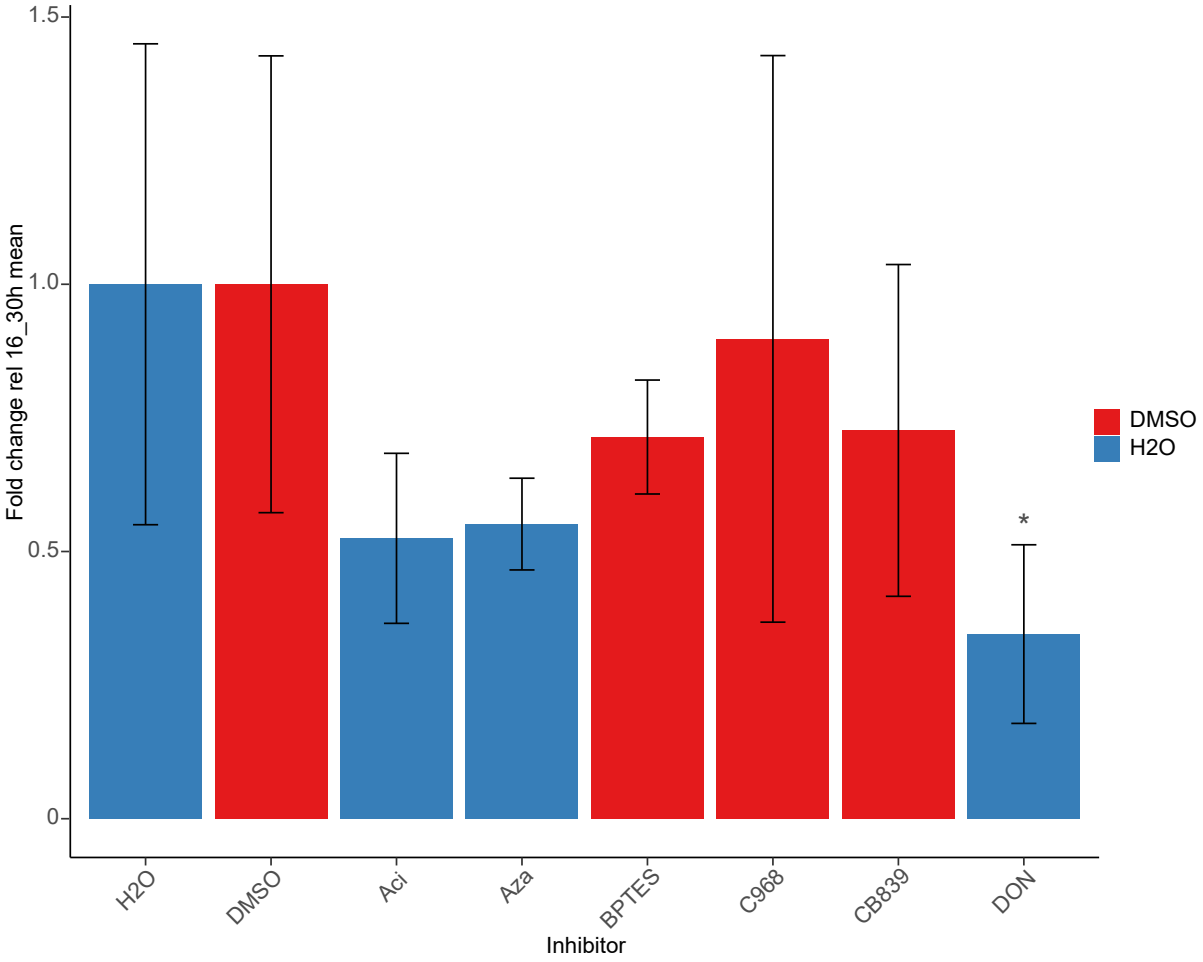

Figure 4.2: Calculated ratio of MYC protein expression upon glutamine starvation and re-addition in normal FBS in RKO cells. Relative quantification of MYC protein expression after glutamine re-addition for 30 min of at least three independent experiments. Each value was normalized to solvent control re-addition for 30 min. Asterisk indicates statistically significant differences.

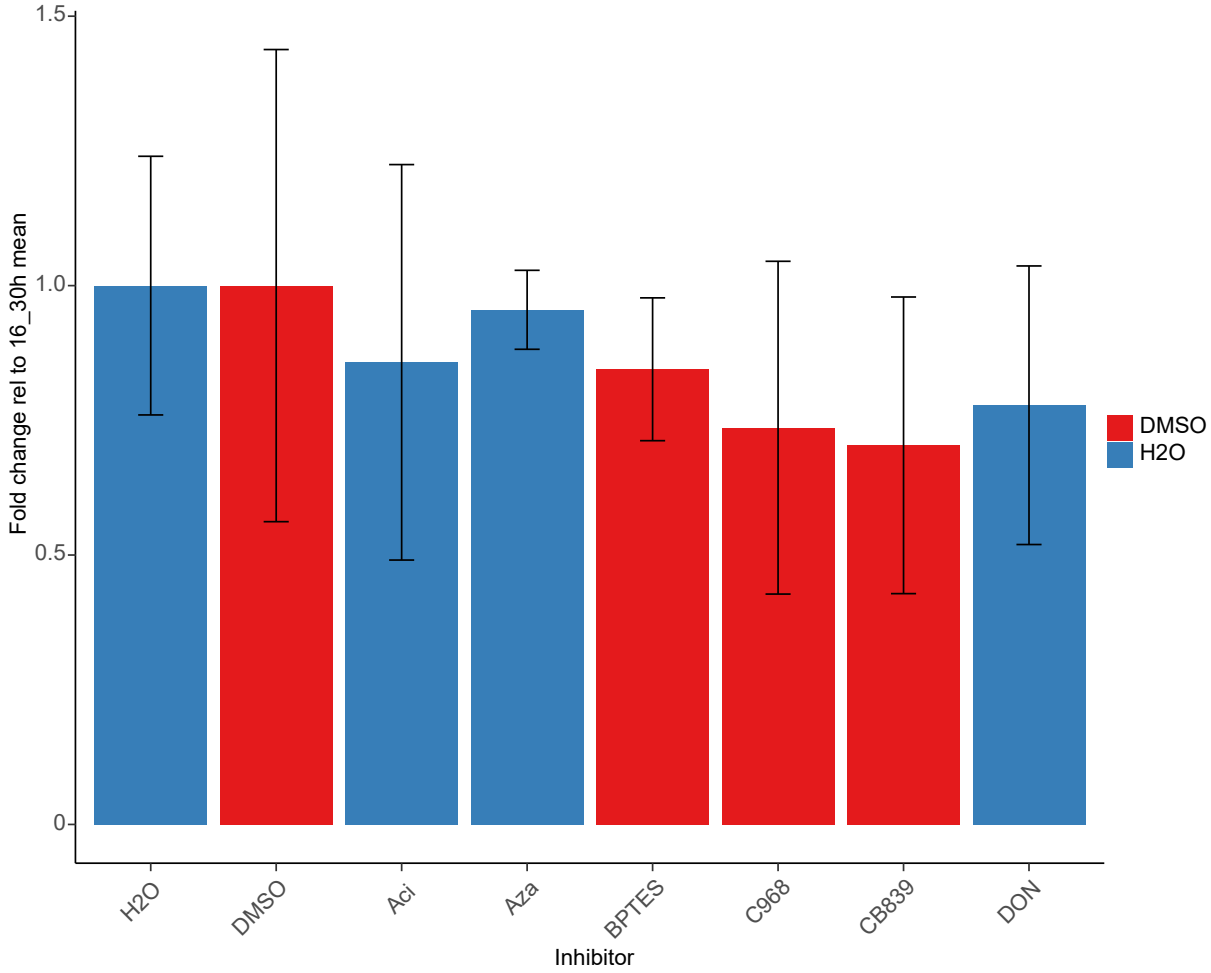

Figure 4.3: Calculated ratio of MYC protein expression upon glutamine starvation and re-addition in normal FBS in HEK293 cells. Relative quantification of MYC protein expression after glutamine re-addition for 30 min of at least three independent experiments. Each value was normalized to solvent control re-addition for 30 min.

4.2 Glutamine deprivation in normal FBS-supplemented medium

The goal was to evaluate the persistent MYC expression in HEK293 cells in glutamine deprived medium compared to glutamine dependent MYC expression in HCT116 and RKO cells. Therefore, data on cell growth and metabolic conversion were integrated, in order to correlate differences in the metabolic profiles of the cell lines with their survival and their MYC expression. To investigate the apparent glutamine dependency in HCT116 and RKO cells, we starved the cells for glutamine in normal FBS-supplemented medium and subsequently analysed their proteome profiles and nucleotide levels.

4.2.1 Proliferation test in normal FBS

The non-cancerous HEK293 cells were shown to grow independent from glutamine. Only when treated with DON, a glutamine analogue, HEK293 showed decreased cell number and MYC expression (Royla (2018), Dejure et al. (2017)). In order to determine whether HEK293 cells can survive and grow in a glutamine independent manner, we first repeated the proliferation experiment and starved the cells for glutamine without additional inhibition of GLS, for 96 h.

In a second approach we extended this growth experiment to 7 d and 14 d. HEK293 and RRO cells were seeded at 2.0 e+6 cells and HCT116 at 2.5 e+6 cells per dish for 24 h with normal FBS medium containing 2 mM glutamine. After 24 h medium was changed to FBS-supplemented medium without glutamine (0 mM) and cells were starved for 96 h for the inital and for at least 14 days for the second experiment. To sustain a sufficient supply of nutrients cell culture media was renewed every 24 h. Cells were splitted at a confluency of 70-80 %. Proliferation rate was determined via cell counts every 24 h for 96 h of the first experiment. For the second approach cell growth was recorded after 16 h, 7 d and 14 d of glutamine deprivation. Regarding the first experiment: The cell growth of colon cancer cell lines HCT116 and RKO are strongly reduced upon glutamine withdrawal compared to glutamine-fed condition for 96 h. Considering the second experiment with a longer period of glutamine depletion, HCT116 cells were able to adapt and survive. In contrast, RKO cells could not adapt to glutamine deprivation and cells were depleted at 14 d. The non cancerous HEK293 cells showed a continued growth in glutamine-fed as well as in glutamine-starved conditions for all tested time points. In conclusion, the findings of the before mentioned glutaminase inhibition assay in combination with pSIRM imply that glutamine-dependent anaplerosis seems not to be the key for the resistance of the tested cells against inhibitors. To gain knowledge about glutamine's nitrogen and the capability of HCT116 cells to adapt to glutamine withdrawal and their differences to RKO cells as well as to glutamine independent HEK293 cells proteome and nucleotide analysis were performed.

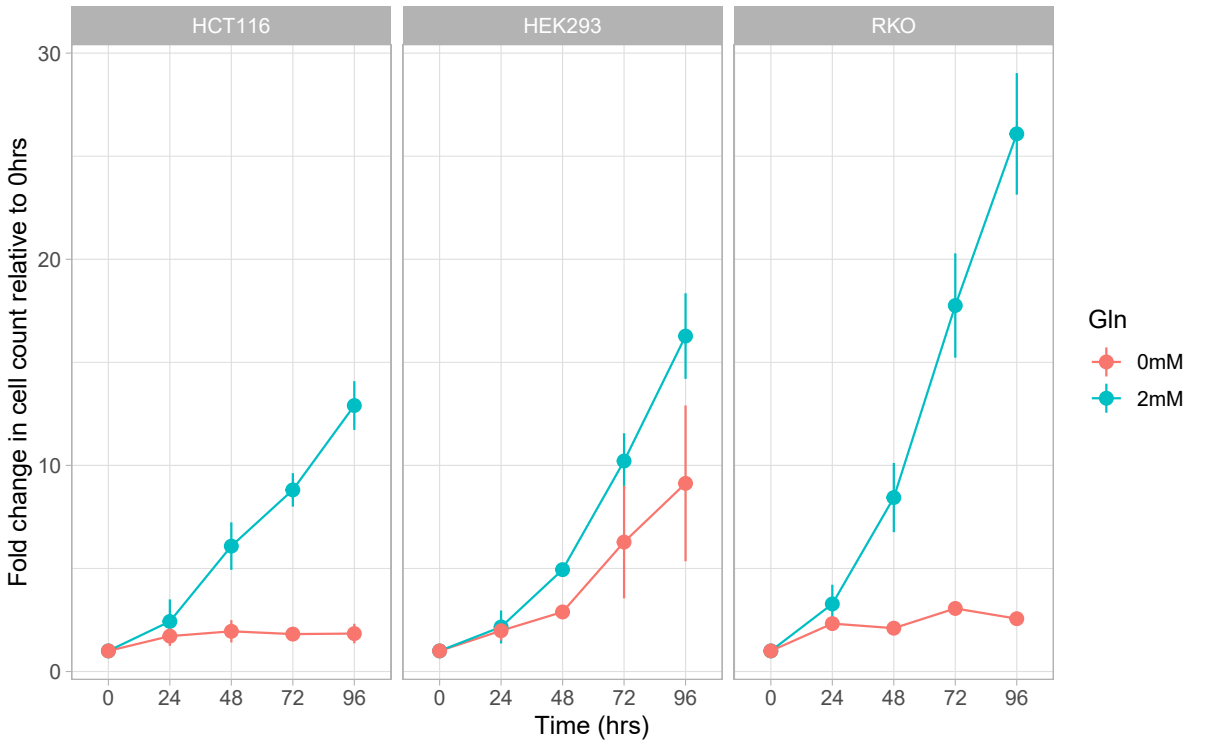

Figure 4.4: Proliferation upon glutamine starvation in normal FBS in total 96 hrs. Cell proliferation upon glutamine starvation in normal FBS medium in HEK293, HCT116 and RKO cell lines. Cells were starved for 96 hrs. Cell number was normalized to 0 h. Results represent mean ± SD (n=3, each measurement was performed in technical duplicates).

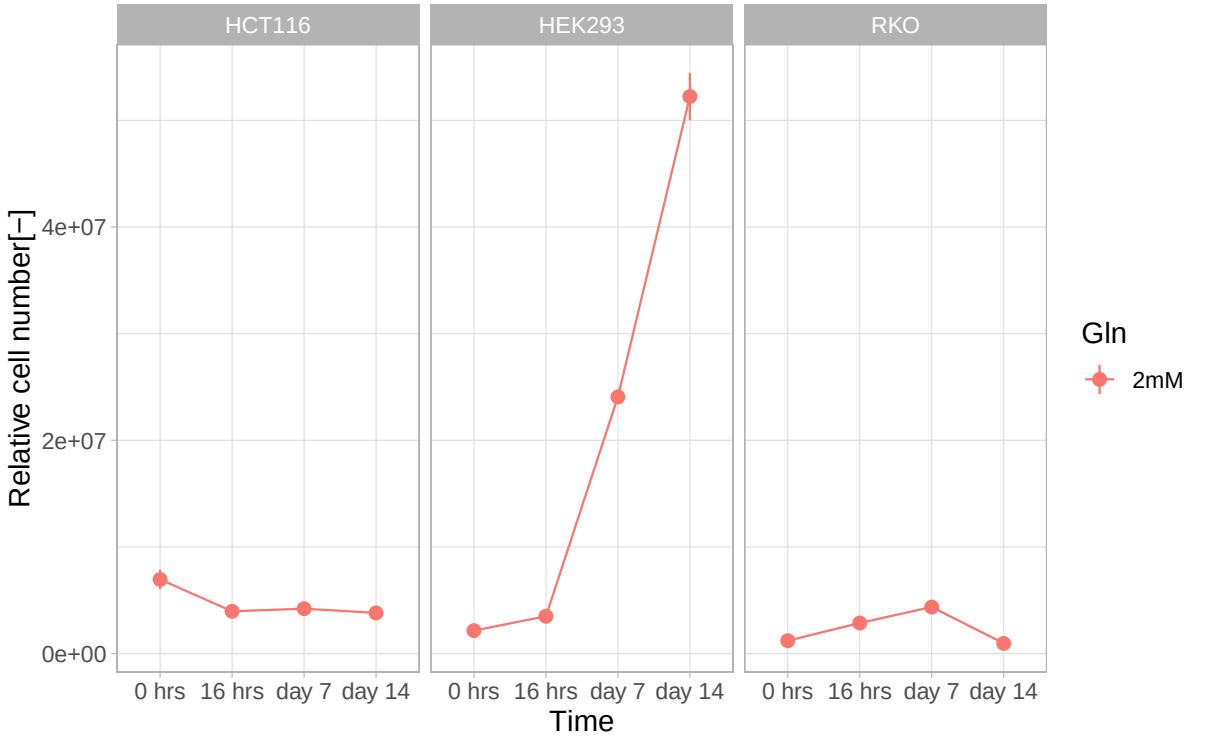

Figure 4.5: Proliferation upon glutamine starvation in normal FBS in total 14 days. Cell proliferation upon glutamine starvation in normal FBS medium in HEK293, HCT116 and RKO cell lines. Cells were starved for 14 days. Cell number presented are relative cell numbers. Results represent mean ± SD (n=3, each measurement was performed in technical duplicates).

4.2.2 Proteome analysis in normal and glutamine deprived conditions

As mentioned in section 4.2.1, a previous proliferation experiment revealed that the glutamine-antagonist DON was the most effective substrate in decreasing cell counts for HCT116, RKO and also HEK293 cells while glutamine's carbon flow was not affected (Royla (2018)). It seems reasonable to assume that GLS is inhibited. However, other bypassing reactions might compensate for the inactivation of the enzyme, especially amidotransferases that are particularly abundant in nucleotide metabolism (Koper et al. (2022)). Therefore, we hypothesized that the efficiency to suppress cell growth by the glutamine analogue DON is not due to the blockage of the conversion of glutamine into glutamate and TCA cycle intermediates. In order to test for correlations between glutamine metabolism and their affect on proliferation a comprehensive data matrix combining cell growth and metabolic conversion data of glutamine starved cells was set up, primarily to see if glutamine-utilizing transaminases might play a key role in glutaminolysis. Hence, the protein abundance of transaminases, that can enlighten the different proliferation phenotypes that have been observed for HCT116, RKO and HEK293 cells, was determined and the protein expression regarding a pattern or escape route, that might elucidate how HEK293 cells continue growing under glutamine withdrawal, was examined. Therefore, the focus was on proteins, for which either glutamine or glutamate serve as substrate. HCT116, RKO and HEK293 cells were plated in standard cell culture medium either with 2 mM, 0.1 mM or 0 mM glutamine for 2 weeks. A shotgun proteome analysis was performed to evaluate protein expression profiles under glutamine fed (0.1 mM and 2 mM) and deprived (0 mM) conditions. As shown in Fig. 4.7 all enzymes involved in glutamine or glutamate metabolism are expressed in HCT116, RKO and HEK293 cells. The two transaminases GOT1 (Glutamate oxaloacetate transaminase1) and GPT2 (Glutamate pyruvate transaminase2) display a compartment-specific differential expression in HCT116 and RKO cells. GOT1 synthesizes L-glutamate from L-aspartate or L-cysteine. GPT2 catalyzes the reversible transamination between alanine and 2-oxoglutarate to form pyruvate and glutamate. These differences could be the reason why the colon cancer cell lines prefer different reactions and pathways to generate glutamate and α-ketoglutarate from glutamine. Interestingly, RKO cells have the highest GLS expression in all tested conditions, whereas the enzymes ASRGL1 (Asparaginase) and ABAT (4-Aminobutyrate aminotransferase) are not expressed in RKO cells. In HCT116 cells the enzyme CCBL1 (Cysteine-S-conjugate beta-lyase) is not expressed. Compared to the colon cancer cell lines HEK293 cells showed a clear increase of GLUL, especially in glutamine starved conditions. However, also HCT116 and RKO cells have an increased expression of glutamine synthetase in the glutamine-deprived medium compared to fed conditions. This observation led to the assumption that all three cell lines are able to synthesize glutamine in glutamine-deprived conditions.

Nevertheless, the observered glutamine independent cell growth in section 4.2.1 can not be explained by the differences in GLUL protein levels alone. Still, in total a remarkable diversity regarding the transaminases that might clarify the different proliferation phenotypes is not detectable. The enyzmes involved in the purine or pyrimidine nucleotide biosynthesis show no significant changes for all three cell lines. Apparently expression of these enzymes is not the reason for the different response upon glutamine starvation. To further address the question if the enzyme GLUL is the decisive difference in HEK293 cells compared to HCT116, RKO

and HEK293 cells further approaches testing the performance of GLUL activity have been performed (see sections 5.4.1, 4.4 and 4.4.1).

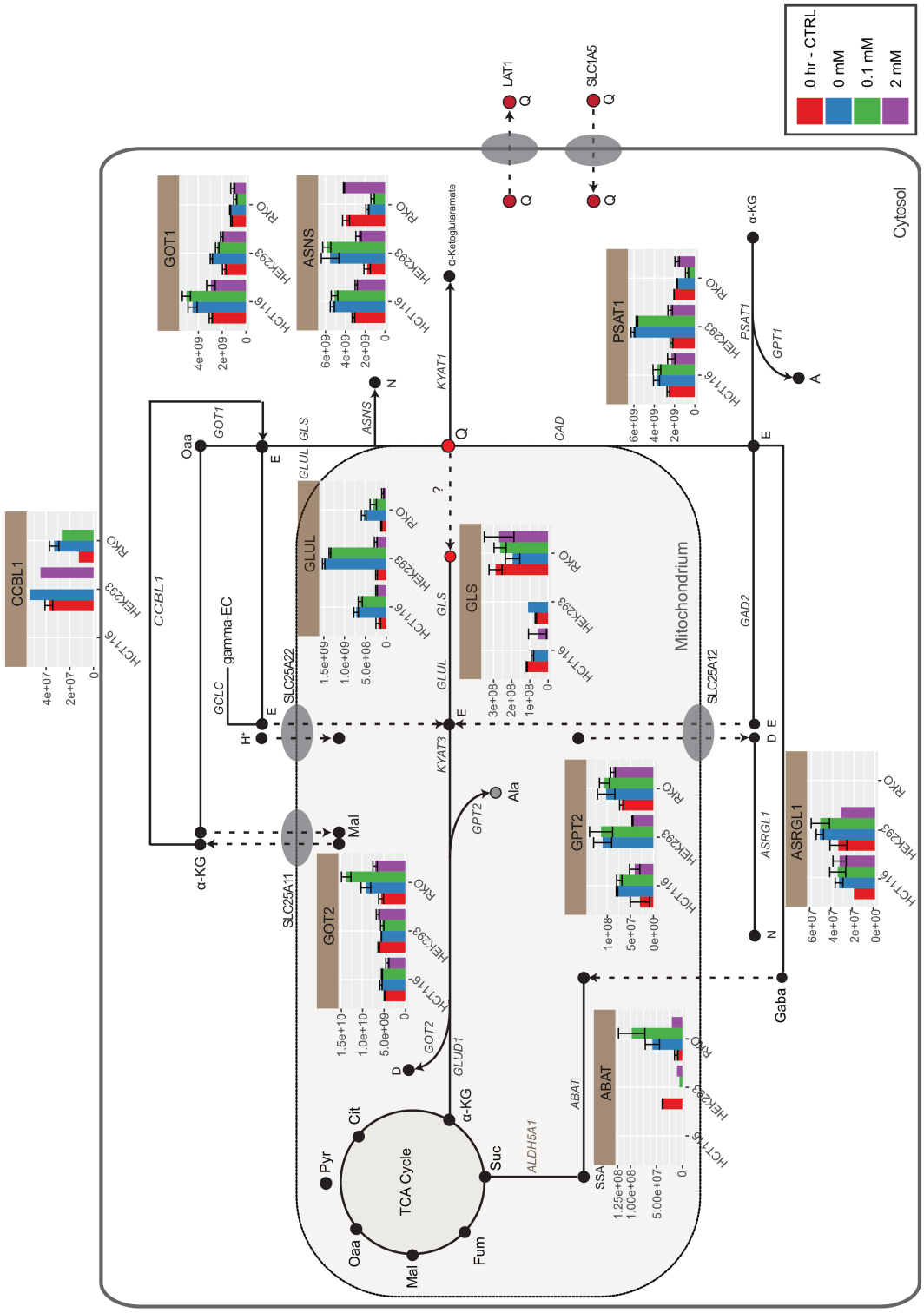

Figure 4.6: Protein expression of glutamine/glutamate utilizing enyzmes in glutamine fed and deprived conditions. LC-MS obtained label-free quantities of selected enzymes are shown for HCT116, RKO and HEK293 cells. Cells were cultivated for 24 hrs in standard cell culture media and subsequently either starved (0 mM) or fed upon glutamine (0.1 mM or 2 mM) for 2 weeks. Results represent mean + SD (n=3). Abbreviations – ABAT: 4-Aminobutyrate aminotransferase ASNS: Asparagine synthetase, ASRGL1: Asparaginase, CCBL1: Cysteine-S-conjugate beta-lyase, GCLC: Glutamate-cysteine ligase catalytic subunit, GOT: Glutamate oxaloacetate transaminase, GPT: Glutamate pyruvate transaminase, GLS: Glutaminase, GLUL: Glutamine synthetase, PSAT: Phosphoserine aminotransferase. For the complete metabolite names refer to the list of abbreviations

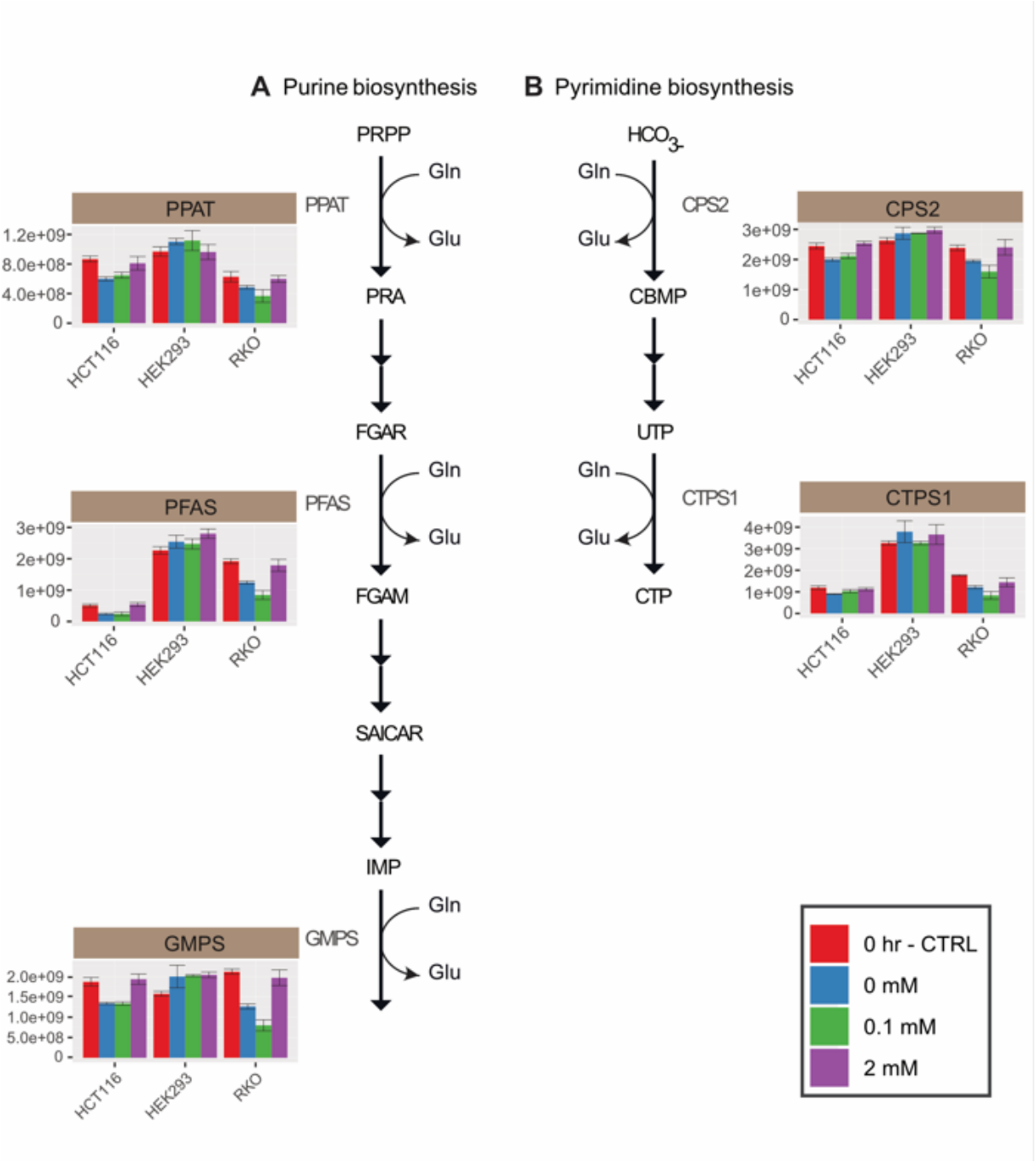

Figure 4.7: Protein expression of glutamine utilizing enyzmes in glutamine fed and deprived conditions. LC-MS obtained label-free quantities of selected enzymes are shown for **A** *de novo* purine biosynthesis and **B** *de novo* for HCT116, RKO and HEK293 cells. Cells were cultivated for 24 hrs in standard cell culture media and subsequently either starved (0 mM) or fed upon glutamine (0.1 mM or 2 mM) for 2 weeks. Results represent mean + SD (n=3). Abbreviations – CPS2: CAD protein, CTPS1: CTP synthase 1, GMPS: GMP synthase, PFAS: Phosphoribosylformylglycinamidine synthase, PPAT: Amidophosphoribosyltransferase. For the complete metabolite names refer to the list of abbreviations

4.2.3 Nucleotide analysis in normal and glutamine deprived conditions

Nucleotide biosynthesis of purine or pyrimidine requires carbon and nitrogen. Therefore, several sources of carbon and nitrogen are used. Besides nitrogen that is released in form of free ammonia by different processes (e.g. protein degradation) or nitrogen from transaminase reactions a major nitrogen donor is the non-essential amino acid glutamine. It contributes either directly the amido (γ-nitrogen) or indirectly the amino (α-nitrogen) group via aminoacids originated from glutamine (e.g. aspartate) to *de novo* nucleotide biosynthesis (Deberardinis and Cheng (2010)).

To investigate changes in deoxy- and ribonucleotide levels upon 2 mM, 0.1 mM and 0 mM glutamine in the cell culture medium, direct infusion MS was employed. For the non-cancerous cell line HEK293 nucleotides were not decreased at 0.1 mM or deprived glutamine concentration compared to the 2 mM condition. Despite limited supply of glutamine, HEK293 cells displayed increased nucleotide levels, likewise cell growth is unaffected. In HCT116 cells nucleotide levels decreased in dependance of glutamine availability, as well as in RKO cells. In particular, in both, HCT116 and RKO cells nucleotides involved in the purine biosynthesis namely ATP, dATP, ADP, AMP, GDP, dGDP, GMP are decreased the most. In the *de novo* purine synthesis glutamine is contributing to three reactions, wherein glutamine's nitrogen is transaminased from three different enzymes (PPAT, PFAS, GMPS). This leads to the question, if one or all of these enzymes are the limiting factor in synthesizing enough purine nucleotides to proliferate in glutamine deprived medium.

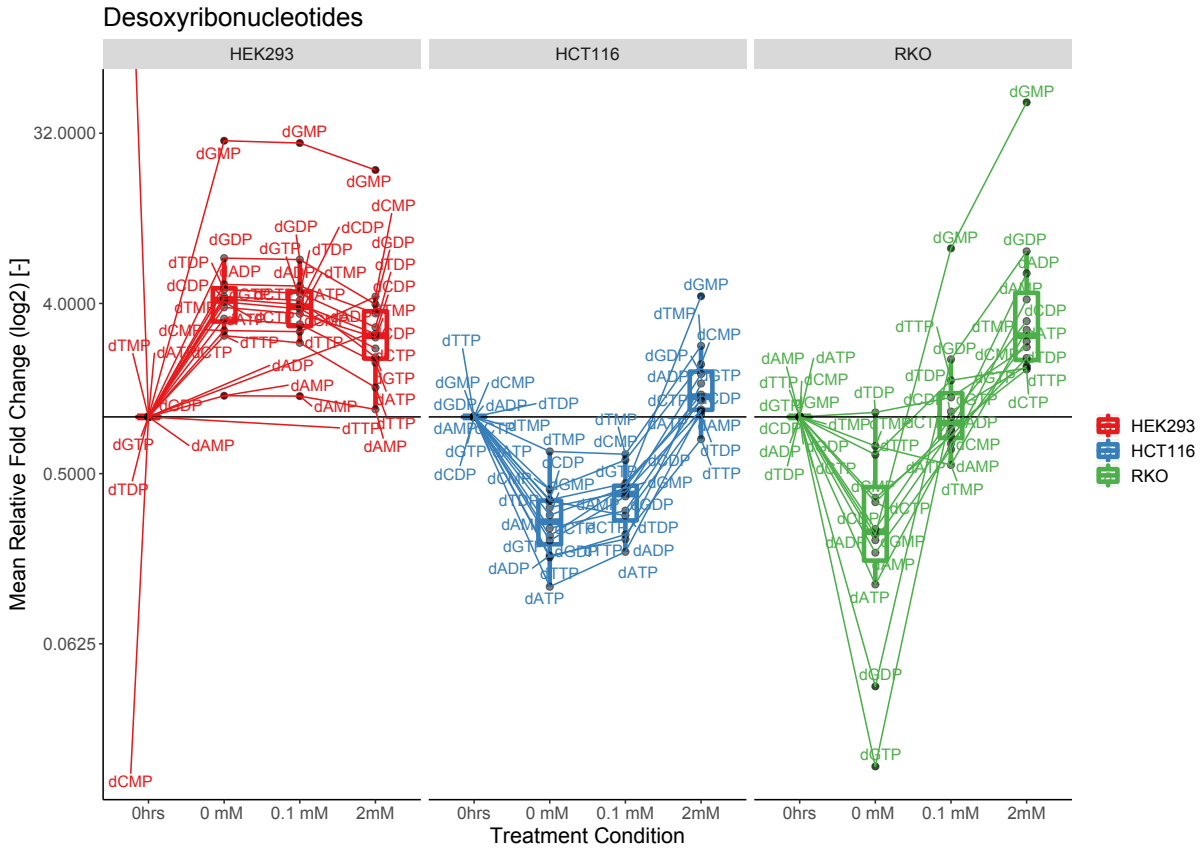

Figure 4.8: Effect of different glutamine concentrations on desoxynucleotide levels. Direct-infusion MS acquired relative fold change of deoxyribonucleotide levels are shown in response to two weeks of different glutamine concentration for HEK293, HCT116 and RKO cells. Cells were starved or treated with low (0.1 mM) or normal cell culture (2 mM) glutamine conditions for 2 weeks. Results representing the mean of three biological replicates. Each measurement was performed in technical triplicates.

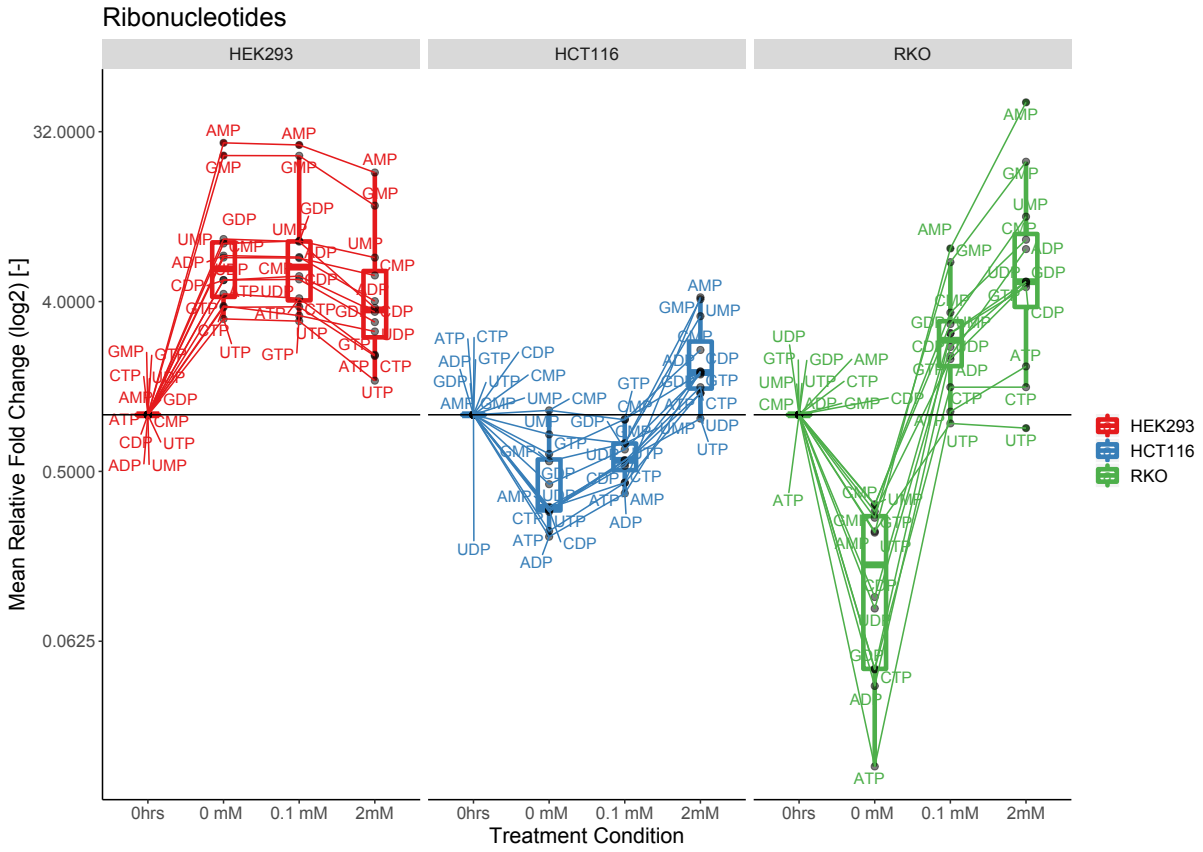

Figure 4.9: Effect of different glutamine concentrations on ribonucleotide levels. Direct-infusion MS acquired relative fold change of ribonucleotide levels are shown in response to two weeks of different glutamine concentration for HEK293, HCT116 and RKO cells. Cells were starved or treated with low (0.1 mM) or cell culture normal (2 mM) glutamine conditions for 2 weeks. Results representing the mean of three biological replicates. Each measurement was performed in technical triplicates.

4.3 HCT116 and HEK293 cells depends on glutamine in dialyzed FBS medium

Different theories exist in the literature regarding "glutamine addiction" in cancer cells. One of these is that MYC-driven cancer becomes dependent on glutamine as MYC induces upregulation of glutamine transporters (SLC1A5, SLC38A5) and the enzyme glutaminase (Altman et al. (2016)). Consequently, glutamine metabolism is elevated. However, Dejure et al. (2017) could demonstrate that glutamine deprivation in colon cancer cell lines did not result in a high degree of apoptosis. Rather, glutamine withdrawal induced a cell cycle arrest, which was fully reversible by glutamine re-addition (Dejure et al. (2017)). They concluded that the human colon carcinoma HCT116 cells are not addicted to glutamine as expected for MYC-driven tumor cells. Based on this statement and the outcome of an initial glutamine starvation assay, where HCT116 and RKO cells arrested (data not shown), the experiment's cell culture system was to be scrutinized. According to the literature, standard cultivation conditions comprise DMEM, FBS, glucose and glutamine. However, under these conditions, glutamine depletion was insufficient to suppress cell growth in the non-cancerous HEK293 cells, while the "glutamine-dependent" cell line HCT116 survived and RKO cells showed a stronger suppressed cell growth. Investigations performed by Yasmin Razzaque (Master student in the Kempa-Lab, BIMSB/MDC, Berlin-Germany) on FBS revealed that the serum contains a mix of undefined nutrients including several amino acids, which led to the hypothesis that the normal fetal bovine serum contains residual glutamine or other small molecules that promote this apparent glutamine independence and enable HCT116 and HEK293 cells to survive in glutamine withdrawal (Razzaque (2021)).

4.3.1 Dialyzed FBS prevents proliferation in HCT116 and HEK293 cells

To verify the presence of residues in FBS medium that might compensate for glutamine absence, the initial proliferation assay was repeated, but with 10 % dialyzed FBS instead of 10 % standard FBS. 2.0 e+6 cells cells were seeded for 24 h with dialyzed FBS-supplemented medium containing 2 mM glutamine. Afterwards medium was exchanged with dialyzed FBS cell culture medium containing 2 mM or 0 mM glutamine. Cells were split at a confluency of 70-80 % and counted via cell counter. If splitting was not possible, only medium was changed to sustain a sufficient supply of nutrients. Proliferation was determined at day 4 and 7. Except for 0 mM glutamine in HCT116 cells. Here, cell count was only detectable for 0 h and day 7. Determination after day 7 was not possible due to too few cells left, which were not countable anymore. All three cell lines showed a decreasing cell number, when glutamine was depleted from the medium. Upon supplementation of the dialyzed cell culture medium with 2 mM glutamine cell numbers were comparable to normal FBS medium. This showed that HEK293 cells were partially glutamine auxotroph and HCT116 and RKO cells glutamine addicted in dialyzed FBS medium (Bayram et al. (2022)). At the same time, these findings confirmed the assumption that cell growth is ensured due to either glutamine residuals or other small molecules in the normal FBS medium when glutamine is deprived (Bayram et al. (2022)).

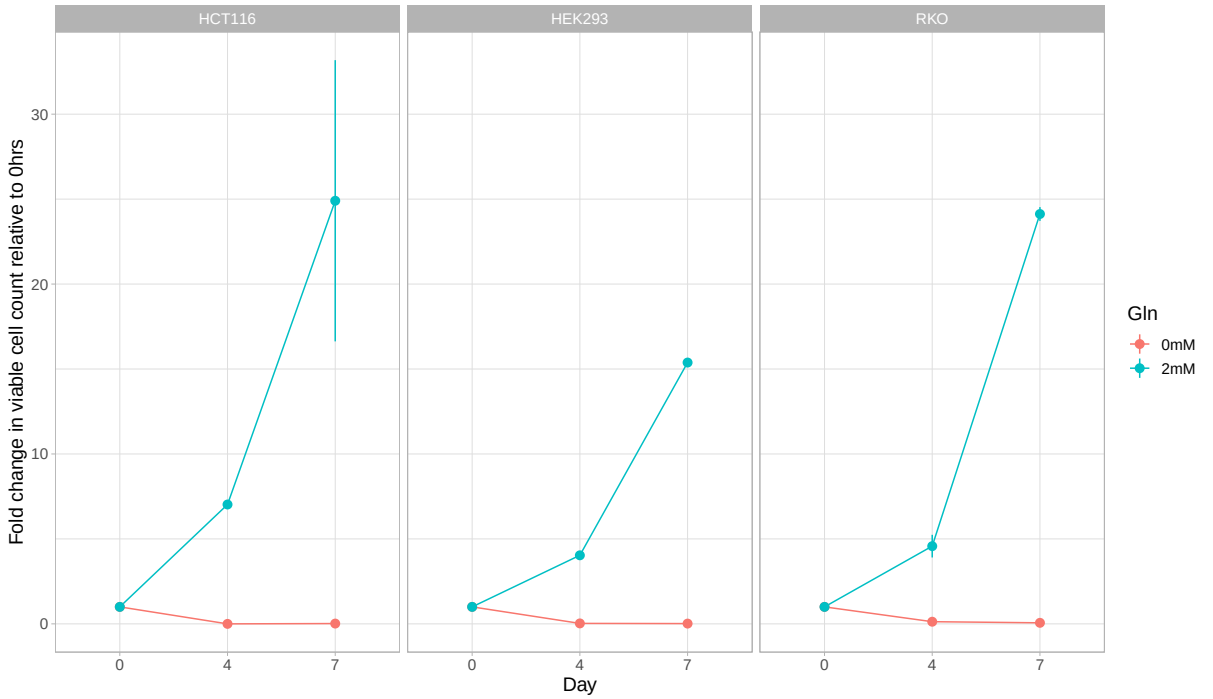

Figure 4.10: Proliferation upon glutamine starvation in dialyzed FBS. Cell proliferation upon glutamine starvation in dialyzed FBS medium in indicated cell lines. Cells were starved for seven days. Cell number was normalized to 0 hrs. Results represent mean ± SD (n=3, each measurement was performed in technical duplicates). Data were published in fig. 2 in (Bayram et al. (2022)).

4.3.2 Supplementation of dialyzed FBS medium

Two previously performed proliferation experiments in standard FBS- supplemented medium first showed an apparent glutamine-addiction for both colon cancer cell lines HCT116 and RKO (see fig. 4.4). In case of a long-term glutamine withdrawal HCT116 cells adapted to this condition and survived, whereas RKO could not adapt and stopped proliferation (see Fig.4.5). The non-cancerous HEK293 cells remained unaffected. Nonetheless, a repetition of the growth experiment in dialyzed FBS medium emphasized the dependency on glutamine for all three tested cell lines. To investigate, if substrates of glutamine's transaminase network can fuel cell growth and in order to identify which metabolic pathways are utilised in cell culture medium with dialyzed FBS and glutamine-depleted conditions a supplemented proliferation assay was performed. Therefore, transaminase substrates that are components of human blood and are associated in local network with glutamine were chosen. Finally, alanine, asparagine, aspartate and glutamate were supplemented individually or in combination with ammonium (see fig.4.11 for detailed composition), which can contribute to synthesize glutamine or is a decomposition product of glutamine. Concentration were chosen based on Human Metabolome Database.

Medium	Supplementation
DMEM + Glc (2.5 g/ L) + dia. FBS (10 %)	+/- Gln (2 mM) +/- Asn (1 mM) +/- Ala (1 mM) +/- Ala (1 mM) + NH_4^+ (0.8 mM) +/- Asp (1 mM) +/- Asp (1 mM) + NH_4^+ (0.8 mM) +/- Glu (1 mM) +/- Glu (1 mM) + NH_4^+ (0.8 mM) +/- NH_4^+ (0.8 mM)

Figure 4.11: Cell Culture media compositions for cell growth assays.

The experiment was assisted by Yasmin Razzaque (Master student in the Kempa-Lab, BIMSB/MDC, Berlin-Germany) under my supervision. For the cell growth assays, all tested cell lines were pre-cultivated and seeded at 2 e+6 cells in 10 cm plates in dialyzed FBS medium containing 2 mM glutamine. The following day, cell count was determined via a cell counter (TC20TM automated, Bio-Rad) and medium was changed to the appropriate supplement condition. Cells were splitted at a confluency of at least 60 %. Thereby, cell count was determined at every passage for at least one month. Each passage was considered as biological replicate. To avoid nutrient limitation medium was replaced every 2-3 days. To account for experimental cell growth cell counts were log transformed and graphically represented (fig. 4.12). A detailed presentation of the results is attached in the supplements (fig. 7.6).

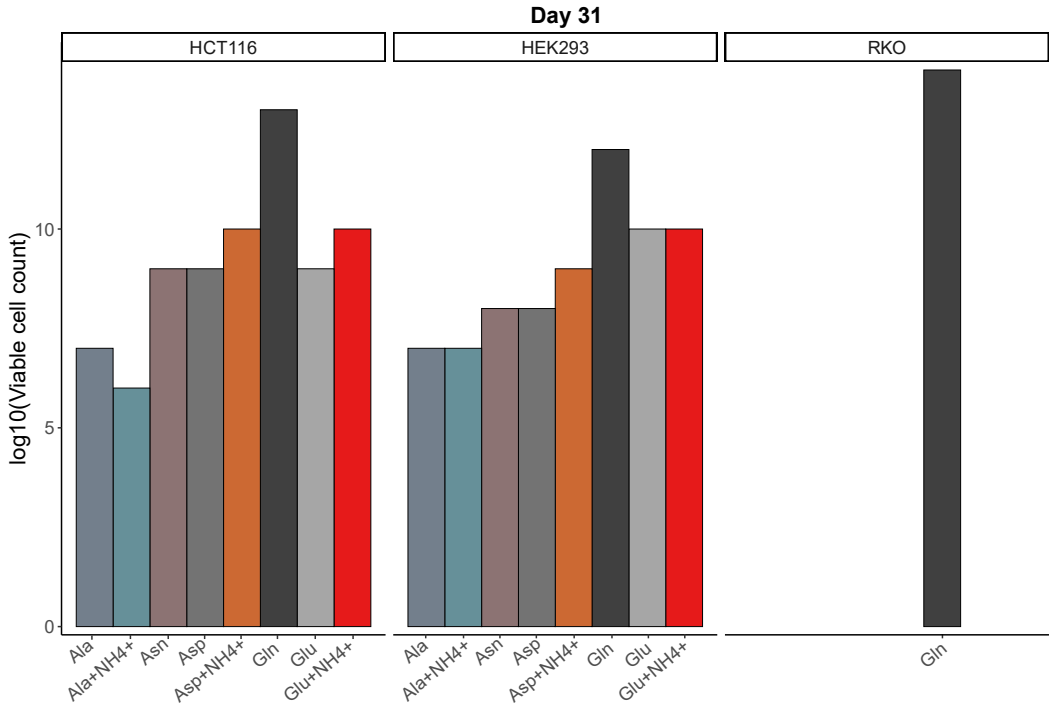

Figure 4.12: Cell Culture media compositions for cell growth assays. Cell proliferation upon the application of various amino acid substrates in dialyzed FBS medium in indicated cell lines. Day 31 is represented graphically. Viable cell count was determined at every passage over one month. Cell count data were Log transformed. Data were published in figure 3 in Bayram et al. (2022).

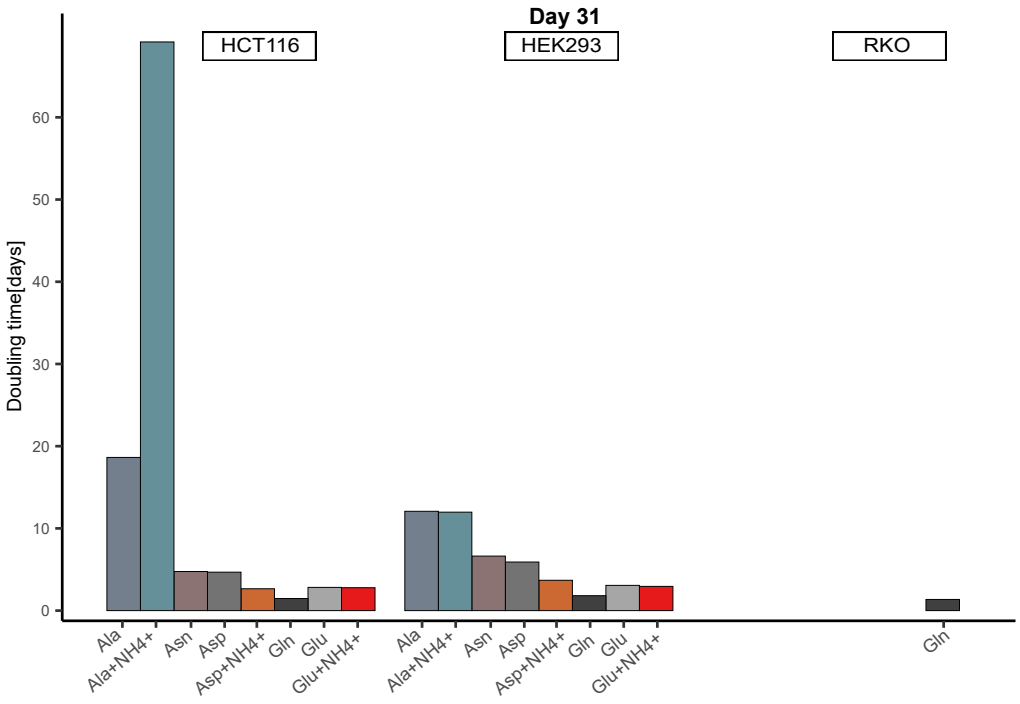

Figure 4.13: Doublingtime. The doubling time was calculated based on the duration in culture and the number of duplications underwent during this time. Data were published in figure 3 in Bayram et al. (2022)

HEK293 cells exhibit the highest proliferation rate in Gln-supplemented medium. Followed by Glu and Glu + NH_4^+, with the doubling time being just 1.6 times higher. For Asp + NH_4^+ and Asp-supplemented media cell proliferation is also observable, whereby Asp with ammonium shows nearly a twofold and without ammonium a threefold higher doubling time compared to gln. Similar to Asp is Asn with a doubling time of 6.63 and thus threefold higher than gln. The lowest proliferation rate as well the highest doubling time are in Ala and Ala + NH_4^+-supplemented medium. It is sixfold higher compared to Gln-supplemented medium. HCT116 cells exhibit the highest proliferation rate in Gln-supplemented medium and the lowest in Ala + NH_4^+-supplemented medium. The second highest proliferation rate is achieved in both Glu + NH_4^+- and Asp + NH_4^+-supplemented media, with the doubling times both being 1.5 times higher than that in Gln-supplemented medium. The corresponding amino acids without ammonium supplementation exhibit lower cell counts, whereas the proliferation rate for Asp is slower compared to Glu. They are 3.1 fold slower for Asp and 1.9 fold slower for Glu. A clear distinction is shown for Alanine, especially with additional ammonium. Here, the doubling time is 69.1 days. In case of Alanine alone the proliferation rate is 18 times slower compared to Gln. Interestingly, RKO cells were able to grow only in glutamine supplemented medium. In the remaining conditions after approximately two weeks RKO cells stopped growing and detached from the plate. Therefore, it was not possible to obtain viable cell count data. In consequence, the proliferation rate of Ala-, Ala + NH_4^+-, Asn-, Asp-, Asp + NH_4^+-, Glu-, Glu + NH_4^+-+-supplemented cell culture media was 0.

Together these results provide important insight into compensating glutamine withdrawal in dialyzed medium to ensure cell proliferation . It emphasizes the assumption that HCT116 cells are sensitive to glutamine depletion whereas RKO are auxotrophic cells that rely on glutamine

only (Bayram et al. (2022)). HCT116 and HEK293 cells prefer Glu + NH_4^+-+-supplemented media in glutamine depleted conditions. One interesting factor is that Glu + NH_4^+ both are relevant substrates for the glutamine-synthesizing enzyme GLUL. A performed proteome analysis revealed increased GLUL expression upon glutamine starvation in HCT116 and HEK293 cells (see fig.4.7). Latterone showed a more significant increase and led to the assumption of glutamine independent cell growth in HEK293 cells. Taken together: Both results strengthen the suspicion that GLUL is the decisive difference regarding RKO cells. This led to the question whether GLUL plays a key role as a survival factor in cellular adaptation to glutamine depletion. Therefore, further experiments were performed with the aim to assess GLUL's role upon glutamine starvation.

4.4 Self-sufficient glutamine production in HCT116 and HEK293 cells

Based on the presented results, the enyzme GLUL was examined as possible survival factor that enables self-sufficient glutamine production in glutamine depleted conditions in HCT116 and HEK293. The investigation should also cover the effect of the GLUL inhibitor Methionine-Sulfoximine (MSO) on synthesizing glutamine and consequently the restricted nitrogen flow to nucleotide biosynthesis.

4.4.1 Glutamine synthesis by the enzyme GLUL

The amino acid glutamine can be synthesized by GLUL-mediated ligation of glutamate and ammonium, with ammonium providing the amido-group. The performed cell growth assays with different supplementation substrates for glutamine's transaminase network showed that in glutamine-depleted dialyzed FBS conditions, HEK293 and HCT116 cells proliferate best when supplemented with the substrates of the enzyme GLUL: Glu + NH_4^+ (see fig.4.12 and fig.7.6). To investigate GLUL's role upon glutamine starvation in dialyzed FBS an inhibitor assay was performed to assess the effect of blocking ***de novo*** glutamine synthesis. The experiment was assisted by Yasmin Razzaque (Master student in the Kempa-Lab, BIMSB/MDC, Berlin-Germany) under my supervision. HCT116 and HEK293 cells were cultivated in Glu + NH_4^+-supplemented dialyzed medium to trace nitrogen and carbon. Subsequently, cells were treated with MSO, which is a competitive inhibitor of GLUL. In order to evaluate the effect of GLUL inhibition on cell growth cell proliferation was monitored every 24 hrs for in total 96 hrs. The cell culture medium was renewed every 24 hrs to sustain a sufficient supply of nutrients. To analyze the simultaneous incorporation of extracellular ^{13}C and ^{15}N within cellular metabolic intermediates and in order to determine metabolic dynamics, especially at nucleotide level, an isotope tracing technique using ultra high-resolution mass spectrometry (SIRM) was designed in the group Kempa. RKO cells are unable to proliferate in glutamine-depleted conditions, they were not subjected to this assay. Each conduction was performed with three biological replicates.

4.4.2 Effects of GLUL inhibition on cell growth

MSO was applied to validate the activity of GLUL to synthesize *de novo* glutamine and the effect of GLUL-inhibition. Initially a pilot assay was performed to calculate IC50 of MSO in HEK293 cells (data shown). Based on these results HCT116 and HEK293 cells were exposed to 500 µg/ 10 mL of the inhibitor MSO. In parallel sterile water was used as control for each cell line. Cell culture medium containing the inhibitor or the solvent control were refreshed daily. Cell count and viability was determined every 24 hours over a 96 hour time period. Each measurement was taken for three biological replicates. The mean and standard deviation of the viable cell counts for each time point were graphically represented in fig.4.14. In the control without MSO-treatment HCT116 cells exhibited similar proliferation rates to those observed in the supplemented cell growth assay (compare fig.7.6). Again HCT116 cells showed highest proliferation rate in Glu + NH_4^+-supplemented medium. In MSO-treated HCT116 cells constant increase of viable cell count was only observable in Gln-supplemented medium. After 72 hours cellular proliferation slowed down and plateaued (Bayram et al. (2022)). In the

conditions with Asn-, Ala-, Ala+NH_4^+-, Asp-, Asp+NH_4^+-, Glu and Glu+NH_4^+-supplemented media with MSO-treatment HCT116 cells decreased viable cell count from 0 hours on. Similar to the colon cancer cell line in HEK293 cells growth rates were alike to the supplementation experiment in the control (7.6). In MSO-treated HEK293 cells proliferation took place only in Gln-supplemented medium. In Glu+NH_4^+-supplemented media a slight increase in cell count was observable for 48 h before decreasing. These findings supported the hypothesis that the enzyme GLUL plays a key role to sustain cell growth in adaptation to glutamine depletion.

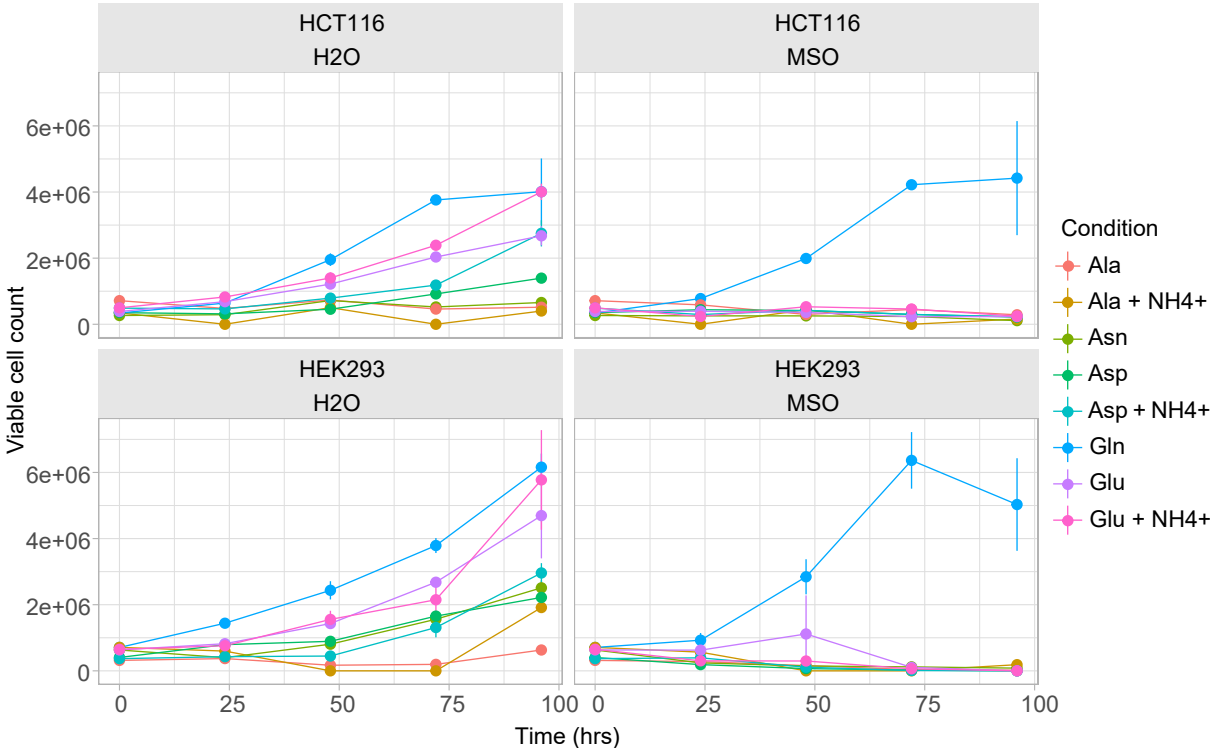

Figure 4.14: Proliferation in untreated and MSO-treated HCT116, RKO and HEK293 cells. Cell proliferation upon MSO treatmeant in the indicated cell lines. Cells were treated for 96 hrs. Cell number was normalized to 0 hrs. Results represent mean ± SD (n=3, each measurement performed in technical duplicates). Data were published in figure 4 in Bayram et al. (2022).

4.4.3 GC-MS analysis of synthesized glutamine during MSO treatment

Based on the results of section 4.4.2 a dual-tracer and targeted Stable Isotope Resolved Metabolomics (SIRM) method was established in order to demonstrate GLUL activity and to determine the metabolic fate of GLUL's substrates (Bayram et al. (2022)). Hence, to monitor the specific biological reaction of GLUL ^{13}C-Glutamate and ^{15}N-ammonium were used and via high resolution mass spectrometry relative contribution of isotopes to intracellular glutamine synthesis and ***de novo*** nucleotide biosynthesis were detected (4.15) (Bayram et al. (2022)).

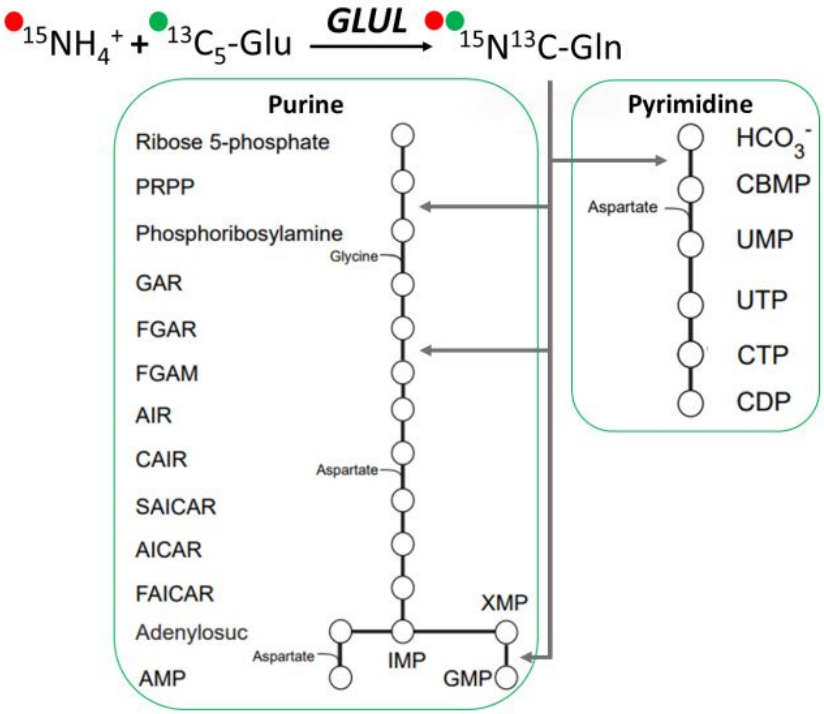

Figure 4.15: Glutamine synthesis via GLUL using ^{15}N-NH$^4_+$ and ^{13}C-Glutamate. Biological reaction of glutamine synthesis by the enzyme GLUL using applied ^{15}N-NH$^4_+$ and ^{13}C-Glutamate. Grey line shows nitrogen donation of newly synthesized glutamine to purine and pyrimidine nucleotide pathway.

HCT116 and HEK293 cells were labelled with ^{13}C and ^{15}N for 24 h. To monitor the ligation of carbon and nitrogen to glutamine $^{13}C_5$-, $^{14}N_1$-, and $^{13}C_5$- $^{15}N_1$-glutamine isotopologues were detected via GC-MS. Tracefinder (Thermo Fisher) was used for automated peak extraction from GC-MS spectra. To calculate mean ^{13}C and ^{15}N enrichment a custom R script was used (Bayram et al. (2022)). For the incorporation into glutamine several characteristic glutamine-3TBDMS fragments were detected, which were indicated by the corresponding ^{13}C and ^{15}N-induced mass shift of the peaks. While fragments of Glutamine-3TBDMS comprising a 5C skeleton and 2N atoms, underwent a mass shift of approximately 6 Da (m+6), fragments comprising a 4C skeleton and 2N atoms underwent a mass shift of 5 Da (m+5), corresponding to $^{13}C_5$-$^{15}N_1$ and $^{13}C_4$-$^{15}N_1$ isotopologues, respectively (Bayram et al. (2022)). As the 5C and 2N fragment 431 m/z showed the cleanest signal it was used for further analysis (Bayram et al. (2022)). In HCT116 cells 87 % enrichment of ^{13}C and 22 % enrichment of ^{15}N in the glutamine-3TBDMS fragment was monitored, whereas for HEK293 cells 51 % enrichment of ^{13}C and 2 % enrichment of ^{15}N was detectable. In both cell lines neither ^{13}C nor ^{15}N incorporating was observable in MSO-treated conditions. RKO cells did not show *de novo* glutamine synthesis. No ^{13}C or ^{15}N enrichment was monitored in untreated and MSO-treated conditions (fig.4.16), albeit the protein could be detected in the proteomic and western blot analyses (4.19).

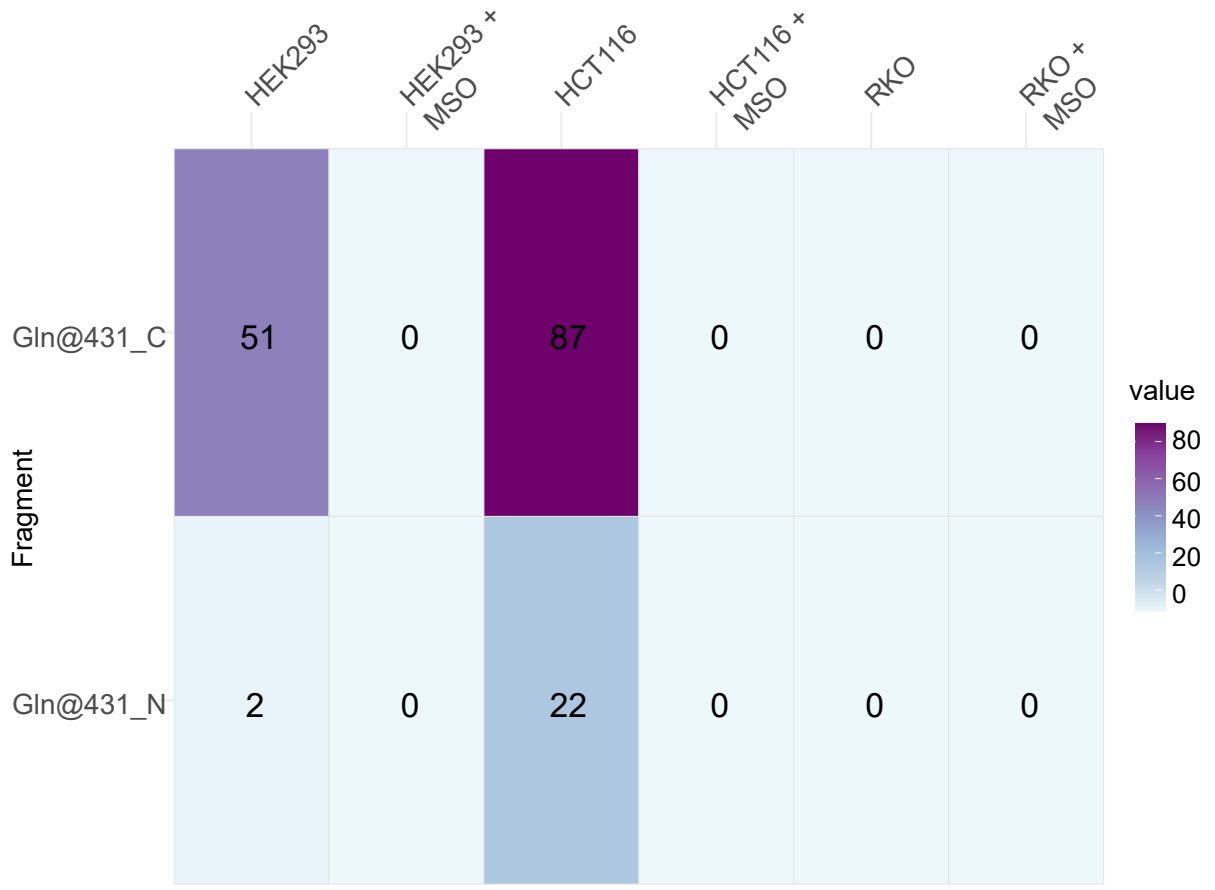

Figure 4.16: Mean ^{13}C and ^{15}N in untreated and MSO-treated cells. Mean ^{13}C and ^{15}N in glutamine in untreated and MSO-treated HCT116, RKO and HEK293 cells. Cells were cultivated with $^{13}C_5$-glutamate and ^{15}N-ammonium for 24 h. After obtaining mass spectra, peak areas were extracted and natural isotope abundance correction and isotope enrichment calculations were performed. Data were published in figure 5 in Bayram et al. (2022).

4.4.4 Direct infusion MS for nucleotide analysis during MSO treatment

To monitor $^{13}C_5$-glutamate and ^{15}N-ammonium contribution of newly synthesized glutamine isotopologues to nucleotide biosynthesis direct-infusion MS was used to detect nucleotide isotopologues. XCalibur Qualbrowser (Thermo Fisher) was used manually for peak extraction from direct infusion-MS spectra (Bayram et al. (2022)). As obligate nitrogen donor glutamine donates two nitrogen atoms to IMP and AMP, and three nitrogen atoms to GMP in the ***de novo*** purine biosynthesis pathway (Bayram et al. (2022)). Hence, the fractional enrichment of nucleotide isotopologues was measured containing up to two ^{15}N atoms (N0, N1 and N2) for IMP and AMP and three ^{15}N atoms (N3) for GMP. In HCT116 and HEK293 cells ^{15}N enrichment in AMP/dGMP and GMP is observable. Both cells have one ^{15}N atom (N1) incorporated into each AMP/dGMP and GMP. Thereby, HCT116 cells have approximately 20 % enrichment of $^{15}N_1$ in AMP/ dGMP and 20 % enrichment in GMP, while HEK293 cells demonstrate 30 % enrichment of $^{15}N_1$ in AMP/ dGMP and 15 % in GMP. Enrichment of ^{15}N nucleotide isotopologues containing two or three ^{15}N atoms (N3) was insignificantly increased for HCT116 as well as HEK293 cells. RKO cells do not demonstrate ^{15}N enrichment of nucleotide isotopologue in AMP and GMP (fig.4.17).

Taken together the outcomes of the GC-MS and direct-infusion MS emphasize the assumption, that GLUL is a survival factor in cellular adaptation to glutamine depletion in HCT116 and HEK293 cells, if substrates are available.

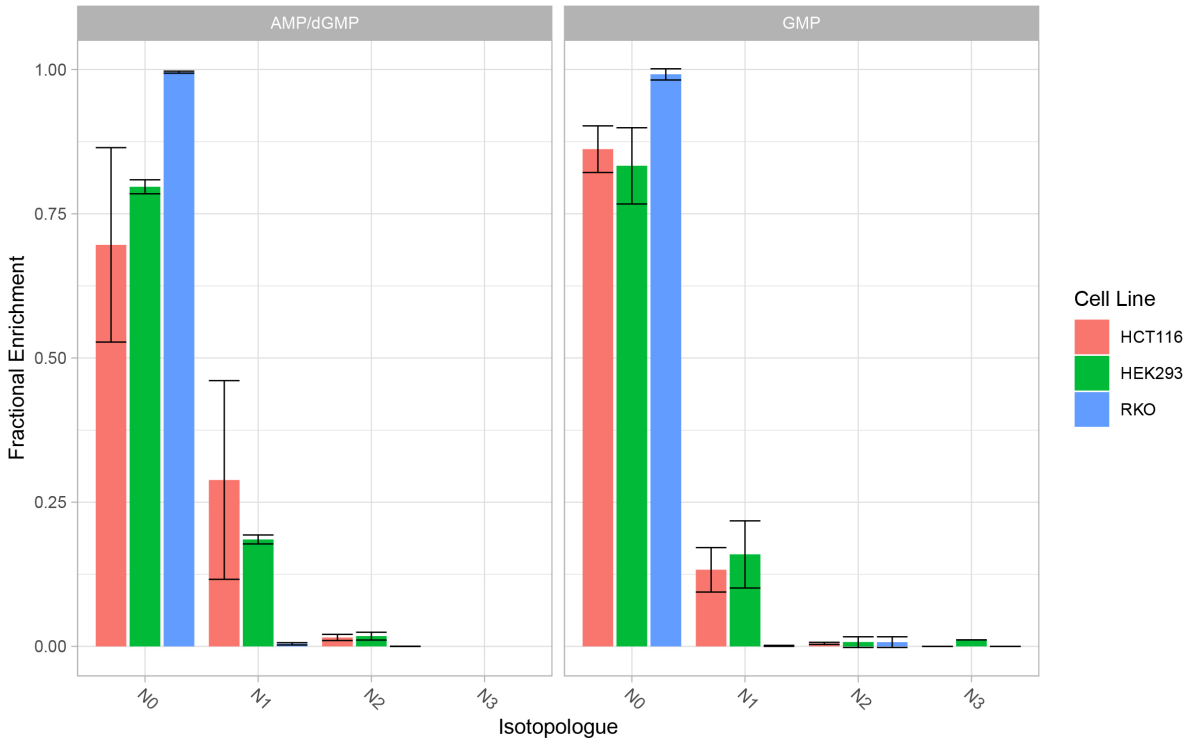

Figure 4.17: ^{15}N Enrichment in AMP/GMP. ^{15}N Enrichment in AMP/GMP in purine nucleotides in HEK293, HCT116 and RKO cells. Cells were cultivated with $^{13}C_5$-glutamate and ^{15}N-ammonium for 24 h. Nucleotide isotopologues were measured via direct-infusion MS and relative quantities are graphically represented. Data represent mean ± SD of three biological replicates. Data were published in figure 6 in Bayram et al. (2022).

4.4.5 Dynamics of glutamine synthesis

A time course experiment by using dual-isotope tracing was performed to analyze the dynamics of glutamine synthesis in HCT116 and HEK293 cells (Bayram et al. (2022)). This work was done in collaboration with Dr. Sabrina Geisberger (Research scientist in the Kempa-Lab, BIMSB/MDC, Berlin-Germany). The tested cell lines were incubated for 15 min, 30 min, 1 h and 3 h with ^{13}C-glutamate and ^{15}N-ammonium. Glutamine label incorporation was analyzed as described above (section 4.4.3). Already after 15 min of labeling incorporation in glutamine was detectable in HCT116 cells and after 30 min in HEK293 cells (Bayram et al. (2022)). Both cell lines showed a fast glutamine synthesis with different kinetics. In HCT116 cells the incorporation of ^{15}N-ammonium into glutamine exceeded the formation of carbon and nitrogen labeled glutamine. Therefore, HCT116 cells have faster ammonium import compared to HEK293 cells (Bayram et al. (2022)).

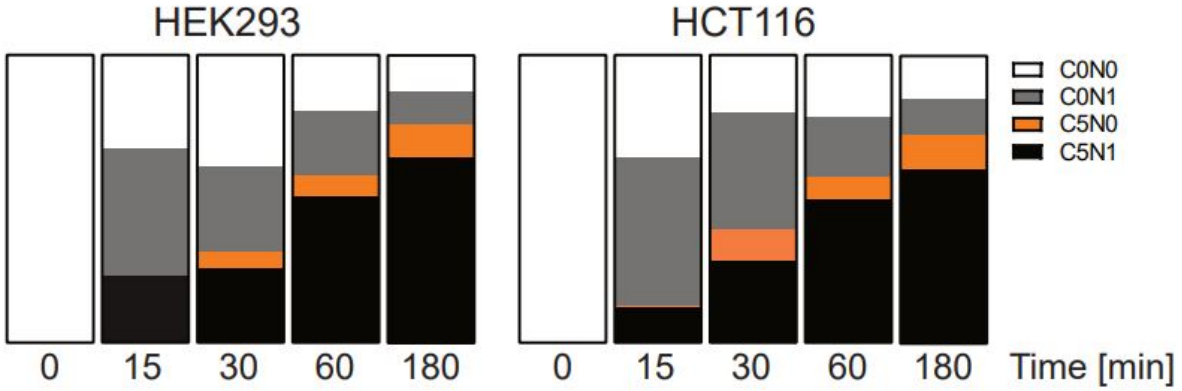

Figure 4.18: Isotope incorporation of $^{13}C_5$-glutamate and ^{15}N-ammonium into Glutamine. Isotope incorporation into glutamine after pulse labelling with $^{13}C_5$-glutamate and ^{15}N-ammonium in HCT116 and HEK293 cells. HCT116 and HEK293 cells were incubated with $^{13}C_5$-glutamate and ^{15}N-ammonium for 15 min, 30 min, 1 h, and 3 h (n = 2 each). Shown are the relative pool sizes of non-labelled (C0N0), ^{15}N labelled (C0N1), $^{13}C_5$ labelled (C5N0) 15N-$^{13}C_5$ labelled (C5N1) glutamine. Data were published in figure 7 in Bayram et al. (2022).

GLUL protein expression via immunoblotting

Considering the results of the above mentioned experiments, particularly in case of RKO cells and the low to no recovery in different medium-supplemented conditions due to glutamine starvation, a western blot analysis was performed to analyze GLUL protein expression in HCT116, RKO and HEK293 cells. In all tested cell lines GLUL protein was present even under normal conditions (Bayram et al. (2022)). Consequently, the reason for the lacking GLUL activity in RKO cells can not be explained by missing GLUL protein levels and must be caused by other factors. The experiment was performed by Carolina Vechiatto (Master student in the Kempa-Lab, BIMSB/MDC, Berlin-Germany).

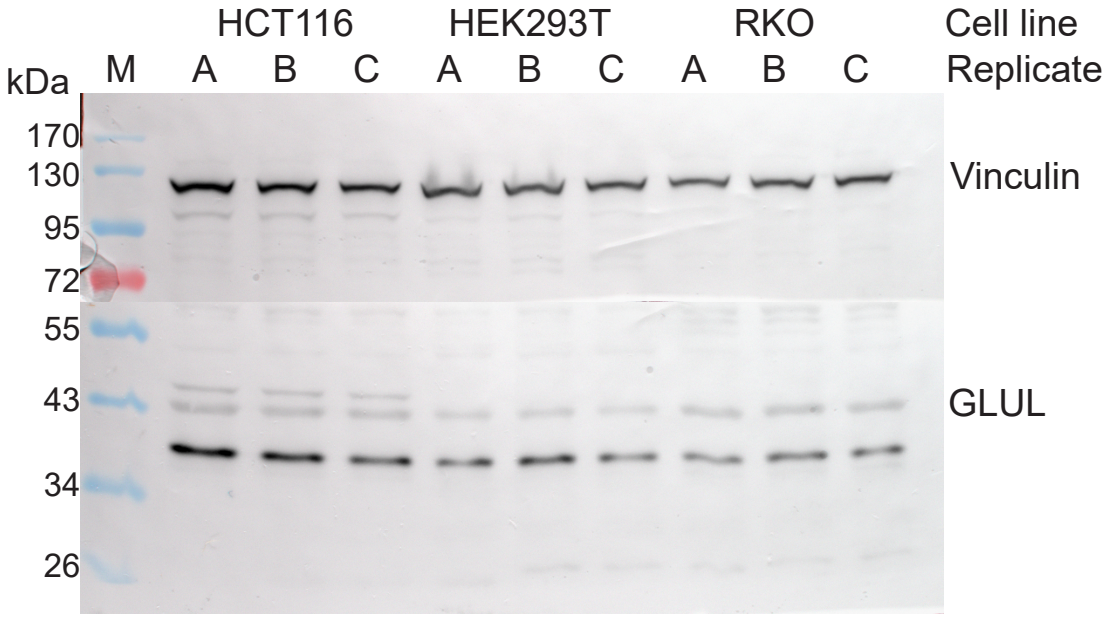

Figure 4.19: GLUL protein expression under normal conditions in HCT116, HEK293 and RKO cells. The representative immunoblot documents GLUL and Vinculin levels under the described condition in the indicated cell lines with in total 3 BR. Abbreviations M: Marker.

4.5 The targets of the glutamine-analogue DON

DON is produced by an undefined Streptomycin strain and is a structural analogue of glutamine (Ahluwalia et al. (1990)). It was evaluated to have potent anti-tumor activity *in vitro* and *in vivo* and has been officially discussed as an inhibitor of glutaminases (Cervantes-Madrid et al. (2015),Lemberg et al. (2018)). Among glutaminases it binds all glutamine-converting enzymes, e.g. ASNS, PPAT and PFAS (Pinkus (1977)). Nevertheless, the targets of DON are not entirely known. An imbalance in nucleotide pools due e.g. drug treatments prevents cell proliferation (Camici et al. (2019),Messina et al. (2004)). Both enzymes, PPAT and PFAS, are involved in purine biosynthesis and are possible DON targets, which should be explored below.

4.5.1 DON treatment affecting nucleotide pools

Royla (2018) and Bayram (2018) revealed in a proliferation inhibition assay pronounced cell growth arrest in HCT116, RKO and HEK293 cells. The pSIRM experiment with applied ^{13}C-glutamine and DON showed no reduction of carbon-13 flow for all tested cell lines (Royla (2018), Bayram (2018)). These results lead to the hypothesis that DON is affecting the flow of nitrogen into the *de novo* nucleotide biosynthesis pathway as glutamine plays a vital role in purine and pyrimidine synthesis (Cory and Cory (2006)). To investigate this assumption HCT116 and HEK293 cells were cultivated in standard DMEM media containing 10 % FBS and 0 mM or 2 mM glutamine for two weeks. Afterwards a pSIRM study with different time points (0 h, 2 h, 8 h and 24 h) of 2 mM DON treatment were set up.

The nucleotide analysis revealed an accumulation of PRPP and a decrease in AICAR and SAICAR. We assumed that PPAT or PFAS, which are amidotransferases and uses glutamine, could be a target of DON. RKO cells did not survive glutamine starvation and could not be tested.

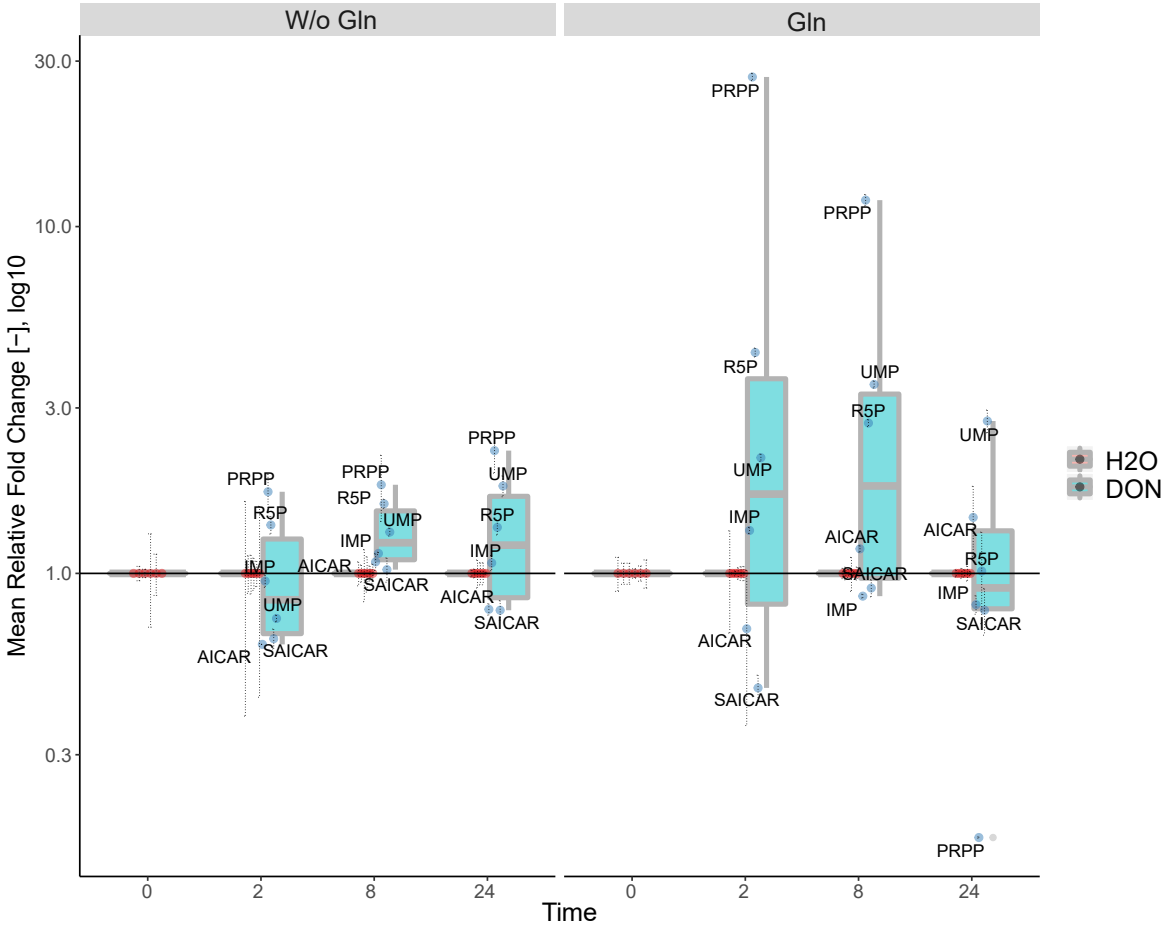

Figure 4.20: Nucleotide precursors in HCT116 cells. Nucleotide precursors. HCT116 cells after two weeks starvation or normal conditions and subsequently DON treatment for 2 h, 8 h and 24 h.

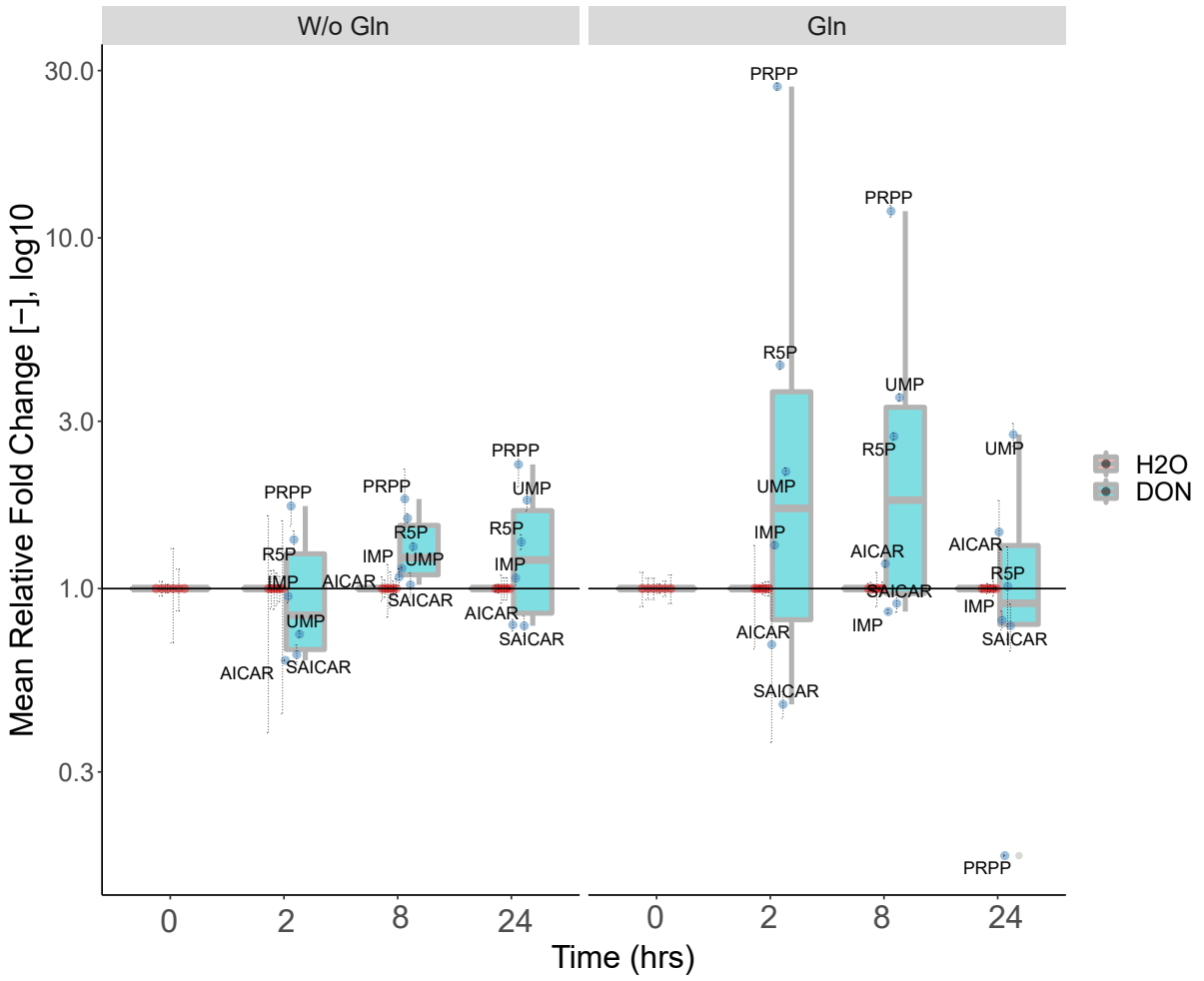

Figure 4.21: Nucleotide precursors in HEK293 cells. Nucleotide precursors. HEK293 cells after two weeks starvation or normal conditions and subsequently DON treatment for 2 h, 8 h and 24 h.

Purine and pyrimidine nucleotide synthesis originates from R5P. For the synthesis of purine nucleotides the intermediates PRPP, 5-PRA, GAR, FGAR, FGAM, AIR, CAIR, SAICAR, AICAR, FAICAR and IMP are required. Thereby, glutamine donates its amido group by producing 5-PRA and FGAM. A protocol was developed to measure those (Rayman (2022)). Therefore, the previously performed nucleotide analysis for quantification in the section before (4.5.1) was repeated with an addition time point. To determine the pool size of each intermediate and nucleotide the isotope intensities for each compound per condition were summed up. In fig. 4.22 compared pool sizes of intermediates involved in the purine biosynthesis are displayed (Rayman (2022)). After 6 h of DON-treatment pool sizes were primarily larger compared to those treated with PBS. At 24 h this was inverted and DON-treated samples showed less intensities than to PBS-treated samples.

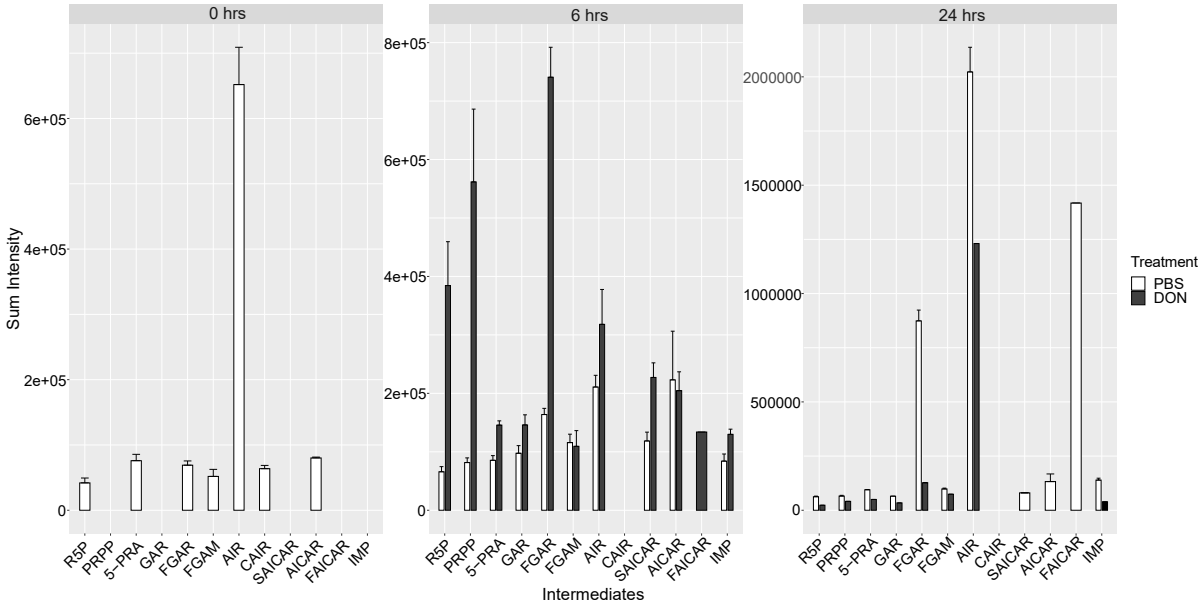

Figure 4.22: Sum intensities of intermediates of HCT116 cells. Sum intensities of intermediates of DON-treated- and PBS-treated-HCT116 cells at 0 h, 6 h and 24 h (Rayman (2022)).

In addition to the intermediates the sum intensities of purine and pyrimidine nucleotides were also measured (Rayman (2022)). Unlike to the intermediates most of the nucleotide intensities were greater in PBS-treated samples at both time points. At 6 h CMP, UMP, UDP and UTP and at 24 h UDP and UTP intensities were higher in DON-treated cells compared to the PBS treated cells.

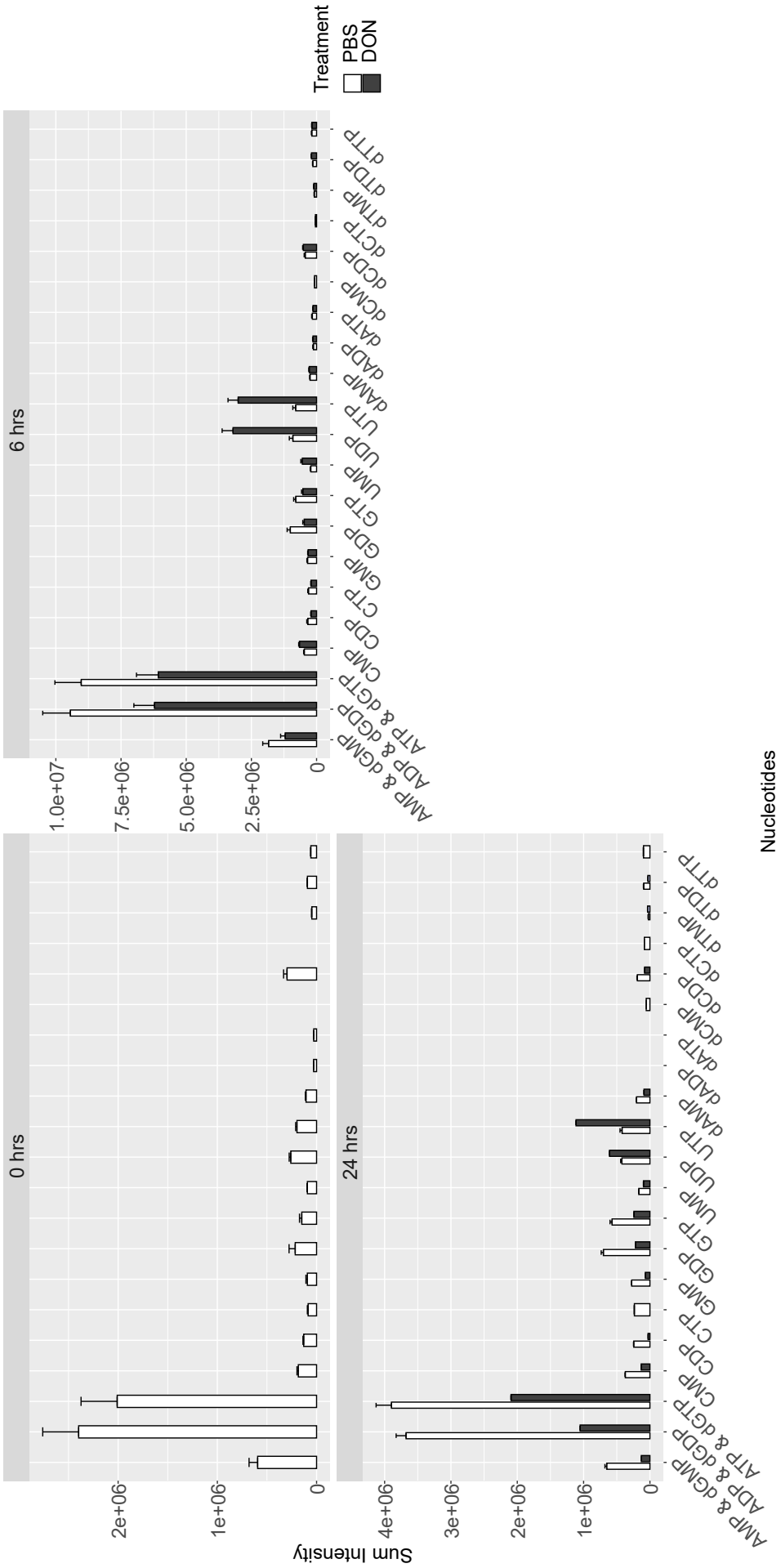

Figure 4.23: Sum intensities of nucleotides of HCT116 cells. Sum intensities of nucleotides of DON-treated- and PBS-treated-HCT116 cells at 0 h, 6 h and 24 h (Rayman (2022)).

4.5.2 Advanced usage of pSIRM to identify DON targets

To study the assumption that DON interrupts glutamine's nitrogen flow in the purine nucleotide biosynthesis due targeting transaminases a new technique was necessary to design. This new approach connects pSIRM with applied inhibitor and parallel dynamic tracing of labelled nitrogen. Furthermore, an extension of detection of nucleotide precursors was required to assess DON impact. Finally, a customized analysis protocol was needed. These tasks were carried out in cooperative work with Dr. Martin Forbes (Research scientist in the Kempa-Lab, BIMSB/MDC, Berlin-Germany) and Liam Rayman (Master student in the Kempa-Lab, BIMSB/MDC, Berlin-Germany). A pSIRM study with different time points of 2 mM DON treatment and 2 mM ^{15}N labelled glutamine was performed. In total four conditions and DON treatment were set up (4.24): (i) Cells were simultaneously treated with DON and labelled glutamine for 24 hours, (ii) Cells were simultaneously treated with DON and labelled glutamine for 6 hours, (iii) Cells were first treated with DON for 6 hours, before ^{15}N-glutamine being added after 2 hours for 4 hours labelling and (iv) Cells were first treated with DON for 6 hours, before ^{15}N-glutamine being added after 5 hours for 1 hour labelling. For each condition PBS was tested as control instead of DON. Furthermore, 2 counting plates were added for each condition and 3 untreated and unlabelled plates to allow for natural abundance determination. The experiment was performed by Liam Rayman (Master student in the Kempa Lab, BIMSB/MDC, Berlin-Germany) under the co-supervision of Dr. Martin Forbes and I (Rayman (2022)).

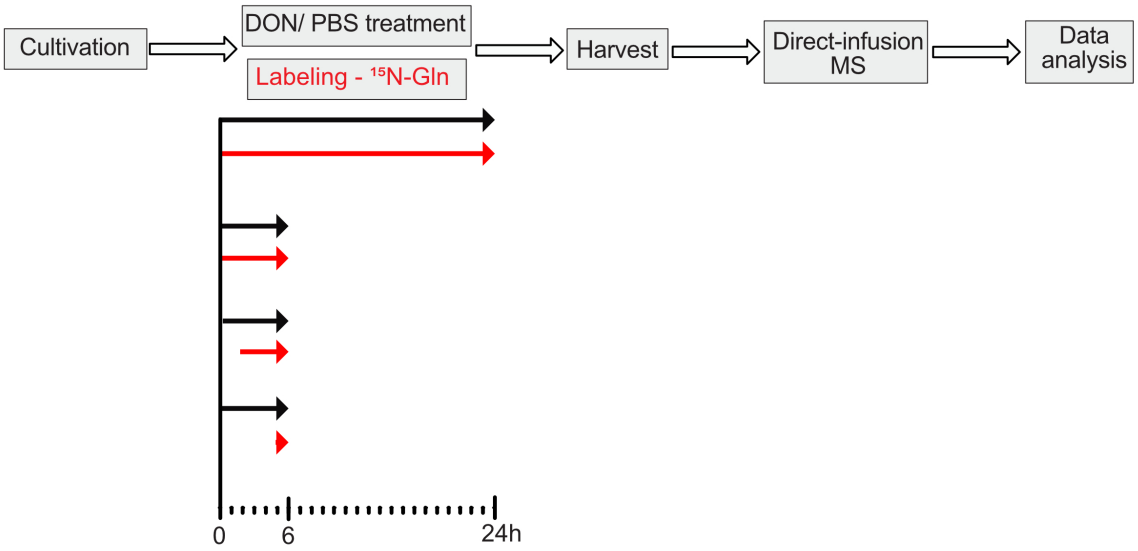

Figure 4.24: Experimental set up: DON treatment and ^{15}N-glutamine labeling. Black arrows present PBS- or DON-treatment starting at time point 0 h for in total 6 or 24 h. Red arrows present ^{15}N-glutamine labeling **i**) simultaneously to PBS- or DON-treatment: started at 0 h for 6 h or 24 h, **ii**) delayed to PBS- or DON-treatment at 2 h and 5 h for 4 h and 1 h labeling, respectively. Cells were harvested after treatment and labeling at 6 h and 24 h.

The implementation of advanced pSIRM allows to measure the dynamic flow of ^{15}N-glutamine in DON-treated and -untreated conditions. By treatment an decreased flow can provide insight into potential targets of DON (fig. 4.25, fig. 4.26).

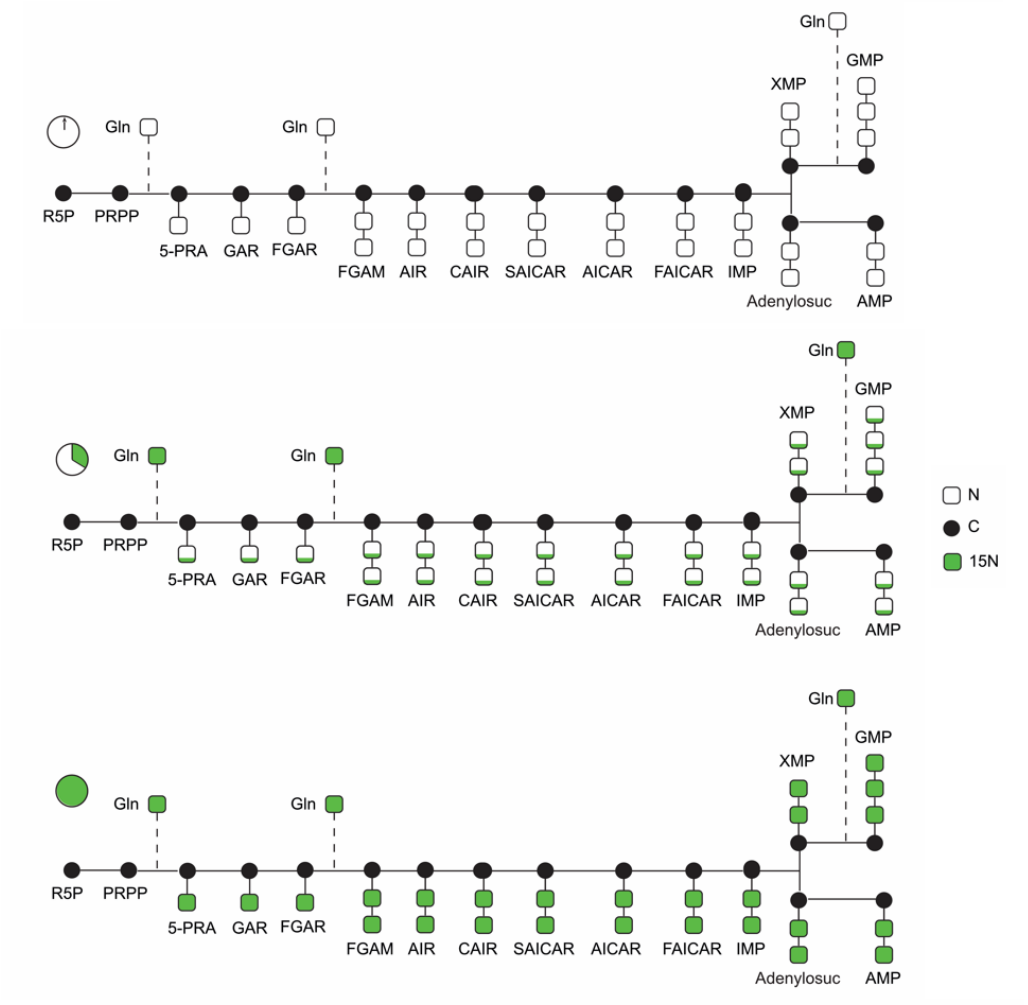

Figure 4.25: Purine biosynthesis pathway with applied ^{15}N-glutamine. Dynamic measuring of purine nucleotide biosynthesis with different time points of applied ^{15}N-glutamine. Essential abbreviations provided in the list of abbreviations.

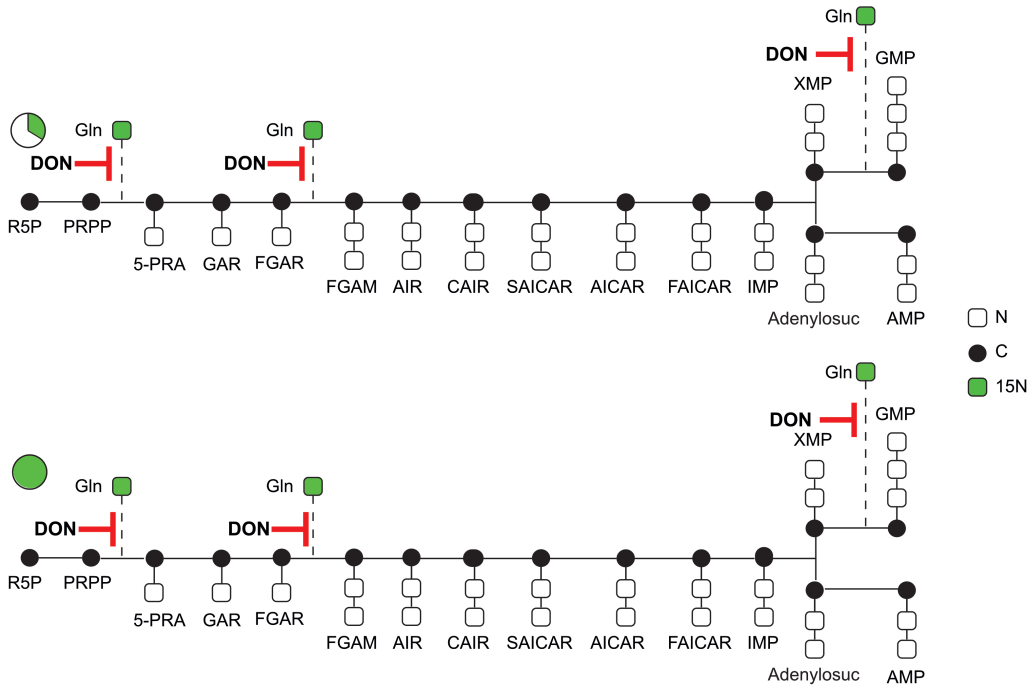

Figure 4.26: Purine biosynthesis pathway with applied ^{15}N-glutamine and DON treatment. Dynamic measuring of purine nucleotide biosynthesis with different time points of applied ^{15}N-glutamine and DON treatment. Essential abbreviations provided in the list of abbreviations.

4.5.3 DON targets PFAS in the purine nucleotide biosynthesis

As stated previously, glutamine serves as a major nitrogen donor as it provides the amido-group directly and amino-group indirectly via aspartate and glycine that originate from glutamine (Deberardinis and Cheng (2010)). To detect ^{15}N-glutamine incorporation peak intensities of each purine synthesis intermediate and nucleotide at each mass shift were measured (Rayman (2022)). Thereby each mass shift represents the addition of ^{15}N to intermediates or nucleotides of *de novo* purine biosynthesis (Rayman (2022)). Intensities of mass shifts of a molecule were compared to the total intensity of that molecule to determine the percentage of nitrogen incorporation. Untreated and unlabelled samples served to determine background noises (Rayman (2022)).

In fig. 4.27 the incorporation of ^{15}N-glutamine into the intermediates of the purine biosynthesis in DON-treated HCT116 cells is depicted (Rayman (2022)). Glutamine's nitrogen was first donated at the conversion of PRPP to 5-PRA by the enzyme PPAT. However, a clear incorporation of the labelled amido was not detectable in 5-PRA at m/z + 1. 5-Pra was followed by GAR and FGAR. The latter showed a clear incorporation pattern at m/z + 1. In DON-treated samples as well as in the PBS-treated samples a continued increase in the percentage of incorporation was observable into FGAR with elevated labelling time. However, a decrease in the percentage of incorporated ^{15}N was observable in DON-treated samples when compared to the control. By converting FGAR to FGAM via the enyzme PFAS another amido-group was donated from glutamine, therefore compounds after this point in the purine biosynthesis were

analysed at m/z + 2.

Purine nucleotides, which comprise adenosine and guanosine were analyzed at m/z + 3 as glutamine donates an amido-group when XMP is converted to GMP via the enzyme GMPS. Due to overlapping of adenosine-based ribonucleotides and guanosine based deoxyribonucleotides m/z, m/z + 3 were used to delineate them (Rayman (2022)).

Taking a look in the purine nucleotides ^{15}N incorporation can be observed for PBS-treated HCT116 cells (Rayman (2022)). While ^{15}N incorporation is increasing in the control, DON-treated samples decrease incorporation below detection over the tested time. Both, m/z + 2 and m/z + 3, showing similar increases of incorporation in the control over the time, whereas DON-treated HCT116 cells having marginal to no ^{15}N incorporation (Rayman (2022)).

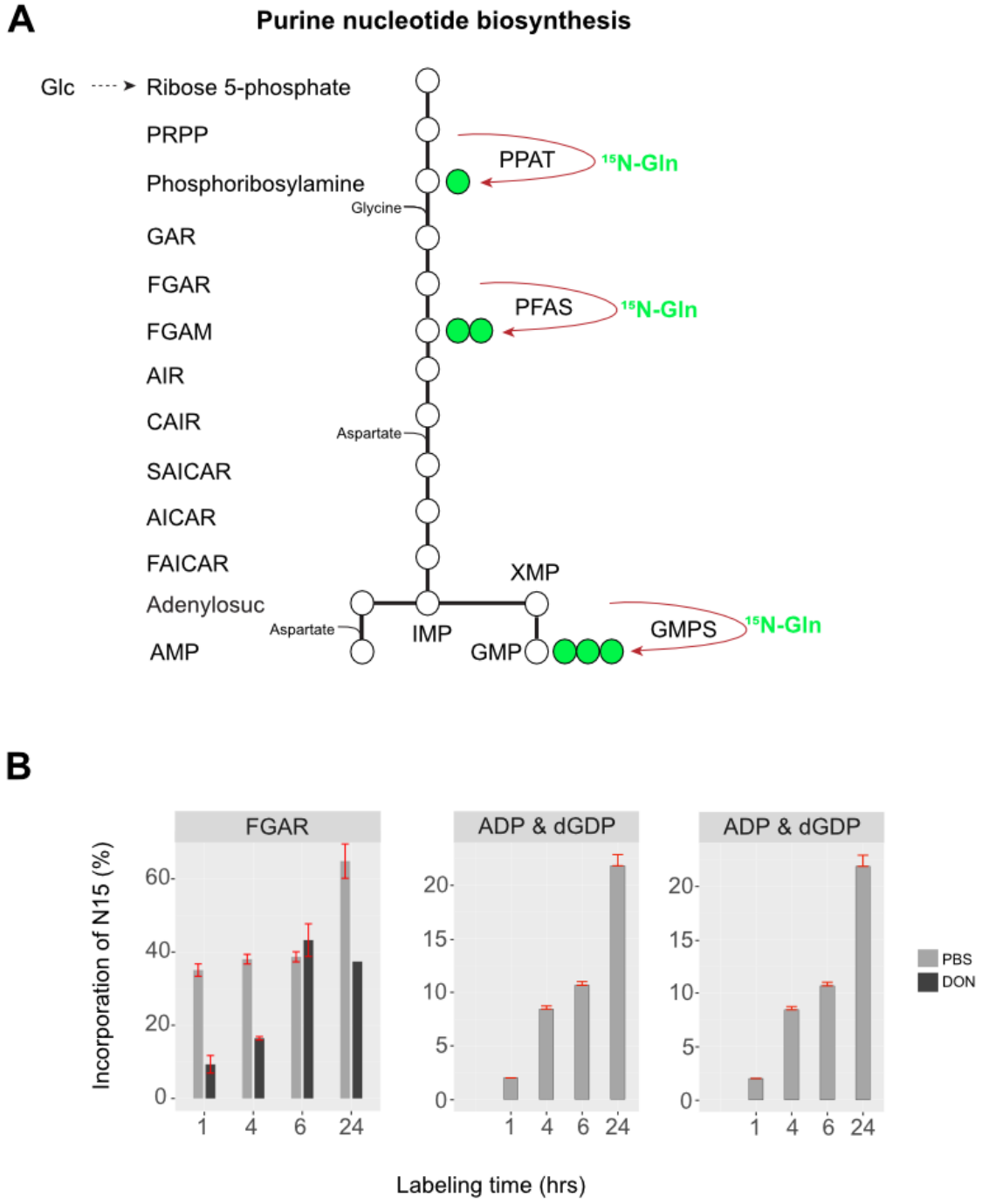

Figure 4.27: Incorporation of ^{15}N into purine synthesis after DON or PBS treatment. **A**: Diagram depicts the intermediates and nucelotides of the purine pathway and the flow of labelled nitrogen from ^{15}N-Glutamine. **B**: Incorporation of ^{15}N into purine synthesis intermediates in DON- or PBS-treated HCT116 cells. FGAR: Single ^{15}N atom incorporation at m + 1. ADP/dGDP: Two ^{15}N atoms incorporation at m + 2. ADP/dGDP: Three ^{15}N atoms incorporation at m + 3. Error bars represent mean ± SEM (Rayman (2022)).

In fig.4.28 the incorporation of ^{15}N-glutamine into the pyrimidine biosynthesis is depicted (Rayman (2022)). The first incorporated glutamine amid into the pyrimidine synthesis pathway occurs with the conversion of HCO_3^- to CBMP by the enzyme CPS2. Therefore UMP, UDP and UTP were analyzed at m/z + 1. Herein, an increasing of ^{15}N incorporation can be observed over the tested time in the control. Similar to decreasing ^{15}N incorporation in DON-treated samples in the purine nucleotides, HCT116-treated DON cells diminished nitrogen incorporation in pyrimidine nucleotides. UMP is converted to cytidine nucleotides, thereby another amid-group is donated from glutamine via the enzyme CTPS1. Hence, CDP was examined at m/z + 2. At time point 1 h of treatment incorporation is not detectable for both conditions. However, an increase in ^{15}N incorporation is observably beginning at 4 h in PBS-treated HCT116 cells over time. While for DON treated cells an incorporation is not detectable at this mass shift.

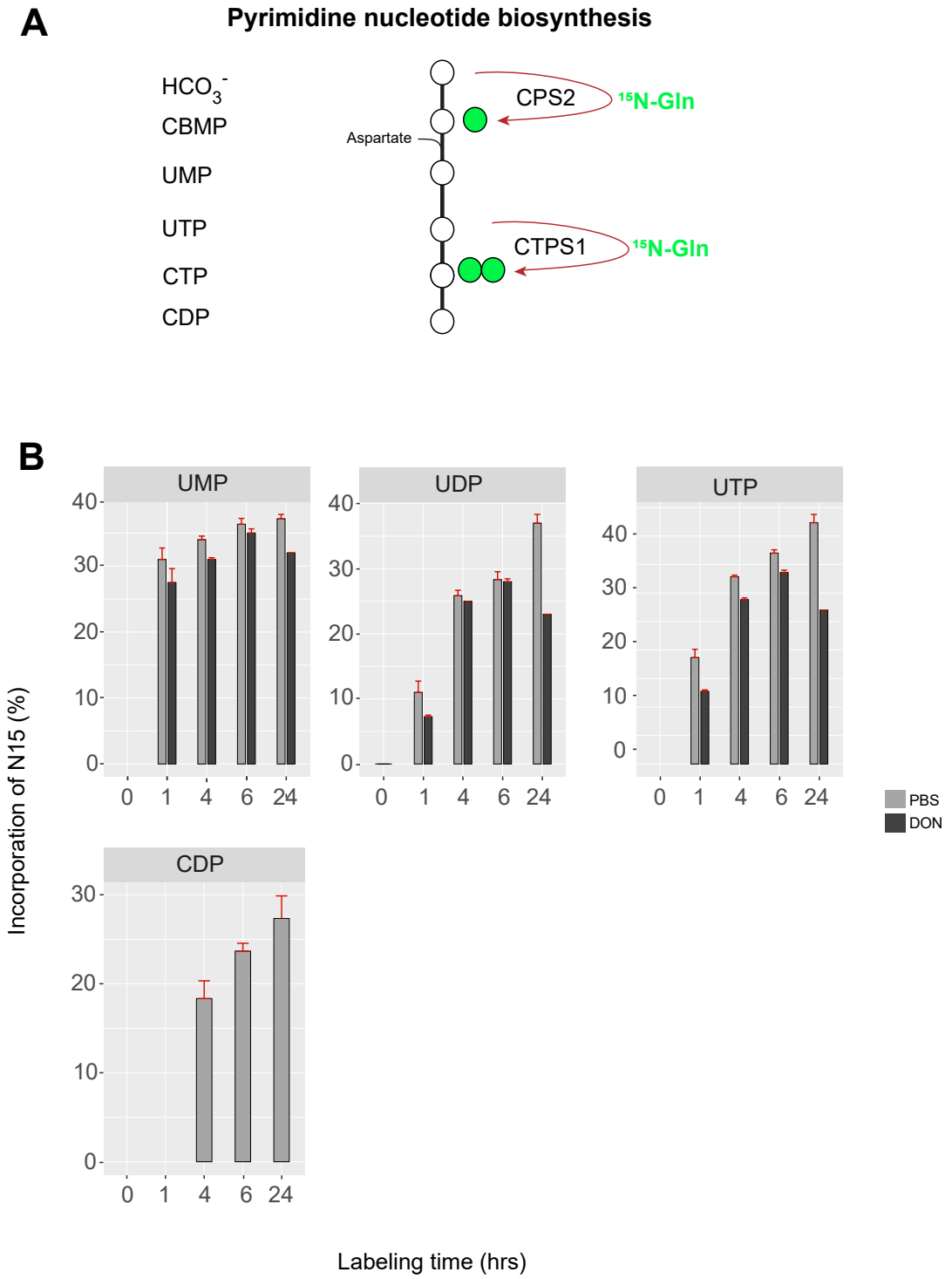

Figure 4.28: Incorporation of ^{15}N into pyrimidine synthesis after DON or PBS treatment. **A**: Diagram depicts the intermediates and nucelotides of the pyrimidine pathway and the flow of labelled nitrogen from ^{15}N-Glutamine. **B**: Incorporation of ^{15}N into purine synthesis intermediates in DON- or PBS-treated HCT116 cells. UMP, UDP, UTP: Single ^{15}N atom incorporation at m + 1. CDP: Two ^{15}N atoms incorporation at m + 2. Error bars represent mean ± SEM (Rayman (2022)).

In conclusion, these findings verify the hypothesis that DON is targeting the nitrogen flow.

Thereby the analysis revealed that DON is inhibiting the enzyme PFAS in the purine nucleotide biosynthesis (Rayman (2022)).

Chapter 5

Discussion

The metabolism of cancer cells is highly flexible as it can be fueled with various substrates that are converted via different pathways. Consequently, this flexibility complicates the dissection of metabolic rewiring processes that are acquired during tumorigenesis and tumor development. Cancer cells undergo significant metabolic changes in order to support proliferation with certain increases in glycolysis and glutaminolysis. This upregulated nutrient supply facilitates solid tumor cells to meet bioenergetic and biosynthetic needs and to run alternative metabolic programs (Hanahan and Weinberg (2011), De Berardinis and Chandel (2016)). The metabolism of the non-essential glutamine is highly accelerated in cancer cells due to the profound expression of glutaminase. The oncogene c-MYC induces a metabolic program that renders tumor cells to be dependent on glutamine for survival (Wise et al. (2008)). Compounds were developed to perturb glutaminolysis by targeting the enyzme GLS.

Prior investigations of the Kempa group focused on the impact of glutaminase inhibition on cell growth and cell metabolism with marginal effects by the specific inhibitors. In line with this, Meric-Bernstam et al. (2016) and DeMichele et al. (2017) demonstrated low antitumor activity of CB839 in clinical trials phase 1. In the proliferation experiment only the glutamine analogue DON was effective in decreasing the cell counts of the tested cell lines. This effect was neither explainable by the inhibition of GLS nor by the fate of the carbon skeleton of glutamine. It is known, that glutamine also has a crucial role in nucleotide synthesis.

Perhaps a reason for the lack of robust clinical effect of selective glutaminase inhibitors is that glutamine metabolism in tumors is more complex and heterogenous than initially hypothesized. The work presented in this thesis describes the sensitivity of HCT116 cells and the auxotrophy of RKO cells on glutamine. In the following I will discuss (i) the pivotal role of glutamine's nitrogen, (ii) the role of GLUL as a survival factor in cellular adaptation to glutamine depletion and (iii) the influence of the glutamine analogue DON on the cell growth via nucleotide analysis.

5.1 Evaluation of glutamine metabolism inhibitors on MYC protein expression

The proto-oncogene c-MYC is frequently activated in human cancer cells to support the high demand of building blocks and energy. MYC is a major regulator of cell growth, metabolism and apoptosis. Deregulated expression of MYC enhances the expression of genes involved in glutamine metabolism and renders cell survival dependent on glutamine as an anaplerotic fuel (Chen and Cui (2015), Yuneva et al. (2007)). This phenomenon is the basis for several therapeutic approaches, targeting the enzyme glutaminase, which converts glutamine into glutamate.

We investigated the effect of 16 h glutamine depletion and glutaminase inhibition by the glutaminase specific inhibitors BPTES, CB839 and C968 and the glutamine analogues Acivizine, Azaserine and DON and subsequently re-addition of glutamine for 30 min, 60 min, 120 min and 240 min in suppressing MYC protein expression. We observed that the quantities of MYC levels were significantly decreased in the absence of glutamine (16 h) in HCT116, RKO and HEK293 cells (7.1, 7.2, 7.3). After 16 h of glutamine starvation the recovery of MYC protein expression levels is particularly observable after 30 min of glutamine re-addition. The fastest recovery were shown in the specific glutaminase inhibitors, while DON-treated samples were significantly strongest delayed in HCT116 and RKO cells. Interestingly, HEK293 cells are not MYC-driven cells and show only a marginal effect in protein levels at 30 min of glutamine re-addition compared to the colon cancer cells.

We focused on DON and aimed to reveal specific targets that actually effect proliferation, and assumed them to fall under the category of numerous transaminases that use glutamine as a nitrogen donor. This will be discussed in the sections below.

5.2 Dependency on the non-essential amino acid glutamine in subject to the choosen FBS medium

Glutamine is the most abundant non-essential amino acid in the blood plasma that provides its carbon skeleton to produce TCA cycle intermediates and at the same time is an obligate nitrogen donor, supporting *de novo* nucleotide biosynthesis (Altman et al. (2016), Oehler and Roth (2003)). It is also required for several cellular processes including essential amino acid (EAA) uptake, macromolecule biosynthesis and autophagy inhibition (Nicklin et al. (2009)). In the cell culture glutamine is supplemented to the medium and so it is plentifully available for the cells. Several *in vivo* and *in vitro* studies focused on MYC-induced glutamine addiction, but not all cancer cell lines require glutamine for proliferation and survival (Yuneva et al. (2007), Nieminen et al. (2013), Le et al. (2012) Timmerman et al. (2013)).

5.2.1 Cell growth is not affected by glutamine absence in normal FBS medium

The concept of glutamine addiction in cancer cells is disputed. Multiple cancer cell lines show a glutamine dependency or addiction. This has spurred to develop inhibitors that effect the glutaminolysis, especially GLS. Some of these inhibitors are in current clinical trials. However, Timmerman et al. (2013) reported increased cell death or decreased cell proliferation due to glutamine withdrawal, differing between cell types. In order to examine the apparent glutamine dependency in HCT116 and RKO cells we starved the cells for glutamine in normal FBS medium and analyzed the effect on proliferation. In addition, we used no to low to normal glutamine concentrations and analysed cellular proteome profiles and nucleotide levels. Furthermore, we set up metabolic profiles of HCT116 and RKO cells to understand correlations about differences regarding cell growth and metabolic conversion. In parallel we tested the non-cancerous HEK293 cells for comparison. In the proliferation assay for at least 96 h of glutamine depletion, we observed that both cancerous cell lines HCT116 and RKO were not able to grow, whereas HEK293 cell continued proliferation. We wondered, if longer glutamine starvation could lead to a adaption of HCT116 and RKO cells as it was shown for the HEK293 cells. Indeed in the second performed proliferation assay for at least two weeks we saw a difference in the colon cancer cell lines. After 16 h HCT116 decreased cell numbers, but kept it up over time. In contrast, RKO cells showed an increase before cell count decreased on day 14. In response to the absence of external glutamine RKO cells seem to exhaust their surrounding glutamine stocks as the cell count was still stable at 7 d time point. However, after splitting and non addition of glutamine RKO cells seem to be unable to proliferate anymore. HCT116 show a fast response to glutamine withdrawal as already after 16 h cell counts are decreased. It could be, that HCT116 have a faster consumption of glutamine and hence have a faster reaction to glutamine depletion. However, in comparison to RKO cells, HCT116 cells did not exhaust glutamine storages. Even more, they adapt to an up to here unknown mechanism to the absence of the non-essential amino acid. It is suspected that this capacity of HCT116 and HEK293 relies on small molecules or residual glutamine in the not further specified normal fetal bovine serum. Additional MYC-driven cancer cell lines have to be tested in regards to glutamine-dependent cell growth in normal FBS. In consequence, cell culture medium composition and supplementation have to be reconsidered.

5.2.2 Increased GLUL protein expression in HEK293 cells

Previous work in the Kempa group could show that glutaminase inhibition only has a small effect, while the glutamine analogue DON has the strongest effect on suppressing cell proliferation in HEK293 cells (Royla (2018)). As stated earlier, glutamine deprivation seems to have no relevant effect in the non-cancerous cell line. We aimed to gain a comprehensive insight to identify key metabolic pathways that enable HEK293 cells to grow independently of glutamine and performed proteome and nucleotide analysis.

More than 8.000 proteins were received in the proteome analysis. However, the focus was set on enzymes with importance for glutamine and glutamate metabolism. The plotted enzymes for the colon cancer cells revealed different abundance in the compartments. As depicted in fig. 4.7, enzymes in HCT116 cells are more abundant in the cytosol and less in the mitochondria. The same enzymes apparently are more abundant in RKO cells in the mitochondria and less in the cytosol. In HEK293 cells a bias is not discernible. The two considered compartments show differently active enzymes in the non-cancerous cells. In a performed proteome analysis, we could see significant changes between the three cell lines (4.7). HEK293 cells showed higher expression of the enzyme GLUL compared to the colon cancer cell lines, especially in the tested conditions with low to no glutamine concentrations. GLUL is the enzyme that synthesizes glutamine from glutamate and a free ammonium. Nonetheless, HCT116 cells showed, similar to HEK293 cells, an increase in GLUL expression upon glutamine withdrawal over the tested time. The same development can be observed for RKO cells although expression is lower. Additionally, while HCT116 cells decreased glutaminase expression, RKO cells did not. Apparently the glutamine-dependent HCT116 cell line changed it's enzymatic activity from favoring glutaminase to aminotransferase to assure glutamine metabolism. In line with our results observed for HCT116 and HEK293 cells, Kung et al. (2011) showed the ability of GLUL to repress GLS expression, but not the other way around.

We assume that HEK293 cells and HCT116 cells synthesize glutamine in depleted conditions in FBS. If so, the pivotal function of glutaminase in glutamine metabolism has to be rethought in cell lines like HCT116. In particular, the property to synthesize glutamine makes this type of cancer less vulnerable to glutamine deprivation treatment and thus therapeutic approaches have to reconsidered.

5.2.3 Proteome analysis showed no significant changes in the nucleotide biosynthesis pathway

Glutamine is also involved in the purine and pyrimidine nucleotide biosynthesis. Transaminases e.g. PFAS, GMPS utilize glutamine's nitrogen to transfer it to an substrate (Deberardinis and Cheng (2010). We examined the protein expression of the intermediates of the corresponding pathway upon various glutamine concentrations. Both colon cancer cell lines have slightly decreased protein expressions in the reduced and depleted glutamine samples compared to the normal cell culture concentration. But no distinct protein expression changes are shown between HCT116 and RKO cells. The non-cancerous cell line HEK293 showed high expression of the measured proteins in all tested conditions. In summary, a significant change could not be observed that provides evidence for the different response on glutamine starvation. Royla (2018) could demonstrate, that carbon-13 flow is not affected by mimicking glutamine depletion via glutaminase inhibition. Moreover, it was speculated that glutamine-utilizing transaminases linked to nucleotide biosynthesis play a pivotal role. In the upcoming sections we provide evidence that the nitrogen flow of glutamine is affected and will discuss them.

5.2.4 Glutamine depletion decreased nucleotide levels in RKO cells

In order to measure the perturbations of lacked glutamine on nucleotides we examined changes in deoxy- and ribonucleotide levels regarding fed, low and no glutamine in the cell culture medium. Therefore, we used direct infusion MS. Glutamine absence does not cause significant changes in HEK293 cells. Nucleotide levels remained upregulated. HCT116 cells showed a slightly decreased trend in the low and depleted conditions. In contrast, a sharp decline can be observed in RKO cells in purine as well as pyrimidine nucleotides. We suspected that nucleotide biosynthesis is not impaired in HEK293 cells due to the capability to produce glutamine. The same applies for HCT116 cells with certain delay because of adaption. RKO do not succeed to produce glutamine and fail in the adaption and thus nucleotide levels decreased.

5.3 Dialyzed FBS medium restricts cell growth without glutamine supplementation

Since we could show that HEK293 and HCT116 cells can grow without glutamine in growth medium containing FBS, we hypothesized that the growth medium contains residual glutamine or other small molecules that promote this apparent glutamine independence. Therefore, we repeated a previously performed starvation experiment using growth medium containing dialyzed fetal bovine serum. Interestingly, neither HCT116 nor HEK293 cells were able to reenter cell proliferation in the absence of glutamine, which emphasizes the importance of glutamine in conditions with dialyzed FBS and without other supplementations. It also provides evidence, that the medium contains molecules or small substrates to overcome glutamine depletion. In line with our results, Muir et al. (2017) observed differential reliance on glutamine as anaplerotic substrate in *in vitro* cultured cancer cells, depending on enviromental conditions, especially when cystine levels were high. However, decades of research for glutamine dependence is well described and still remains elusive and poorly understood (Coles and Johnstone (1962), Kovacević and Morris (1972), Reitzer et al. (1979), DeBerardinis et al. (2007), Wise et al. (2008)).

5.3.1 Substrates of the enzyme GLUL allowed optimal proliferation in dialyzed FBS-supplemented medium for HCT116 and HEK293 cells

In further starvation experiments we supplemented the dialyzed FBS medium with substrates of glutamine-centric metabolic pathways and free ammonium after starvation (see fig. 5.1). We wanted to know if other substrates can replace glutamine and allow cell growth. The colon cancer cell lines HCT116 and RKO as well the non-cancerous cell line HEK293 demonstrated the highest proliferation rate upon glutamine supplementation. RKO cells appear to have restricted metabolic flexibility, given that they only proliferate with extracellular glutamine, while HCT116 cells demonstrated to be adaptable. HCT116 and HEK293 showed that the supplementation of GLU+NH_4^+ - the substrates of the enzyme GLUL- allowed optimal proliferation. Moreover, this result implicates that glutamine withdrawal is rather rescued by glutamine prototrophy than due to TCA cycle replenishment. Consistent with our findings Tardito et al. (2015) observed autonomously synthesized glutamine by GLUL in glioblastoma cells rather than anaplerotic reactions. This strengthened our presumption of a decisive role of GLUL.

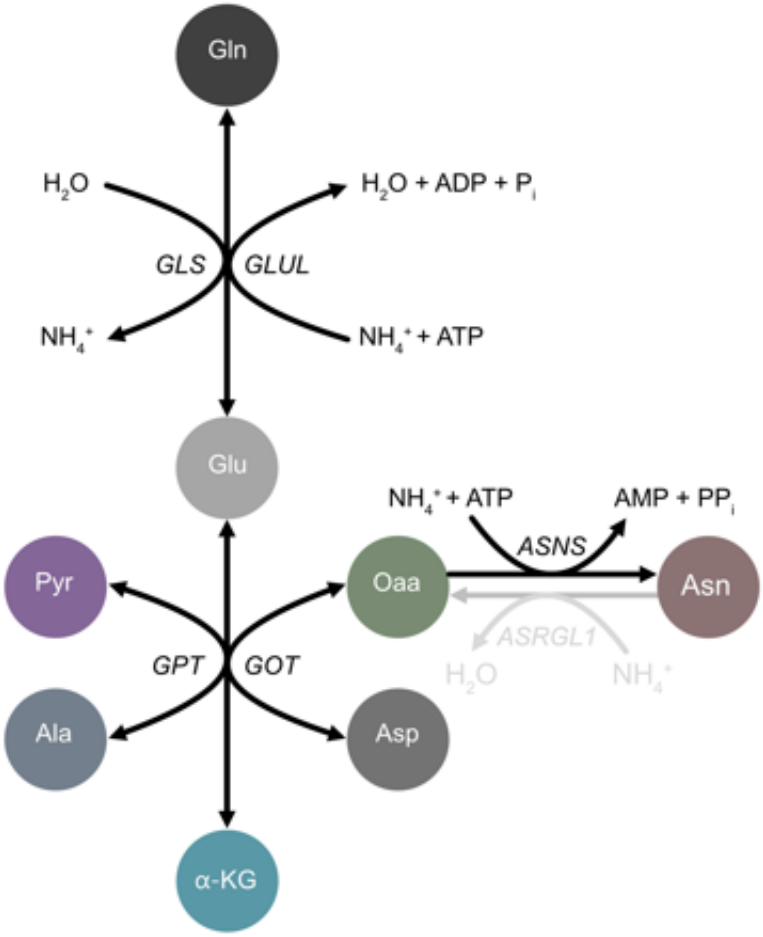

Figure 5.1: The Local Transaminase Network of Glutamine. Transaminase reactions enable the interconversion of amino acids including the generation of glutamate, a substrate required for de novo glutamine synthesis. Established metabolic pathways are shown in black. Hypothetical metabolic pathway is shown in grey. Abbreviations: Ala = alanine, Asn = asparagine, ASNS = asparagine synthetase, Asp = aspartate, ASRGL1 = asparaginase-like 1, Gln = glutamine, GLS = glutaminase, Glu = glutamate, GLUL = glutamine synthetase, GOT = Glutamic-oxaloacetic transaminase, GPT = Glutamate-Pyruvate transaminase, Oaa = oxaloacetate, Pyr = pyruvate, α-KG = α-ketoglutarate.

5.3.2 GLUL acts as a survival factor

To demonstrate GLUL activity, a SIRM study was performed in which stable isotope labeled substrates of GLUL ($^{13}C_5$-glutamate and ^{15}N-ammonium) were applied to the cells, after which ^{13}C and ^{15}N incorporation into newly synthesised metabolites was detected via GC-MS and direct-infusion MS (Bayram et al. (2022)). To demonstrate the essentiality of GLUL activity, MSO treatment was also applied.

The in fig. 4.16 depicted heatmap shows incorporation of ^{13}C and ^{15}N into glutamine for the fragment glutamine-3TBDMS at 431 m/z in HCT116 and HEK293. In RKO cells an incorporation is not detectable. We investigated also incorporation in nucleotide biosynthesis and could observe ^{13}C and ^{15}N incorporation in purine and ^{15}N incorporation in pyrimidine nucleotides in HEK293 and HCT116 cells while RKO cells did not show incorporation.

These findings provide evidence that GLUL is active and subsequently allows glutamine independency because all pathways funnel into *de novo* glutamine synthesis in HEK293 and HCT116 cells (Bayram et al. (2022)). RKO did not show GLUL activity as none of the supplements could contribute to cell growth and survival. This could be attributed to mutations, which cause loss of GLUL activity and thus less catalytical activity (Bayram et al. (2022)).

Furthermore, a literature research on "DepMap Portal" revealed (based on a calculation for each gene score in a cell line the probability of dependency with a score higher than 0.5) that RKO cells with 5.5 has a dependency on GLUL. Further work is required to investigate GLUL activity. In addition, we demonstrated MSO-treatment abolished GLUL activity and consequently HCT116 and HEK293 were incapable to overcome glutamine-depletion by using the supplemented nutrients. However, once more GLUL has been verified as a key player in regard of glutamine independency.

We highlighted the combination of innovative MS-based approaches via simultaneous application of ^{13}C-glutamate and ^{15}N-ammonium. This allows new insights into biological reactions. The simultaneous application of ^{13}C-glutamate and ^{15}N-ammonium and MSO-treatment allowed us to detect the relative contribution of extracellular glutamate and ammonium to intracellular glutamine synthesis. In addition, the downstream contribution of glutamine's carbon and nitrogen into the *de novo* nucleotide biosynthesis could be monitored.

5.4 DON effects transaminases involved in the nucleotide pathway

5.4.1 Cell growth and off-target effect of DON

Investigation of the impact of glutaminase inhibitors revealed resistance in colon cancer cells and outlined preserved glutaminolysis due to glutamine-utilising transaminases (Royla (2018), Bayram et al. (2020)).

The glutamine analogue DON does not impair glutamine to glutamate conversion although it does affect proliferation (Royla (2018),Bayram et al. (2020)). Apparently, off-target effects take place that are not based on the carbon skeleton of glutamine. Therefore, we focused on DON, as it was the most efficient inhibitor in suppressing cell growth. We aimed to reveal specific targets that actually affect proliferation and assumed them to fall under the category of numerous transaminases that use glutamine as a nitrogen donor, especially those involved in nucleotide biosynthesis.

Therefore, we examined DON's affect on nucleotide precursors under normal conditions and after glutamine withdrawal for two weeks in HCT116 and HEK293 cells (see fig. 4.20). RKO cells were excluded due inability to overcome glutamine depletion. We observed an accumulation of PRPP and decrease in AICAR and SAICAR. So far the detection of all purine synthesis intermediates is still missing. Methods to describe purine synthesis are either nucleotide levels or certain intermediates by direct tracing via radioactive labelling (Zhao et al. (2015), Sant et al. (1989), Mádrová et al. (2018)). Therefore, Dr. Martin Forbes (Research scientist in the Kempa-Lab, BIMSB/MDC, Berlin-Germany) and Liam Rayman (Master student in the Kempa-Lab, BIMSB/MDC, Berlin-Germany) explored the possibility to characterize further precursors of *de novo* produced purine nucleotides by direct infusion mass spectrometry (Rayman (2022)). In addition, in collaboration with Dr. Guido Mastrobuoni (Research scientist in the Kempa-Lab, BIMSB/MDC, Berlin-Germany) a method was established that combines nitrogen flow with pSIRM and applied treatment based on direct infusion MS (fig. 5.2). Furthermore, a computational analysis and custom R script were developed (Rayman (2022)). Based on this method we examined DON's affect on the nitrogen flow of intermediates involved in *de novo* nucleotide biosynthesis and illuminated the mechanism of action.

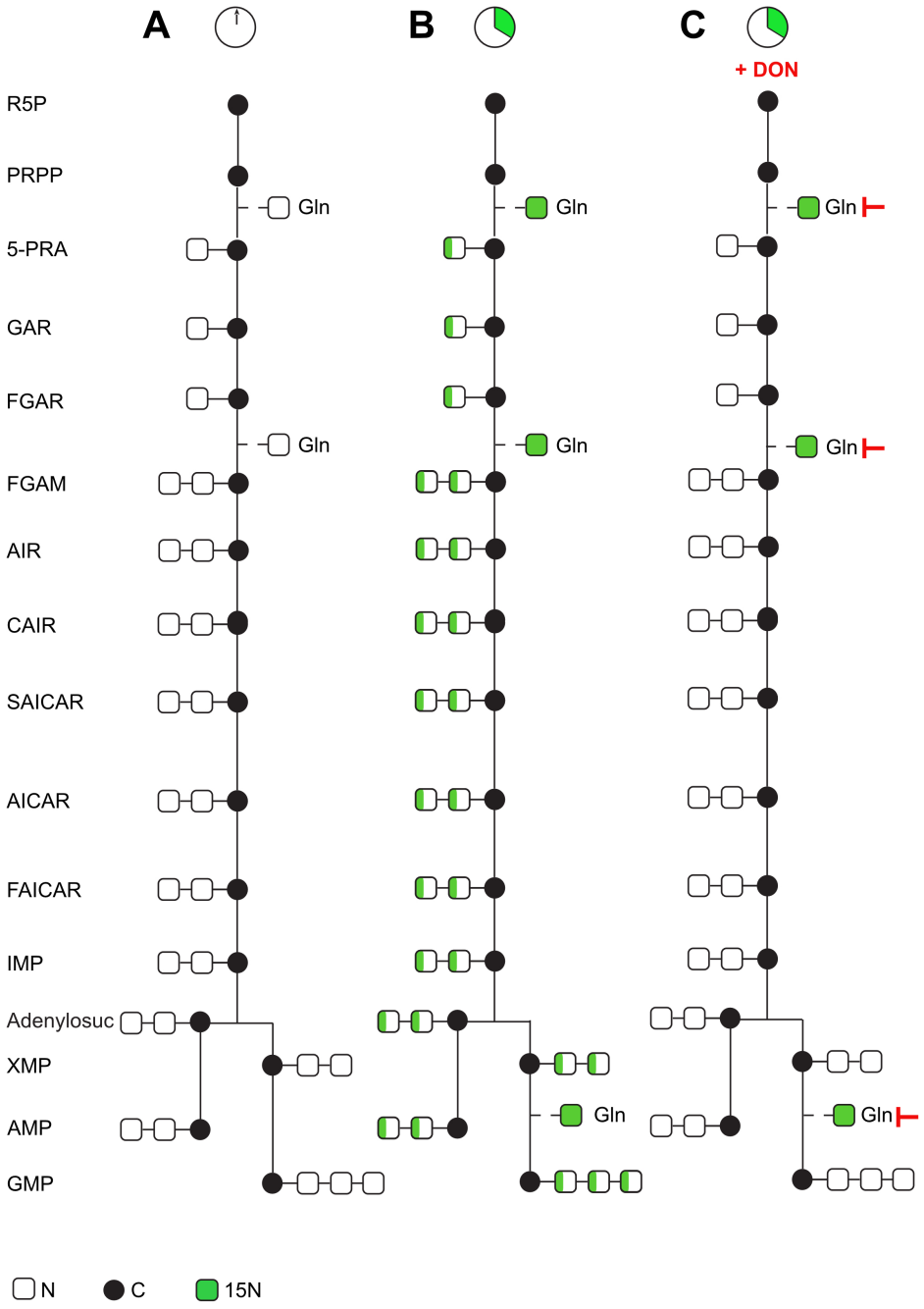

Figure 5.2: Purine nucleotide biosynthesis with ^{15}N-glutamine labeling and DON treatment. Dynamic incorporation of ^{15}N-glutamine in the purine nucleotide biosynthesis. **A** Time-resolved pulsed labeling at time point 0 without labeling and treatment. **B** Time-resolved pulsed labeling with appropriated ^{15}N-glutamine labeling and without treatment. **C** Time-resolved pulsed labeling with appropriated ^{15}N-glutamine labeling and with DON treatment. .

We repeated the first experiment and extended by a further 6 h time point for HCT116 cells. Regarding purine precursors a variation of intensities is shown after 6 h and 24 h in fig. 4.22 (Rayman (2022)). While intensities are increased at 6 hours in DON-treated cells, 24 hours intensities are greater in PBS-treated cells. Furthermore, an increased precursor intensity was as well as shown for the 2 h DON-treatment from the first experiment (fig. 4.20). This indicates that the cells increases nucleotide precursor levels as a result of DON-treatment.

In fig. 4.23 we observed changes in pool sizes between the nucleotides in PBS-treated and DON-treated samples. Purine intensities were greater in PBS-treated samples compared to DON-treated samples, which implies a greater pool in the PBS-treated cells (Rayman (2022)). In contrast, CMP, UMP, UDP and UTP of pyrimidine nucleotides exhibited some increase in pool size in DON-treated samples relative to PBS-treated samples. We suggest that purine and pyrimidine synthesis are affected differently by DON as varied nitrogen from glutamine contributes to nucleotide biosynthesis. Subsequently, DON interferes with purine differently than with pyrimidine nucleotide biosynthesis (Rayman (2022)).

As only a single replicate treated with DON could be used, further experiments will be necessary to be able to make a more general statement on changed pool sizes caused by DON (Rayman (2022)).

5.4.2 DON interacts with the aminotransferase PFAS

1963 Hartman (1963) reported that DON is inhibiting PPAT. Over the following decades further investigations revealed PPAT as another target Ahluwalia et al. (1990). Both enzymes transaminate glutamine and contribute its amido-group into the pathway. The studies used radioactive approaches. We provided HCT116 cells with ^{15}N-glutamine to demonstrate changes in the flux of the purine synthesis pathway. Subsequently, we displayed DON's inhibitory effect (Rayman (2022)).

5-PRA is the first intermediate of the purine pathway, that is donated with glutamine's nitrogen via the enzyme PPAT. However, 5-PRA has a half-life of 5 seconds and is unstable *in vivo*. Thus, a full degree of incorporation in these samples is not delineated (Rudolph and Stubbe (1995)).

A clear incorporation of ^{15}N was seen in the intermediate FGAR at m/z + 1 (Rayman (2022)). PBS-treated as well as DON-treated cells show an incorporation of labelling over time, while DON samples show this to a lesser extent. It seems, glutamine's nitrogen is prevented from being incorporated into the purine pathway. However, the 6 h time point has a higher increase of ^{15}N incorporation when treated with DON. A reason for that is the simultaneous application of DON-treatment and labeling. Obviously to assess DON efficiency on the nucleotide pathway a time gap before labelling is more conclusive.

FGAR is converted to FGAM via the enzyme PFAS, which contributes a nitrogen from glutamine. Therefore, FGAM is detected at m + 2. However, FGAM showed low abundances and was undetected. The observed signals could be noises or exaggerated signals from the other mass shifts and were not shown.

We examined incorporation of ^{15}N into nucleotides (Rayman (2022)). In PBS-treated HCT116 cells an incorporation was noted in the purine nucleotides in all mass shifts. Interestingly, DON-treated samples showed little to no ^{15}N incorporation, suggesting incorporation is below detection as a result of treatment. We assume that DON treatment causes the reduced flow of ^{15}N to the nucleotides, which leads to stalled production in purine nucleotides as we also noted decreased pool sizes in fig. 4.23 (Rayman (2022)). Same was noted for pyrimidine nucleotide CDP at m + 2 as shown in figure 4.28(Rayman (2022)). Adenosine-based nucleotides contain two and guanosine-based nucleotides three nitrogenes of glutamine. Mass shift at + 3 for AMP/ dGMP, ADP/ dGDP, ATP/dGTP denotes ^{15}N incorporation into dGMP, dGDP and dGTP. However, mass shift at M + 2 represents nucleotides from adenosine- and guanosine-based nucleotides.

Examination of pyrimidine nucleotides showed incorporation of ^{15}N into UMP, UDP and UTP at m + 1 (fig. 4.28) (Rayman (2022)). Glutamine's nitrogen is contributed in the first step of pyrimidine synthesis via the enzyme CTPS Ter-Ovanessian et al. (2021).

In samples treated with DON a decreased incorporation of ^{15}N into UMP, UDP and UTP was noted. Indicating that DON could be affecting the enzyme CTPS. Further MS analysis of the intermediates involved in pyrimidine synthesis are required for a better understanding of the data.

Based on our examination we can state that DON is effecting different transaminases of the nucleotide pathway as earlier studies have demonstrated (fig. 5.3) (Hartman (1963), Ahluwalia et al. (1990)).

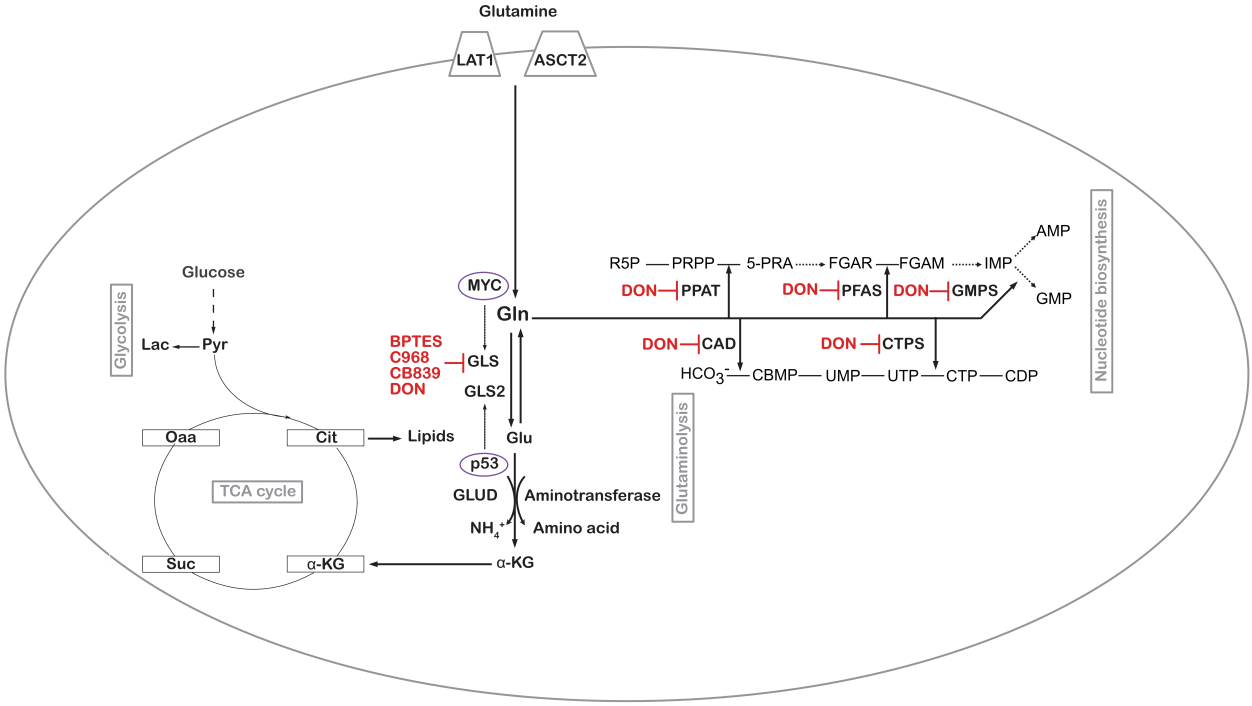

Figure 5.3: Glutamine centric pathway with inhibitors.. Glutamine is converted to glutamate by GLS or GLS2. BPTES, C968 and CB839 are GLS specific inhibitors, while DON is a glutamine analoq inhibiting all glutamine-utilizing enzymes. The counter-reaction is performed by GLUL, which synthesizes glutamine. MSO is an inhibitor of GLUL. PPAT, PFAS and GMPS are glutamine-transaminases involved in the purine pathway. CAD and CTPS are glutamine-transaminases involved in the pyrimidine pathway. Essential abbreviations provided in the list of abbreviations.).

5.5 c-MYC and glutamine connection

Another important phenomenon is the interaction between glutamine and c-MYC. C-MYC is a proto-oncogene that plays a key role in regulating cell growth, proliferation, metabolism and apoptosis. MYC expression levels are low in non-cancerous cells and the expression is tightly controlled. In human cancer, c-MYC expression is deregulated, which leads to a transcriptional imbalance (Kalkat et al. (2017)). This in turn causes a constitutive cell growth cascade, which induces a dependence of cancer cells on the non-essential amino acid glutamine. In cancer cells with MYC-overexpression, the metabolism of glutamine is changed by the oncogene that enhances the expression of enzymes that utilize the amino acid (Yuneva et al. (2007), Wise et al. (2008)). As mentioned before, glutamine addicted cells were shown to undergo apoptosis when deprived of the amino acid glutamine. Interestingly, glutamine deprivation decreases adenosine levels, which also decreases MYC levels. Evidently there is a mutual interaction between glutamine and MYC that is mediated by translational control, but has not been elucidated (Dejure et al. (2017)).

5.5.1 Glutamine's effect on the oncogene cMYC

In previous work by the Kempa group, it was shown that MYC protein expression is controlled by glutamine availability via adenosine derived nucleotides (Royla (2018)). Glutamine depletion leads to changes in adenosine nucleotide levels, which has a suppressive effect on MYC translation. This metabolic feedback protects cells from MYC-driven apoptosis. In this process, decreasing MYC levels have a protecting effect on cancer cells, probably by a RNA binding protein sensitive to low nucleotide levels, adenine in particular.

As stated earlier glutamine depletion in dialyzed FBS stopped cell growth in HCT116, RKO as well as HEK293 cells. Latter showed still MYC expression in glutamine deprived medium when normal FBS was used. A western blot analysis was performed to analyze MYC expression in HCT116, RKO and HEK293 cells in dialyzed FBS and glutamine withdrawal. Regarding MYC levels, a diminished expression upon glutamine deprivation can be observed when using growth medium containing dialyzed FBS for all three cell lines.

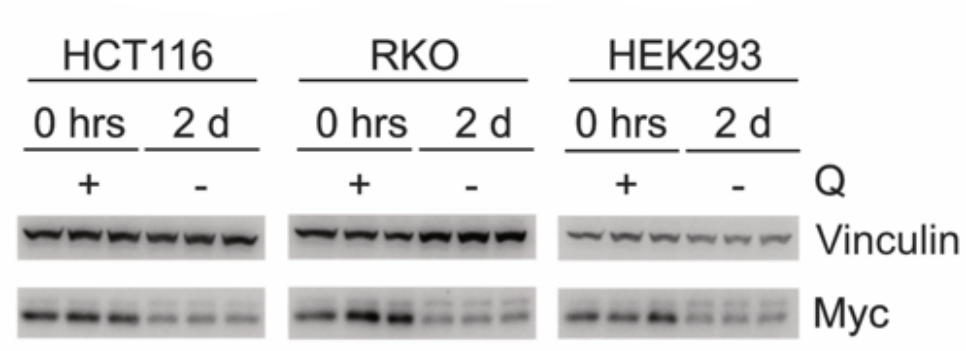

Figure 5.4: MYC protein expression in HCT116, HEK293 and RKO cells. The representative immunoblot documents MYC and Vinculin levels under the described condition in the indicated cell lines with in total 3 BR.

Chapter 6

Conclusion and Outlook

This thesis describes recent efforts to investigate glutamine addiction in colon cancer cell lines and their altered glutamine metabolism. In order to gain insights into that a comprehensive analysis of cell growth, metabolism, protein expression and nucleotide levels was carried out. The non-cancerous HEK293 cells were analyzed in parallel and used as a comparison only. We showed that HCT116 cells are sensitive and RKO cells are auxotrophic to glutamine depletion in FBS. While HCT116 cells as well as HEK293 become auxotrophic to glutamine when dialyzed FBS was used. However, we demonstrated that HCT116 cells can overcome glutamine addiction in dialyzed FBS medium by supplementation with different substrates, especially in Glu + NH_4^+ supplemented medium. A proteome analysis revealed high protein expression of GLUL. We speculated that GLUL serves as a survival factor. A performed SIRM study demonstrated GLUL activity by sustaining *de novo* nucleotide biosynthesis. Additionally, these findings were confirmed via a proliferation assay with applied GLUL-inhibitor (MSO). An immunoblotting confirmed GLUL expression in all three cell lines. Nevertheless activity could not be displayed for RKO cells. We assume, that GLUL is inactive due to gene mutations or impaired transport of substrates for GLUL reaction (Bayram et al. (2022)). Therefore, we propose to perform DNA-sequencing of the RKO colon cancer cell line. Furthermore, to demonstrate and evaluate the inactivity of GLUL in RKO cells and consequently glutamine dependency, an approach by applying recombinant produced GLUL protein in Glu + NH_4^+ supplemented medium in RKO cells should be investigated. Moreover, other glutamine-sensitive cells should be contemplated and analysed concerning GLUL as survival factor in glutamine depleted conditions. Altogether, we could only shed light on a small part of the complex metabolism of cancer cells, regarding glutamine. We found evidence for GLUL as a survival factor in glutamine-sensitive cells, which should be considered as an additional therapeutic agent in targeting glutamine metabolism. A monotherapy does not seem to be useful as glutamine is a versatile used substrate with the opportunity to circumvent the restriction as already adaption of colon cancer cells to single-sided treatment has been demonstrated (Royla (2018), Bayram (2018), Bayram et al. (2020), Bayram et al. (2022)). Another important but not further discussed fact is cancer-associated drug resistance due to cancer-associated fibroblasts, which secrete GLUL-synthesized glutamine and induce proliferation and differentitaion (Li et al. (2021)). This corollary finding emphasizes our conclusion of dual targeting of glutamine metabolism. The glutamine analogue DON has shown strong effectiveness to suppress cell growth in HCT116, RKO and HEK293 cells. We demonstrated reduced ^{15}N-incorporation in purine nucleotides when HCT116 cells were

treated with DON. To gain further information of DON's effect on nucleotide synthesis, intermediates' MS analysis would be required to provide further context to this. The effect of DON in RKO and HEK293 cells should also be investigates. In addition, we propose to knock out glutamine-utilizing enzymes involved in the nucleotide biosynthesis in order to see if the protective mechanism induced by suppressing MYC levels can be circumvented. We assume, those belong to the glutamine-utilizing enzymes targeted by DON. Nonetheless, the heterogeneity of glutamine metabolism regarding tissue types and the associated cancer genetics as well as the tumor microenviroment shows the intricate network of cancer cell. However, a closer look on cell culture medium and conditions is recommended and should be modified to human plasma concentrations to avoid misinterpretation of results. In particular, the high concentration of glutamine can effectuate favoured routes of cultured cells that re-orientate themselves if glutamine is depleted (Pavlova et al. (2022), Cheng et al. (2011)). Subsequently, glutamine dependency or addiction or to put it another way glutamine sensitive or auxtrophic cells can be better categorized and perhaps the phenomenon termed glutamine addiction can be cleared up.

Bibliography

G. S. Ahluwalia, J. L. Grem, Z. Hao, and D. A. Cooney. Metabolism and action of amino acid analog anti-cancer agents, 1990. ISSN 01637258.

B. J. Altman, Z. E. Stine, and C. V. Dang. From Krebs to clinic: Glutamine metabolism to cancer therapy, 2016. ISSN 14741768.

I. Amelio, F. Cutruzzolá, A. Antonov, M. Agostini, and G. Melino. Serine and glycine metabolism in cancer, 2014. ISSN 09680004.

N. Amoêdo, J. Valencia, M. Rodrigues, A. Galina, and F. Rumjanek. How does the metabolism of tumour cells differ from that of normal cells. *Bioscience Reports*, 33(6):865–873, 2013. ISSN 0144-8463. doi: 10.1042/BSR20130066. URL `http://bioscirep.org/cgi/doi/10.1042/BSR20130066`.

S. N. Baharum and K. A. Azizan. Metabolomics in systems biology. In *Advances in Experimental Medicine and Biology*. 2018. doi: 10.1007/978-3-319-98758-3_4.

S. Bayram. Analysis of the Differential Response of Colon Cancer Cell Lines Upon Glutaminase Inhibition. 2018.

S. Bayram, S. Fürst, M. Forbes, and S. Kempa. Analysing central metabolism in ultra-high resolution: At the crossroads of carbon and nitrogen, 2020. ISSN 22128778.

S. Bayram, Y. S. Razzaque, S. Geisberger, M. Pietzke, S. Fürst, C. Vechiatto, M. Forbes, G. Mastrobuoni, and S. Kempa. Investigating the role of glul as a survival factor in cellular adaptation to glutamine depletion via targeted stable isotope resolved metabolomics. *Frontiers in Molecular Biosciences*, 9, 2022. ISSN 2296-889X. doi: 10.3389/fmolb.2022.859787. URL `https://www.frontiersin.org/articles/10.3389/fmolb.2022.859787`.

J. M. Berg, J. L. Tymoczko, and L. Stryer. *Stryer Biochemie*. 2013. doi: 10.1007/978-3-8274-2989-6.

J. Bergström, P. Fürst, L. O. Norée, and E. Vinnars. Intracellular free amino acid concentration in human muscle tissue. *Journal of Applied Physiology*, 36(6):693–697, 1974. ISSN 0021-8987. URL `http://www.ncbi.nlm.nih.gov/pubmed/4829908`.

L. Berlicki. Inhibitors of Glutamine Synthetase and their Potential Application in Medicine. *Mini-Reviews in Medicinal Chemistry*, 2008. ISSN 13895575. doi: 10.2174/138955708785132800.

A. J. Bott, S. Maimouni, and W. X. Zong. The pleiotropic effects of glutamine metabolism in cancer, 2019. ISSN 20726694.

R. C. Bruntz, A. N. Lane, R. M. Higashi, and T. W. Fan. Exploring cancer metabolism using Stable isotope-resolved metabolomics (SIRM), 2017. ISSN 1083351X.

J. M. Buescher and E. M. Driggers. Integration of omics: more than the sum of its parts. *Cancer & Metabolism*, 2016. doi: 10.1186/s40170-016-0143-y.

A. Bush, M. Mateyak, K. Dugan, A. Obaya, S. Adachi, J. Sedivy, and M. Cole. c-myc null cells misregulate cad and gadd45 but not other proposed c- Myc targets. *Genes and Development*, 1998. ISSN 08909369. doi: 10.1101/gad.12.24.3797.

R. A. Cairns, I. S. Harris, and T. W. Mak. Regulation of cancer cell metabolism, 2011. ISSN 1474175X.

M. Camici, M. Garcia-Gil, R. Pesi, S. Allegrini, and M. G. Tozzi. Purine-metabolising enzymes and apoptosis in cancer, 2019. ISSN 20726694.

J. R. Cantor and D. M. Sabatini. Cancer cell metabolism: One hallmark, many faces, 2012. ISSN 21598274.

D. Cervantes-Madrid, Y. Romero, and A. Dueñas-González. Reviving Lonidamine and 6-diazo-5-oxo-l-norleucine to be used in combination for metabolic cancer therapy. *BioMed Research International*, 2015, 2015. ISSN 23146141. doi: 10.1155/2015/690492.

L. Chen and H. Cui. Targeting glutamine induces apoptosis: A cancer therapy approach, 2015. ISSN 14220067.

L. Chen, H. Cui, J. Fang, H. Deng, P. Kuang, H. Guo, X. Wang, and L. Zhao. Glutamine deprivation plus BPTES alters etoposide- and cisplatin-induced apoptosis in triple negative breast cancer cells. *Oncotarget*, 7(34):54691–54701, 2016. ISSN 1949-2553. doi: 10.18632/oncotarget.10579. URL `http://www.oncotarget.com/fulltext/10579`.

T. Cheng, J. Sudderth, C. Yang, A. R. Mullen, E. S. Jin, J. M. Matés, and R. J. DeBerardinis. Pyruvate carboxylase is required for glutamine-independent growth of tumor cells. *Proceedings of the National Academy of Sciences of the United States of America*, 2011. ISSN 00278424. doi: 10.1073/pnas.1016627108.

I. Chiodi, C. Perini, D. Berardi, and C. Mondello. Asparagine sustains cellular proliferation and c-Myc expression in glutamine-starved cancer cells. *Oncology Reports*, 2021. ISSN 17912431. doi: 10.3892/or.2021.8047.

A. A. Cluntun, M. J. Lukey, R. A. Cerione, and J. W. Locasale. Glutamine Metabolism in Cancer: Understanding the Heterogeneity, 2017. ISSN 24058033.

N. W. Coles and R. M. Johnstone. Glutamine metabolism in Ehrlich ascites-carcinoma cells. *The Biochemical journal*, 1962. ISSN 02646021. doi: 10.1042/bj0830284.

H. A. Coller. Is cancer a metabolic disease? 9582978472, 2014. ISSN 00029440.

J. G. Cory and A. H. Cory. Critical roles of glutamine as nirogen donors in purine and pyrimidine nucleotide synthesis: Asparaginase treatment in childhood acute lymphoblastic leukemia, 2006. ISSN 0258851X.

J. Cox, N. Neuhauser, A. Michalski, R. A. Scheltema, J. V. Olsen, and M. Mann. Andromeda: A peptide search engine integrated into the MaxQuant environment. *Journal of Proteome Research*, 2011. ISSN 15353893. doi: 10.1021/pr101065j.

F. Crick. Central dogma of molecular biology. *Nature*, 1970. ISSN 00280836. doi: 10.1038/227561a0.

V. Cruzat, M. M. Rogero, K. N. Keane, R. Curi, and P. Newsholme. Glutamine: Metabolism and immune function, supplementation and clinical translation, 2018. ISSN 20726643.

C. V. Dang. Links between metabolism and cancer, 2012a. ISSN 08909369.

C. V. Dang. MYC on the path to cancer. *Cell*, 149(1):22–35, Mar. 2012b.

C. V. Dang. MYC, metabolism, cell growth, and tumorigenesis. *Cold Spring Harb Perspect Med*, 3(8), Aug. 2013.

R. J. De Berardinis and N. S. Chandel. Fundamentals of cancer metabolism, 2016. ISSN 23752548.

R. J. Deberardinis and T. Cheng. Q's next: The diverse functions of glutamine in metabolism, cell biology and cancer. *Oncogene*, 29(3):313–324, 2010. ISSN 09509232. doi: 10.1038/onc.2009.358. URL `http://dx.doi.org/10.1038/onc.2009.358`.

R. J. DeBerardinis, A. Mancuso, E. Daikhin, I. Nissim, M. Yudkoff, S. Wehrli, and C. B. Thompson. Beyond aerobic glycolysis: Transformed cells can engage in glutamine metabolism that exceeds the requirement for protein and nucleotide synthesis. *Proceedings of the National Academy of Sciences of the United States of America*, 2007. ISSN 00278424. doi: 10.1073/pnas.0709747104.

F. R. Dejure, N. Royla, S. Herold, J. Kalb, S. Walz, C. P. Ade, G. Mastrobuoni, J. T. Vanselow, A. Schlosser, E. Wolf, S. Kempa, and M. Eilers. The MYC mRNA 3'-UTR couples RNA polymerase II function to glutamine and ribonucleotide levels . *The EMBO Journal*, 2017. ISSN 0261-4189. doi: 10.15252/embj.201796662.

B. Delabarre, S. Gross, C. Fang, Y. Gao, A. Jha, F. Jiang, J. Song J., W. Wei, and J. B. Hurov. Full-length human glutaminase in complex with an allosteric inhibitor. *Biochemistry*, 50(50):10764–10770, 2011. ISSN 00062960. doi: 10.1021/bi201613d.

A. DeMichele, J. Harding, M. Telli, P. Münster, R. McKay, O. Iliopoulos, S. Whiting, K. Orford, M. Bennett, J. Mier, T. Owonikoko, M. Patel, K. Kalinsky, R. Carvajal, J. Infante, and F. Merit-Bernstam. Abstract P6-11-05: Phase 1 study of CB-839, a small molecule inhibitor of glutaminase (GLS), in combination with paclitaxel (Pac) in patients (its) with triple negative breast cancer (TNBC). *Cancer Research*, 2017. ISSN 0008-5472. doi: 10.1158/1538-7445.sabcs16-p6-11-05.

H. W. Dion, S. A. Fusari, Z. L. Jakubowski, J. G. Zora, and Q. R. Bartz. 6-Diazo-5-oxo-L-norleucine, a new tumor-inhibitory substance. II. Isolation and characterization. *Journal of the American Chemical Society*, 78(13):3075–3077, 1956. ISSN 15205126. doi: 10.1021/ja01594a036.

R. Dringen, O. Kranich, and B. Hamprecht. The γ-glutamyl transpeptidase inhibitor acivicin preserves glutathione released by astroglial cells in culture. *Neurochemical Research*, 1997. ISSN 03643190. doi: 10.1023/A:1027310328310.

E. Dudley and L. Bond. Mass spectrometry analysis of nucleosides and nucleotides. *Mass Spectrometry Reviews*, 2014. ISSN 10982787. doi: 10.1002/mas.21388.

H. Eagle. Nutrition needs of mammalian cells in tissue culture. *Science (New York, N.Y.)*, 122(3168):501–14, 1955. ISSN 0036-8075. doi: 10.1002/9780470114735.hawley00624. URL `http://www.jstor.org/stable/2893079{%}0Ahttp://about.jstor.org/terms{%}0Ahttp://www.ncbi.nlm.nih.gov/pubmed/8539599{%}0Ahttp://doi.wiley.com/10.1002/9780470114735.hawley00624{%}0Ahttp://www.ncbi.nlm.nih.gov/pubmed/13255879`.

J. Ehrlich, G. L. Coffey, M. W. Fisher, A. B. Hillegas, D. L. Kohberger, H. E. Machamer, W. A. Rightsel, and F. R. Roegner. 6-Diazo-5-oxo-L-norleucine, a new tumor-inhibitory substance. I. Biologic studies. *Antibiot. Chemother. (Washington, D. C.)*, 6:487–497, 1956. ISSN 05703123.

D. Eisenberg, H. S. Gill, G. M. Pfluegl, and S. H. Rotstein. Structure-function relationships of glutamine synthetasesre, 2000. ISSN 01674838.

A. Elgogary, Q. Xu, B. Poore, J. Alt, S. C. Zimmermann, L. Zhao, J. Fu, B. Chen, S. Xia, Y. Liu, M. Neisser, C. Nguyen, R. Lee, J. K. Park, J. Reyes, T. Hartung, C. Rojas, R. Rais, T. Tsukamoto, G. L. Semenza, J. Hanes, B. S. Slusher, and A. Le. Combination therapy with BPTES nanoparticles and metformin targets the metabolic heterogeneity of pancreatic cancer. *Proceedings of the National Academy of Sciences*, 113(36):E5328–E5336, 2016. ISSN 0027-8424. doi: 10.1073/pnas.1611406113. URL `http://www.pnas.org/lookup/doi/10.1073/pnas.1611406113`.

E. Emberley, A. Pan, J. Chen, R. Dang, M. Gross, T. Huang, W. Li, A. MacKinnon, D. Singh, N. Sotirovska, S. M. Steggerda, T. Wang, and F. Parlati. The glutaminase inhibitor telaglenastat enhances the antitumor activity of signal transduction inhibitors everolimus and cabozantinib in models of renal cell carcinoma. *PLoS ONE*, 2021. ISSN 19326203. doi: 10.1371/journal.pone.0259241.

E. L. Esmans, P. Geboes, Y. Luyten, and F. C. Alderweireldt. Direct liquid introduction LC/MS microbore experiments for the analysis of nucleoside material present in human urine. *Biological Mass Spectrometry*, 1985. ISSN 10969888. doi: 10.1002/bms.1200120511.

C. T. Ferrara, P. Wang, E. C. Neto, R. D. Stevens, J. R. Bain, B. R. Wenner, O. R. Ilkayeva, M. P. Keller, D. A. Blasiole, C. Kendziorski, B. S. Yandell, C. B. Newgard, and A. D. Attie. Genetic networks of liver metabolism revealed by integration of metabolic and transcriptional profiling. *PLoS Genetics*, 2008. ISSN 15537390. doi: 10.1371/journal.pgen.1000034.

D. Gaglio, C. M. Metallo, P. A. Gameiro, K. Hiller, L. S. Danna, C. Balestrieri, L. Alberghina, G. Stephanopoulos, and F. Chiaradonna. Oncogenic K-Ras decouples glucose and glutamine metabolism to support cancer cell growth. *Molecular Systems Biology*, 2011. ISSN 17444292. doi: 10.1038/msb.2011.56.

P. Gao, I. Tchernyshyov, T.-C. Chang, Y.-S. Lee, K. Kita, T. Ochi, K. I. Zeller, A. M. De Marzo, J. E. Van Eyk, J. T. Mendell, and C. V. Dang. c-myc suppression of mir-23a/b enhances mitochondrial glutaminase expression and glutamine metabolism. *Nature*, 458(7239):762–765, 2009. doi: 10.1038/nature07823.

W. J. Griffiths, T. Koal, Y. Wang, M. Kohl, D. P. Enot, and H. P. Deigner. Targeted metabolomics for biomarker discovery, 2010. ISSN 14337851.

A. R. Hanaford, J. Alt, R. Rais, S. Z. Wang, H. Kaur, D. L. Thorek, C. G. Eberhart, B. S. Slusher, A. M. Martin, and E. H. Raabe. Orally bioavailable glutamine antagonist prodrug JHU-083 penetrates mouse brain and suppresses the growth of MYC-driven medulloblastoma. *Translational Oncology*, 2019. ISSN 19365233. doi: 10.1016/j.tranon.2019.05.013.

D. Hanahan and R. A. Weinberg. Hallmarks of cancer: The next generation. *Cell*, 144(5):646–674, 2011. ISSN 00928674. doi: 10.1016/j.cell.2011.02.013. URL `http://dx.doi.org/10.1016/j.cell.2011.02.013`.

S. C. Hartman. The Interaction of 6-Diazo-5-oxo-l-norleucine with Phosphoribosyl Pyrophosphate Amidotransferase. *Journal of Biological Chemistry*, 1963. ISSN 00219258. doi: 10.1016/s0021-9258(18)51862-7.

N. Hay. Reprogramming glucose metabolism in cancer: Can it be exploited for cancer therapy?, 2016. ISSN 14741768.

P. P. Hsu and D. M. Sabatini. Cancer cell metabolism: Warburg and beyond, 2008. ISSN 00928674.

P. Icard, A. Coquerel, Z. Wu, J. Gligorov, D. Fuks, L. Fournel, H. Lincet, and L. Simula. Understanding the central role of citrate in the metabolism of cancer cells and tumors: An update, 2021. ISSN 14220067.

M. Kalkat, J. De Melo, K. A. Hickman, C. Lourenco, C. Redel, D. Resetca, A. Tamachi, W. B. Tu, and L. Z. Penn. MYC deregulation in primary human cancers, 2017. ISSN 20734425.

Y. V. Karpievitch, A. D. Polpitiya, G. A. Anderson, R. D. Smith, and A. R. Dabney. Liquid Chromatography Mass Spectrometry-Based Proteomics: Biological and Technological Aspects. *Ann Appl Stat*, 4(4):1797–1823, 2011. ISSN 1932-6157. doi: 10.1214/10-AOAS341.Liquid.

W. P. Katt and R. A. Cerione. Glutaminase regulation in cancer cells: A druggable chain of events, 2014. ISSN 18785832.

E. R. Kaufman. Isolation and characterization of a mutant Chinese hamster cell line resistant to the glutamine analog 6-diazo-5-oxo-l-norleucine. *Somatic Cell and Molecular Genetics*, 1985. ISSN 07407750. doi: 10.1007/BF01534729.

G. W. Kim, D. H. Lee, Y. H. Jeon, J. Yoo, S. Y. Kim, S. W. Lee, H. Y. Cho, and S. H. Kwon. Glutamine synthetase as a therapeutic target for cancer treatment, 2021. ISSN 14220067.

K. Koper, S.-W. Han, D. C. Pastor, Y. Yoshikuni, and H. A. Maeda. Evolutionary origin and functional diversification of aminotransferases. *Journal of Biological Chemistry*, 298(8):102122, 2022. ISSN

0021-9258. doi: https://doi.org/10.1016/j.jbc.2022.102122. URL https://www.sciencedirect.com/science/article/pii/S0021925822005634.

Z. Kovacević and H. P. Morris. The role of glutamine in the oxidative metabolism of malignant cells. *Cancer Research*, 1972. ISSN 00085472.

J. S. Kovach, R. T. Eagan, G. Powis, J. Rubin, E. T. Creagan, and C. G. Moertel. Phase I and pharmacokinetic studies of DON. *Cancer treatment reports*, 65(11-12):1031–6, 1981. ISSN 0361-5960. URL http://www.ncbi.nlm.nih.gov/pubmed/7296548.

J. T. Ku, A. Y. Chen, and E. I. Lan. Metabolic engineering design strategies for increasing acetyl-coa flux, 2020. ISSN 22181989.

H. N. Kung, J. R. Marks, and J. T. Chi. Glutamine synthetase is a genetic determinant of cell type-specific glutamine independence in breast epithelia. *PLoS Genetics*, 2011. ISSN 15537390. doi: 10.1371/journal.pgen.1002229.

U. K. Laemmli. Cleavage of structural proteins during the assembly of the head of bacteriophage T4. *Nature*, 1970. ISSN 00280836. doi: 10.1038/227680a0.

A. N. Lane and T. W. Fan. Regulation of mammalian nucleotide metabolism and biosynthesis, 2015. ISSN 13624962.

D. P. Lane. P53 and human cancers. *British Medical Bulletin*, 1994. ISSN 14718391. doi: 10.1093/oxfordjournals.bmb.a072911.

N. Laronde-Leblanc, M. Resto, and B. Gerratana. Regulation of active site coupling in glutamine-dependent NAD + synthetase. *Nature Structural and Molecular Biology*, 2009. ISSN 15459993. doi: 10.1038/nsmb.1567.

A. N. Lau, Z. Li, L. V. Danai, A. M. Westermark, A. M. Darnell, R. Ferreira, V. Gocheva, S. Sivanand, E. C. Lien, K. M. Sapp, J. R. Mayers, G. Biffi, C. R. Chin, S. M. Davidson, D. A. Tuveson, T. Jacks, N. J. Matheson, O. Yilmaz, and M. G. Vander Heiden. Dissecting cell-type-specific metabolism in pancreatic ductal adenocarcinoma. *eLife*, 2020. ISSN 2050084X. doi: 10.7554/eLife.56782.

A. Le, A. N. Lane, M. Hamaker, S. Bose, A. Gouw, J. Barbi, T. Tsukamoto, C. J. Rojas, B. S. Slusher, H. Zhang, L. J. Zimmerman, D. C. Liebler, R. J. Slebos, P. K. Lorkiewicz, R. M. Higashi, T. W. Fan, and C. V. Dang. Glucose-independent glutamine metabolism via TCA cycling for proliferation and survival in b cells. *Cell Metabolism*, 15(1):110–121, 2012. ISSN 15504131. doi: 10.1016/j.cmet.2011.12.009. URL http://dx.doi.org/10.1016/j.cmet.2011.12.009.

K. M. Lemberg, J. J. Vornov, R. Rais, and B. S. Slusher. We're not "don" yet: Optimal dosing and prodrug delivery of 6-diazo-5-oxo-L-norleucine, 2018. ISSN 15388514.

B. Levenberg, I. MELNICK, and J. M. BUCHANAN. Biosynthesis of the purines. XV. The effect of aza-L-serine and 6-diazo-5-oxo-L-norleucine on inosinic acid biosynthesis de novo. *The Journal of biological chemistry*, 1957. ISSN 00219258.

A. Levitzki, W. B. Stallcup, and D. E. Koshland. Half-of-the-Sites Reactivity and the Conformational States of Cytidine Triphosphate Synthetase. *Biochemistry*, 1971. ISSN 15204995. doi: 10.1021/bi00794a009.

B. Li and M. C. Simon. Molecular pathways: Targeting MYC-induced metabolic reprogramming and oncogenic stress in cancer. *Clinical Cancer Research*, 2013. ISSN 10780432. doi: 10.1158/1078-0432.CCR-12-3629.

X. Li, H. Zhu, W. Sun, X. Yang, Q. Nie, and X. Fang. Role of glutamine and its metabolite ammonia in crosstalk of cancer-associated fibroblasts and cancer cells, 2021. ISSN 14752867.

P. Lorkiewicz, R. M. Higashi, A. N. Lane, and T. W. Fan. High information throughput analysis of nucleotides and their isotopically enriched isotopologues by direct-infusion fticr-ms. *Metabolomics*, 8, 2012. ISSN 15733882. doi: 10.1007/s11306-011-0388-y.

G. Lubes and M. Goodarzi. GC–MS based metabolomics used for the identification of cancer volatile organic compounds as biomarkers. *Journal of Pharmaceutical and Biomedical Analysis*, 147:313–322, 2018. ISSN 1873264X. doi: 10.1016/j.jpba.2017.07.013. URL `https://doi.org/10.1016/j.jpba.2017.07.013`.

M. J. Lukey, K. F. Wilson, and R. A. Cerione. Therapeutic strategies impacting cancer cell glutamine metabolism. *Future medicinal chemistry*, 5(14):1685–700, 2013. ISSN 1756-8927. doi: 10.4155/fmc.13.130. URL `/pmc/articles/PMC4154374/?report=abstract`.

L. Mádrová, M. Krijt, V. Barešová, J. Václavík, D. Friedecký, D. Dobešová, O. Součková, V. Škopová, T. Adam, and M. Zikánová. Mass spectrometric analysis of purine de novo biosynthesis intermediates. *PLoS ONE*, 2018. ISSN 19326203. doi: 10.1371/journal.pone.0208947.

F. Meric-Bernstam, N. M. Tannir, J. W. Mier, A. DeMichele, M. L. Telli, A. C. Fan, P. N. Munster, R. D. Carvajal, K. W. Orford, M. K. Bennett, O. Iliopoulos, T. K. Owonikoko, M. R. Patel, R. McKay, J. R. Infante, M. H. Voss, and J. J. Harding. Phase 1 study of CB-839, a small molecule inhibitor of glutaminase (GLS), alone and in combination with everolimus (E) in patients (pts) with renal cell cancer (RCC). *Journal of Clinical Oncology*, 2016. ISSN 0732-183X. doi: 10.1200/jco.2016.34.15_suppl.4568.

E. Messina, P. Gazzaniga, V. Micheli, M. R. Guaglianone, S. Barbato, S. Morrone, L. Frati, A. M. Aglianó, and A. Giacomello. Guanine nucleotide depletion triggers cell cycle arrest and apoptosis in human neuroblastoma cell lines. *International Journal of Cancer*, 2004. ISSN 00207136. doi: 10.1002/ijc.11642.

R. Motzer, C.-H. Lee, H. Emamekhoo, M. Matrana, I. Percent, J. Hsieh, A. Hussain, U. Vaishampayan, R. Graham, S. Liu, S. McCune, M. Shaheen, H. Parmar, Y. Shen, S. Whiting, and N. Tannir. ENTRATA: Randomized, double-blind, phase II study of telaglenastat (tela; CB-839) + everolimus (E) vs placebo (pbo) + E in patients (pts) with advanced/metastatic renal cell carcinoma (mRCC). *Annals of Oncology*, 2019. ISSN 09237534. doi: 10.1093/annonc/mdz394.048.

A. Muir, L. V. Danai, D. Y. Gui, C. Y. Waingarten, C. A. Lewis, and M. G. Vander Heiden. Environmental cystine drives glutamine anaplerosis and sensitizes cancer cells to glutaminase inhibition. *eLife*, 2017. ISSN 2050084X. doi: 10.7554/eLife.27713.

H. Nam, B. C. Chung, Y. Kim, K. Y. Lee, and D. Lee. Combining tissue transcriptomics and urine metabolomics for breast cancer biomarker identification. *Bioinformatics*, 2009. ISSN 13674803. doi: 10.1093/bioinformatics/btp558.

R. W. Newcomb. Selective inhibition of glutaminase by bis-thiadiazoles. *US Patent*, 2001.

P. Nicklin, P. Bergman, B. Zhang, E. Triantafellow, H. Wang, B. Nyfeler, H. Yang, M. Hild, C. Kung, C. Wilson, V. E. Myer, J. P. MacKeigan, J. a. Porter, Y. K. Wang, L. C. Cantley, P. M. Finan, and L. O. Murphy. Bidirectional Transport of Amino Acids Regulates mTOR and Autophagy. *Cell*, 136(3):521–534, feb 2009. ISSN 00928674. doi: 10.1016/j.cell.2008.11.044. URL `http://linkinghub.elsevier.com/retrieve/pii/S0092867408015195`.

A. I. Nieminen, V. M. Eskelinen, H. M. Haikala, T. A. Tervonen, Y. Yan, J. I. Partanen, and J. Klefström. Myc-induced AMPK-phospho p53 pathway activates Bak to sensitize mitochondrial apoptosis. *Proceedings of the National Academy of Sciences of the United States of America*, 2013. ISSN 00278424. doi: 10.1073/pnas.1208530110.

R. Oehler and E. Roth. Regulative capacity of glutamine, 2003. ISSN 13631950.

T. Opialla, S. Kempa, and M. Pietzke. Towards a more reliable identification of isomeric metabolites using pattern guided retention validation. *Metabolites*, 2020. ISSN 22181989. doi: 10.3390/metabo10110457.

F. Parlati, S. D. Demo, M. I. Gross, J. R. Janes, E. R. Lewis, A. L. MacKinnon, M. L. Rodriguez, P. J. Shwonek, T. Wang, J. Yang, D. Zhang, F. Zhao, and M. K. Bennett. Abstract 1416: CB-839, a novel potent and selective glutaminase inhibitor, has broad antiproliferative activity in cell lines derived from both solid tumors and hematological malignancies. *Cancer Research*, 2014. ISSN 0008-5472. doi: 10.1158/1538-7445.am2014-1416.

N. N. Pavlova and C. B. Thompson. The Emerging Hallmarks of Cancer Metabolism, 2016. ISSN 19327420.

N. N. Pavlova, J. Zhu, and C. B. Thompson. The hallmarks of cancer metabolism: Still emerging, 2022. ISSN 19327420.

M. Pietzke and S. Kempa. Pulsed stable isotope-resolved metabolomic studies of cancer cells. In *Methods in Enzymology*. 2014. ISBN 9780128013298. doi: 10.1016/B978-0-12-801329-8.00009-X.

L. M. Pinkus. Glutamine Binding Sites. *Methods in Enzymology*, 1977. ISSN 15577988. doi: 10.1016/S0076-6879(77)46049-X.

C. J. Poole and J. van Riggelen. MYC—master regulator of the cancer epigenome and transcriptome, 2017. ISSN 20734425.

R. Quinn, M. Basanta-Sanchez, R. E. Rose, and D. Fabris. Direct infusion analysis of nucleotide mixtures of very similar or identical elemental composition. *Journal of Mass Spectrometry*, 2013. ISSN 10969888. doi: 10.1002/jms.3207.

S. Ramachandran, C. Q. Pan, S. C. Zimmermann, B. Duvall, T. Tsukamoto, B. C. Low, and J. Sivaraman. Structural basis for exploring the allosteric inhibition of human kidney type glutaminase. *Oncotarget*, 2016. ISSN 19492553. doi: 10.18632/oncotarget.10791.

J. Rappsilber, M. Mann, and Y. Ishihama. Protocol for micro-purification, enrichment, pre-fractionation and storage of peptides for proteomics using StageTips. *Nature Protocols*, 2(8):1896–1906, 2007. ISSN 17542189. doi: 10.1038/nprot.2007.261.

L. Rayman. Understanding nucleotide pool depletion in neuroblastoma and colon cancer cells treated with glutamine analogues and glycolytic inhibitors. 2022.

Y. Razzaque. Investigating the Role of Asparaginase in Cancer Cell Metabolism. 2021.

L. J. Reitzer, B. M. Wice, and D. Kennell. Evidence that glutamine, not sugar, is the major energy source for cultured HeLa cells. *Journal of Biological Chemistry*, 1979. ISSN 00219258. doi: 10.1016/s0021-9258(17)30124-2.

S. Ren, Y. Shao, X. Zhao, C. S. Hong, F. Wang, X. Lu, J. Li, G. Ye, M. Yan, Z. Zhuang, C. Xu, G. Xu, and Y. Sun. Integration of metabolomics and transcriptomics reveals major metabolic pathways and potential biomarker involved in prostate cancer. *Molecular and Cellular Proteomics*, 2016. ISSN 15359484. doi: 10.1074/mcp.M115.052381.

M. Robinson, S. Mcbryant, T. Tsukamoto, C. Rojas, D. Ferraris, S. Hamilton, J. Hansen, and N. Curthoys. Novel mechanism of inhibition of rat kidney-type glutaminase by bis-2-(5-phenylacetamido-1,2,4-thiadiazol-2-yl)ethyl sulfide (BPTES). *Biochemical Journal*, 406(3):407–414, 2007. ISSN 0264-6021. doi: 10.1042/BJ20070039. URL `http://biochemj.org/lookup/doi/10.1042/BJ20070039`.

N. Royla. *Analysis of metabolic feedbacks regulating c-MYC*. PhD thesis, Freie Universität Berlin, 2018.

J. Rudolph and J. Stubbe. Investigation of the Mechanism of Phosphoribosylamine Transfer from Glutamine Phosphoribosylpyrophosphate Amidotransferase to Glycinamide Ribonucleotide Synthetase. *Biochemistry*, 1995. ISSN 15204995. doi: 10.1021/bi00007a019.

S. K. Saha, S. M. Riazul Islam, M. Abdullah-Al-Wadud, S. Islam, F. Ali, and K. S. Park. Multiomics analysis reveals that GLS and GLS2 differentially modulate the clinical outcomes of cancer. *Journal of Clinical Medicine*, 2019. ISSN 20770383. doi: 10.3390/jcm8030355.

M. E. Sant, A. Poiner, M. C. Harsanyi, S. D. Lyons, and R. I. Christopherson. Chromatographic analysis of purine precursors in mouse L1210 leukemia. *Analytical Biochemistry*, 1989. ISSN 10960309. doi: 10.1016/0003-2697(89)90728-8.

M. Scalise, L. Pochini, M. Galluccio, L. Console, and C. Indiveri. Glutamine transport and mitochondrial metabolism in cancer cell growth, 2017. ISSN 2234943X.

C. A. Schneider, W. S. Rasband, and K. W. Eliceiri. NIH Image to ImageJ: 25 years of image analysis, 2012. ISSN 15487091.

K. Sellers, M. P. Fox, M. B. Ii, S. P. Slone, R. M. Higashi, D. M. Miller, Y. Wang, J. Yan, M. O. Yuneva, R. Deshpande, A. N. Lane, and T. W. Fan. Pyruvate carboxylase is critical for non-small-cell lung cancer proliferation. *Journal of Clinical Investigation*, 2015. ISSN 15588238. doi: 10.1172/JCI72873.

S. Tardito, A. Oudin, S. U. Ahmed, F. Fack, O. Keunen, L. Zheng, H. Miletic, P. Ø. Sakariassen, A. Weinstock, A. Wagner, S. L. Lindsay, A. K. Hock, S. C. Barnett, E. Ruppin, S. Harald MØrkve, M. Lund-Johansen, A. J. Chalmers, R. Bjerkvig, S. P. Niclou, and E. Gottlieb. Glutamine synthetase activity fuels nucleotide biosynthesis and supports growth of glutamine-restricted glioblastoma. *Nature Cell Biology*, 2015. ISSN 14764679. doi: 10.1038/ncb3272.

L. M. Ter-Ovanessian, B. Rigaud, A. Mezzetti, J. F. Lambert, and M. C. Maurel. Carbamoyl phosphate and its substitutes for the uracil synthesis in origins of life scenarios. *Scientific Reports*, 2021. ISSN 20452322. doi: 10.1038/s41598-021-98747-6.

K. Thangavelu, Q. Y. Chong, B. C. Low, and J. Sivaraman. Structural Basis for the Active Site Inhibition Mechanism of Human Kidney-Type Glutaminase (KGA). *Scientific Reports*, 4:1–7, 2015. ISSN 20452322. doi: 10.1038/srep03827.

A. G. Thomas, C. Rojas, C. Tanega, M. Shen, A. Simeonov, M. B. Boxer, D. S. Auld, D. V. Ferraris, T. Tsukamoto, and B. S. Slusher. Kinetic characterization of ebselen, chelerythrine and apomorphine as glutaminase inhibitors. *Biochemical and Biophysical Research Communications*, 2013. ISSN 0006291X. doi: 10.1016/j.bbrc.2013.06.110.

L. A. Timmerman, T. Holton, M. Yuneva, R. J. Louie, M. Padró, A. Daemen, M. Hu, D. A. Chan, S. P. Ethier, L. J. Van'tVeer, K. Polyak, F. McCormick, and J. W. Gray. Glutamine Sensitivity Analysis Identifies the xCT Antiporter as a Common Triple-Negative Breast Tumor Therapeutic Target. *Cancer Cell*, 2013. ISSN 18783686. doi: 10.1016/j.ccr.2013.08.020.

V. Tolstikov. Metabolomics: Bridging the gap between pharmaceutical development and population health, 2016. ISSN 22181989.

S. Tyanova, T. Temu, P. Sinitcyn, A. Carlson, M. Y. Hein, T. Geiger, M. Mann, and J. Cox. The perseus computational platform for comprehensive analysis of (prote)omics data, 2016. ISSN 15487105.

M. Vander Heiden, L. Cantley, and C. Thompson. Understanding the Warburg effect: The metabolic Requiremetns of cell proliferation. *Science*, 324(5930):1029–1033, 2009. ISSN 1095-9203. doi: 10.1126/science.1160809.Understanding.

C. Wagener, C. Stocking, and O. Müller. *Cancer Signaling: From Molecular Biology to Targeted Therapy*. Wiley-Blackwell, 2016. ISBN 978-3-527-33658-6.

E. Wang. A Roadmap of Cancer Systems Biology. *Systems Biology*, 83:1–28, 2010. doi: 10.1038/npre.2010.4322.2. URL http://precedings.nature.com/documents/4322/version/2.

T. Wang, B. Cai, M. Ding, Z. Su, Y. Liu, and L. Shen. c-Myc Overexpression Promotes Oral Cancer Cell Proliferation and Migration by Enhancing Glutaminase and Glutamine Synthetase Activity. *American Journal of the Medical Sciences*, 2019. ISSN 15382990. doi: 10.1016/j.amjms.2019.05.014.

O. Warburg. On the Origin of Cancer Cells On the Origin of Cance. *Source: Science, New Series*, 123(123):309–314, 1956. ISSN 0036-8075. doi: 10.1126/science.123.3191.309. URL http://www.jstor.org/stable/1750066{%}5Cnhttp://www.jstor.org/stable/1750066?seq=1{&}cid=pdf-reference{#}references{_}tab{_}contents{%}5Cnhttp://about.jstor.org/terms.

D. R. Wise and C. B. Thompson. Glutamine Addiction: A New Therapeutic Target in Cancer. *Trends in Biochemical Sciences*, 35(8):427–433, 2011. ISSN 0968-0004. doi: 10.1016/j.tibs.2010.05.003.Glutamine. URL http://www.sciencedirect.com/science/article/pii/S0968000410000915.

D. R. Wise, R. J. Deberardinis, A. Mancuso, N. Sayed, X. Y. Zhang, H. K. Pfeiffer, I. Nissim, E. Daikhin, M. Yudkoff, S. B. McMahon, and C. B. Thompson. Myc regulates a transcriptional program that stimulates mitochondrial glutaminolysis and leads to glutamine addiction. *Proceedings of the National Academy of Sciences of the United States of America*, 2008. ISSN 00278424. doi: 10.1073/pnas.0810199105.

F. Xie, T. Liu, W. J. Qian, V. A. Petyuk, and R. D. Smith. Liquid chromatography-mass spectrometry-based quantitative proteomics. *Journal of Biological Chemistry*, 286(29):25443–25449, 2011. ISSN 00219258. doi: 10.1074/jbc.R110.199703.

K. Yanagida, Y. Maejima, P. Santoso, Z. Otgon-Uul, Y. Yang, K. Sakuma, K. Shimomura, and T. Yada. Hexosamine pathway but not interstitial changes mediates glucotoxicity in pancreatic β-cells as assessed by cytosolic Ca2+ response to glucose. *Aging*, 2014. ISSN 19454589. doi: 10.18632/aging.100647.

L. Yang, S. Venneti, and D. Nagrath. Glutaminolysis: A Hallmark of Cancer Metabolism. *Annual Review of Biomedical Engineering*, 2017. ISSN 15454274. doi: 10.1146/annurev-bioeng-071516-044546.

H. C. Yoo, S. J. Park, M. Nam, J. Kang, K. Kim, J. H. Yeo, J. K. Kim, Y. Heo, H. S. Lee, M. Y. Lee, C. W. Lee, J. S. Kang, Y. H. Kim, J. Lee, J. Choi, G. S. Hwang, S. Bang, and J. M. Han. A Variant of SLC1A5 Is a Mitochondrial Glutamine Transporter for Metabolic Reprogramming in Cancer Cells. *Cell Metabolism*, 2020. ISSN 19327420. doi: 10.1016/j.cmet.2019.11.020.

M. Yuneva, N. Zamboni, P. Oefner, R. Sachidanandam, and Y. Lazebnik. Deficiency in glutamine but not glucose induces MYC-dependent apoptosis in human cells. *Journal of Cell Biology*, 178(1):93–105, 2007. ISSN 00219525. doi: 10.1083/jcb.200703099.

M. O. Yuneva, T. W. Fan, T. D. Allen, R. M. Higashi, D. V. Ferraris, T. Tsukamoto, J. M. Matés, F. J. Alonso, C. Wang, Y. Seo, X. Chen, and J. M. Bishop. The metabolic profile of tumors depends on both the responsible genetic lesion and tissue type. *Cell Metabolism*, 2012. ISSN 15504131. doi: 10.1016/j.cmet.2011.12.015.

G. Zhang, P. He, H. Tan, A. Budhu, J. Gaedcke, B. Michael Ghadimi, T. Ried, H. G. Yfantis, D. H. Lee, A. Maitra, N. Hanna, H. Richard Alexander, and S. Perwez Hussain. Integration of metabolomics and transcriptomics revealed a fatty acid network exerting growth inhibitory effects in human pancreatic cancer. *Clinical Cancer Research*, 2013. ISSN 10780432. doi: 10.1158/1078-0432.CCR-13-0209.

J. Zhang, N. N. Pavlova, and C. B. Thompson. Cancer cell metabolism: the essential role of the nonessential amino acid, glutamine. *The EMBO Journal*, 2017. ISSN 0261-4189. doi: 10.15252/embj.201696151.

H. Zhao, C. R. Chiaro, L. Zhang, P. B. Smith, C. Y. Chan, A. M. Pedley, R. J. Pugh, J. B. French, A. D. Patterson, and S. J. Benkovic. Quantitative analysis of purine nucleotides indicates that purinosomes increase de Novo purine biosynthesis. *Journal of Biological Chemistry*, 2015. ISSN 1083351X. doi: 10.1074/jbc.M114.628701.

Y. Zhao, X. Zhao, V. Chen, Y. Feng, L. Wang, C. Croniger, R. A. Conlon, S. Markowitz, E. Fearon, M. Puchowicz, H. Brunengraber, Y. Hao, and Z. Wang. Colorectal cancers utilize glutamine as an anaplerotic substrate of the TCA cycle in vivo. *Scientific Reports*, 2019. ISSN 20452322. doi: 10.1038/s41598-019-55718-2.

H. R. Zielke, C. M. Sumbilla, C. L. Zielke, J. T. Tildon, and P. T. Ozand. Glutamine Metabolism by Cultured Mammalian Cells. In *Glutamine Metabolism in Mammalian Tissues*. 1984. doi: 10.1007/978-3-642-69754-8_16.

Publications

1. Bayram Şafak, Razzaque YS, Geisberger S, et al. Investigating the role of GLUL as a survival factor in cellular adaptation to glutamine depletion via targeted stable isotope resolved metabolomics. Front Mol Biosci. 2022;9. doi:10.3389/fmolb.2022.859787

2. Bayram S, Fürst S, Forbes M, Kempa S. Analysing central metabolism in ultra-high resolution: At the crossroads of carbon and nitrogen. Mol Metab. Published online 2020. doi:10.1016/j.molmet.2019.12.002

Chapter 7

Supplementary Data

7.1 Materials

Table 7.1: Cell culture reagents and supplements

Name	Supplier
2-Deoxyglucose	Sigma-Aldrich, D - Darmstadt
3-Bromopyruvate	Sigma-Aldrich, D - Darmstadt
Dimethyl sulfoxide	Sigma-Aldrich, D - Darmstadt
DMEM, no glucose, glutamine, phenol red	Gibco, USA - Waltham
Fetal bovine serum	Gibco, USA - Waltham
Dialyzed Fetal bovine serum	Gibco, USA - Waltham
Glucose	Sigma-Aldrich, D - Darmstadt
L-Glutamine	Gibco, USA - Waltham
Phosphate-buffered saline	Gibco, USA - Waltham
Trypan Blue Solution (0.4%)	Gibco, USA - Waltham
TrypLE Express	Gibco, USA - Waltham
U-^{13}C-Glutamate	Campro-Scientific, D - Berlin
^{15}N-Ammonium	Campro-Scientific, D - Berlin

Table 7.2: Chemicals

Compound	Supplier
Acetic acid	Fluka, D - Darmstadt
Acetonitrile	VWR, USA - Radnor
Acrylamide	Carl Roth, D - Karlsruhe
Ammonium bicarbonate	Fluka, D - Darmstadt
Ammonium persulfate	Sigma-Aldrich, D - Darmstadt
Bromphenol blue	AppliChem GmbH, D - Darmstadt
BSA	SERVA, D - Heidelberg
$CaCl_2$ (1 M), nuclease-free	Sigma-Aldrich, D - Darmstadt
Chloroform	Sigma-Aldrich, D - Darmstadt
Chloroform-isoamyl alcohol (24:1)	Carl Roth, D - Karlsruhe
Cinnamic acid	Sigma-Aldrich, D - Darmstadt
DTT	Sigma-Aldrich, D - Darmstadt
EDTA	Carl Roth, D - Karlsruhe
Ethanol (EtOH)	LiChrosolv, D - Darmstadt
Formaldehyde (16%)	Polysciences, USA - Warrington

Continued on next page

Table 7.2: Continued from previous page

Compound	Supplier
Formamide	AppliChem GmbH, D - Darmstadt
Formic acid	Fluka, D - Darmstadt
Glucose	Sigma-Aldrich, D - Darmstadt
Glycerol	Carl Roth, D - Karlsruhe
Glycine	Carl Roth, D - Karlsruhe
HEPES	Sigma-Aldrich, D - Darmstadt
Hexylamine	Sigma-Aldrich, D - Darmstadt
IAA	Sigma-Aldrich, D - Darmstadt
Isopropanol	Carl Roth, D - Karlsruhe
$MgCl_2$	Sigma-Aldrich, D - Darmstadt
MeOH	Merck, D - Darmstadt
MeOx	Sigma-Aldrich, D - Darmstadt
Skim milk powder	Sigma-Aldrich, D - Darmstadt
MSTFA	VWR, USA - Radnor
NaCl	Sigma-Aldrich, D - Darmstadt
Na-deoxycholate	Sigma-Aldrich, D - Darmstadt
NaOAc	Thermo Fisher, USA - Waltham
NH_4Ac	Carl Roth, D - Karlsruhe
NH_4OH	Sigma-Aldrich, D - Darmstadt
NP-40	Sigma-Aldrich, D - Darmstadt
Page ruler prestained protein ladder	Bio-Rad, D - München
PBS (10x)	Biochrom, D - Darmstadt
Phophatase inhibitor cocktail	Sigma-Aldrich, D - Darmstadt
Protease Inhibitor Cocktail, EDTA-free	Roche, D - Darmstadt
Pyridine	Sigma-Aldrich, D - Darmstadt
Sodium acetate (3 M), pH 5.5, nuclease free	Invitrogen, USA - Waltham
SDS (20%)	Carl Roth, D - Karlsruhe
TEMED	Carl Roth, D - Karlsruhe
Triflouracetic acid	Merck, D - Darmstadt
TrisBase	Carl Roth, D - Karlsruhe
TrisHCl	Carl Roth, D - Karlsruhe
Triton x-100	Carl Roth, D - Karlsruhe
Trypsin Beads	Aplied Biosystems, USA - Waltham
Tween-20	Carl Roth, D - Karlsruhe
Urea	Carl Roth, D - Karlsruhe

Table 7.3: SDS-PAGE gel preparation

Component	4%	8%	10%	12%
H_2O	6.1 mL	4.6 mL	4.0 mL	3.3 mL
Acrylamide 30%	1.33 mL	2.7 mL	3.3 mL	4.0 mL
0.5 M Tris (pH 6.8)	2.5 mL	-	-	-
1.5 M Tris (pH 8.8)	-	2.5 mL	2.5 mL	2.5 mL
SDS 10%	100 µL	50 µL	50 µL	50 µL
Ammonium persulfate 10%	50 µL	50 µL	50 µL	50 µL
TEMED	10 µL	6 µL	4 µL	4 µL

Table 7.4: Commercial kits

Kit	Supplier
ECL Prime Western Blotting Detection Reagent	GE Healthcare, UK - Little Chalfont
MycoAlert Mycoplasma Detection Kit	Lonza, CH - Basel
Pierce BCA Protein Assay Kit	Thermo Fisher, USA - Waltham

Table 7.5: Antibodies

Antibody	Cat.-No	Manufacturer
Anti-MYC	5605	Cell Signaling
Anti-GLUL(MSO)	PA1-46165	Cell Signaling
Mouse, horseradish peroxidase-linked	7075	Cell Signaling
Goat, horseradish peroxidase-linked	7074	Cell Signaling
Rabbit, horseradish peroxidase-linked	7076	NEB, DE, Frankfurt am Main
Vinculin	V9131	Sigma-Aldrich, D - Darmstadt

Table 7.6: Consumables

Name	Supplier
Cell lifter	Sigma-Aldrich, D - Darmstadt
Counting slides	Biorad, D - München
Gas liner, CI34	Gerstel, D - Mühlheim an der Ruhr
Glass vials	Th.Geyer, D - Berlin
Nytran N Blotting Membrane	GE Healthcare, UK - Little Chalfont
PVDF membrane	GE Healthcare, UK - Little Chalfont
Whatman Blotting paper	Biorad, D - München

Table 7.7: Equipment

Name	Manufacturer
Autosampler - MPS2XL-Twister	Gerstel, DE - Mühlheim an der Ruhr
Autosampler, ESI ion source - TriVersa NanoMate	Advion, DE - Ithaca
Blotting device - TransBlot Turbo	Biorad, DE - München
Cell counter - TC20	Biorad, DE - München
Centrifuge - 5417R	Eppendorf, DE - Hamburg
Centrifuge - 5430	Eppendorf, DE - Hamburg
Electrophoresis system - ReadySub-Cell	Biorad, DE - München
Electrophoresis system - Protean Tetra cell	Biorad, DE - München
Gas chromatograph - Agilent 78903	LECO, USA - St. Joseph
Imager - Vilber fusion	GE Healthcare, UK - Little Chalfont
Mass Spectrometer - Q Exactive Plus	Thermo Fisher, USA - Waltham
Mass Spectrometer - TSQ Quantiva	Thermo Fisher, USA - Waltham
Mass Spectrometer-TOF - Pegasus IV	LECO, USA - St. Joseph
Microplate reader-Infinite M200	Tecan, CH - Männedorf
Microplate reader- Spectramax iD microplate reader	Molecular Devices, USA, California
Microscope- Keyence Bz-x700	Keyence
Japan, Osaka	
Microscope-Eclipse TS2 microscope	Nikon, DE- Düsseldorf
Nano Liquid Chromatograph 400	Eksigent, DE - Darmstadt

Continued on next page

Table 7.7: Continued from previous page

Name	Manufacturer
pH meter - VMS C7	VWR, USA - Radnor
Power supply - PowerPac Universal	Biorad, DE - München
Vacuum concentrator - 2-33 CD plus	Christ, DE - Osterode
Sonicator - Sonorex Digitech DT 100	Bandelin, DE - Berlin
Tube roller - SRT6D	Stuart, UK - Staffordshire

Table 7.8: Software

Name
ChromaToF (Version 4.51.6.0)
FlowJo (Version.10)
Fuji
Adobe Illustrator (Version 5.6)
Adobe infinity (Version X.X)
ImageJ
MAUI-SILVIA (Version 1.0.5)
MaxQuant (Version 1.5.3.30)
MetMax
Perseus (Version 1.5.6.0)
RStudio Desktop (Version 1.1.383

7.1.1 Nucleotides

Table 7.9: Direct infusion MS transition parameters

Compound	Precursor [m/z]	Product [m/z]	Collision Energy [V]	RF lens [V]
ADP	426.02	134.06	24	92
ADP	426.02	158.92	27	92
AICAR	337.00	79.00	29	93
AICAR	337.00	97.00	20	93
AMP	346.06	107.08	47	80
AMP	346.06	134.06	31	80
ATP	505.99	158.96	29	92
ATP	505.99	408.04	20	92
cAMP	328.02	107.08	44	78
cAMP	328.02	134.07	25	78
CDP	402.01	159.03	25	94
CDP	402.01	272.94	23	94
CMP	322.04	79.03	26	72
CMP	322.04	97.01	22	72
CTP	481.98	159.05	29	85
CTP	481.98	383.93	20	85
dADP	410.09	158.94	25	94
dADP	410.09	256.96	24	94
dAMP	330.09	134.12	27	68
dAMP	330.09	194.94	27	68
dATP	490.05	158.94	26	136

Continued on next page

Table 7.9: Continued from previous page

Compound	Precursor [m/z]	Product [m/z]	Collision Energy [V]	RF lens [V]
dATP	490.05	256.96	29	136
dCDP	86.05	158.96	23	78
dCDP	86.05	177.01	22	78
dCMP	306.08	97.00	23	80
dCMP	306.08	110.11	23	80
dCTP	66.01	158.94	26	111
dCTP	466.01	256.80	28	111
dGDP	426.05	158.96	24	99
dGDP	426.05	176.94	24	99
dGMP	346.09	79.00	22	73
dGMP	346.09	150.07	25	73
dGTP	506.11	159.03	28	120
dGTP	506.11	238.97	26	120
dTDP	401.05	158.94	24	82
dTDP	401.05	256.96	23	82
dTMP	321.11	125.05	22	69
dTMP	321.11	194.95	16	69
dTTP	480.98	158.94	30	90
dTTP	480.98	256.84	15	90
GDP	442.00	158.93	26	105
GDP	442.00	343.96	16	105
GMP	362.05	133.05	40	83
GMP	362.05	150.06	29	83
GTP	522.03	240.96	29	163
GTP	522.03	320.90	26	163
IMP	347.00	97.07	22	80
IMP	347.00	135.05	27	80
NAD+	622.09	272.91	34	68
NAD+	622.09	539.94	15	68
NADH	664.07	396.94	31	231
NADH	664.07	407.94	31	231
NADP+	742.05	272.92	40	80
NADP+	742.05	619.88	16	80
NADPH	744.06	272.92	33	97
NADPH	744.06	407.94	16	97
PRPP	389.00	621.66	16	75
PRPP	389.00	177.00	18	75
SAICAR	453.00	294.00	21	124
SAICAR	453.00	355.00	17	124
UDP	402.99	158.91	22	95
UDP	402.99	272.89	22	95
UMP	323.03	79.04	28	70
UMP	323.03	97.02	23	70
UTP	482.98	158.93	28	118
UTP	482.98	403.01	24	118

7.1.2 Metabolomics

Table 7.10: GC-MS masses used for quantification. Peak areas under the indicated masses, were summed and normalised to Cinnamic acid and cell counts.

Metabolite	Derivate	RI	Quantification masses [m/z]
Alanine	(2TMS)	1106	110;133;114;100;188;190
Aspartic acid	(2TMS)	1442	160
Cinnamic acid, trans-	(1TMS)	1555	205
Citric acid	(4TMS)	1848	149.0;273.0;183.0;133.0;211.0;275.0;277.0;278.0
Cysteine	(3TMS)	1574	116;100;132;218;220
Dihydroxyacetone-phosphate	(1MEOX)(3TMS)	1773	133;103;142;89;315;400;403
Fructose-1,6-diphosphate	(1MEOX)(7TMS)	2795	217;299;387;315;129;220
Fructose-6-phosphate	(1MEOX)(6TMS)	2385	129;217;299;315;103;220
Fumaric acid	(2TMS)	1369	143;246;133;115;245;247;249
Gluconic acid	(6TMS)	2060	292
Gluconic acid-6-phosphate	(7TMS)	2512	129;299;133;387;101;220
Glucose-6-phosphate	(1MEOX)(6TMS)	2420	160;299;129;387;133;220;162;132
Glutamic acid	(3TMS)	1640	246
Glutaric acid, 2-hydroxy-	(3TMS)	1596	129
Glutaric acid, 2-oxo-	(1MEOX)(2TMS)	1596	156;112;170;89;198;200;203
Glyceric acid	(3TMS)	1362	189
Glyceric acid-3-phosphate	(4TMS)	1840	211;227;299;101;133;357;359
Glycerol	(3TMS)	1303	205
Glycerol-3-phosphate	(4TMS)	1794	101;299;133;357;103;359
Glycine	(2TMS)	1124	86.0;133.0;175.0;100.0;174.0
Glycine	(3TMS)	1330	86.0;133.0;175.0;100.0;174.0
Isoleucine	(1TMS)	1179	86
Lactic acid	(2TMS)	1065	118.0; 190.0; 191.0; 117.0; 133.0;119.0; 193.0; 219.0; 222.0
Leucine	(1TMS)	1158	86
Lysine	(3TMS)	1867	174
Malic acid	(3TMS)	1507	101;133;117;149;233;245;247;249
Methionine	(2TMS)	1532	176
Phenylalanine	(2TMS)	1642	192
Proline	(2TMS)	1318	142
Putrescine	(4TMS)	1754	174
Pyroglutamic acid	(2TMS)	1534	157
Pyruvic acid	(1MEOX)(1TMS)	1053	100.0 ;99.0 ;89.0; 174.0; 115.0 ;177.0
Ribose-5-phosphate	(1MEOX)(5TMS)	2161	299.0;315.0;217.0;133.0;129.0;220.0
Serine	(3TMS)	1391	116;218;133;204;100;206
Succinic acid	(2TMS)	1336	149;247;129;133;172;249;251
Threonine	(3TMS)	1417	218
Uracil	(2TMS)	1363	241
Urea	(2TMS)	1253	171
Uridine	(3TMS)	2506	217
Valine	(2TMS)	1230	144

Table 7.11: GC-MS fragment ranges used for determination of stable isotope incorporation

Metabolite	Derivate	Fragment Min	Fragment Max
Alanine	(2TMS)	116	120
Aspartic acid	(2TMS)	245	251
Citric acid	(4TMS)	273	279
Fructose-1,6-diphosphate	(1MEOX)(7TMS)	217	222
Fructose-6-phosphate	(1MEOX) (6TMS)	217	222
Fumaric acid	(2TMS)	245	251
Gluconic acid-6-phosphate	(7TMS)	217	220
Glucose-6-phosphate	(1MEOX) (6TMS)	217	220
Glutamic acid	(3TMS)	246	250
Glutamine, DL-	(3TMS)	156	163
Glutaric acid, 2-hydroxy-	(3TMS)	247	252
Glutaric acid, 2-oxo-	(1MEOX) (2TMS)	198	205
Glutaric acid, 2-oxo-	(1MEOX)(2TMS)	288	295
Glyceric acid	(3TMS)	357	361
Glyceric acid-3-phosphate	(4TMS)	357	361
Glycerol	(3TMS)	218	222
Glycerol-3-phosphate	(4TMS)	357	361
Glycine	(3TMS)	276	279
Lactic acid	(2TMS)	219	224
Malic acid	(3TMS)	245	251
Pyruvic acid	(1MEOX)(1TMS)	174	179
Serine	(3TMS)	204	208
Serine	(2TMS)	116	120
Succinic acid	(2TMS)	247	252

7.2 Additional results

7.2.1 Cell biology

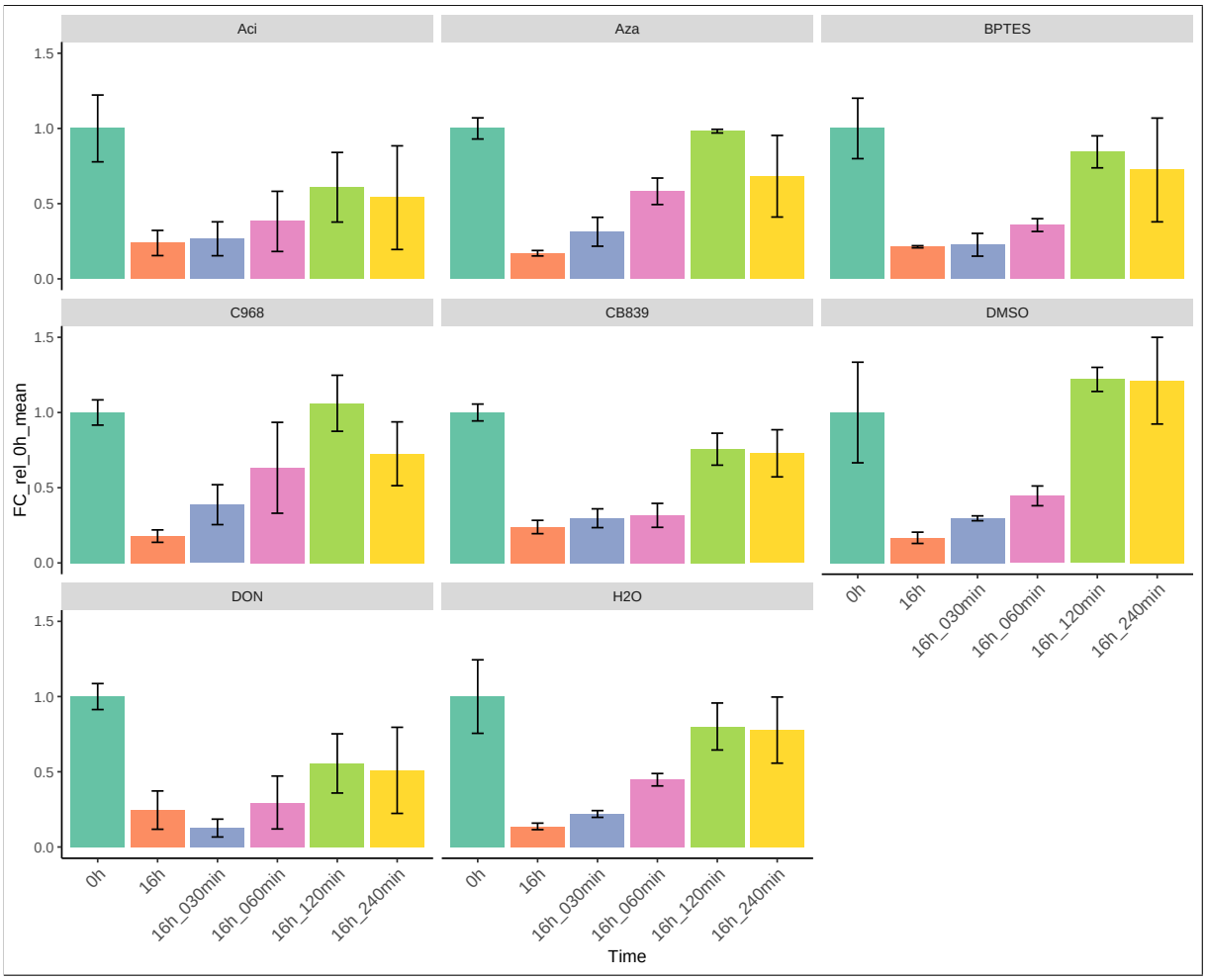

Figure 7.1: MYC protein expression upon glutamine starvation and readdition in normal FBS in HCT116 cells. MYC regulation after 16 h glutamine starvation and subsequent re-addition of glutamine for 30 min, 60 min, 120 min and 240 min in normal FBS medium in HCT116 cells. Quantification of MYC protein expression of at least three independent experiments. Each value was normalized to 0 h.).

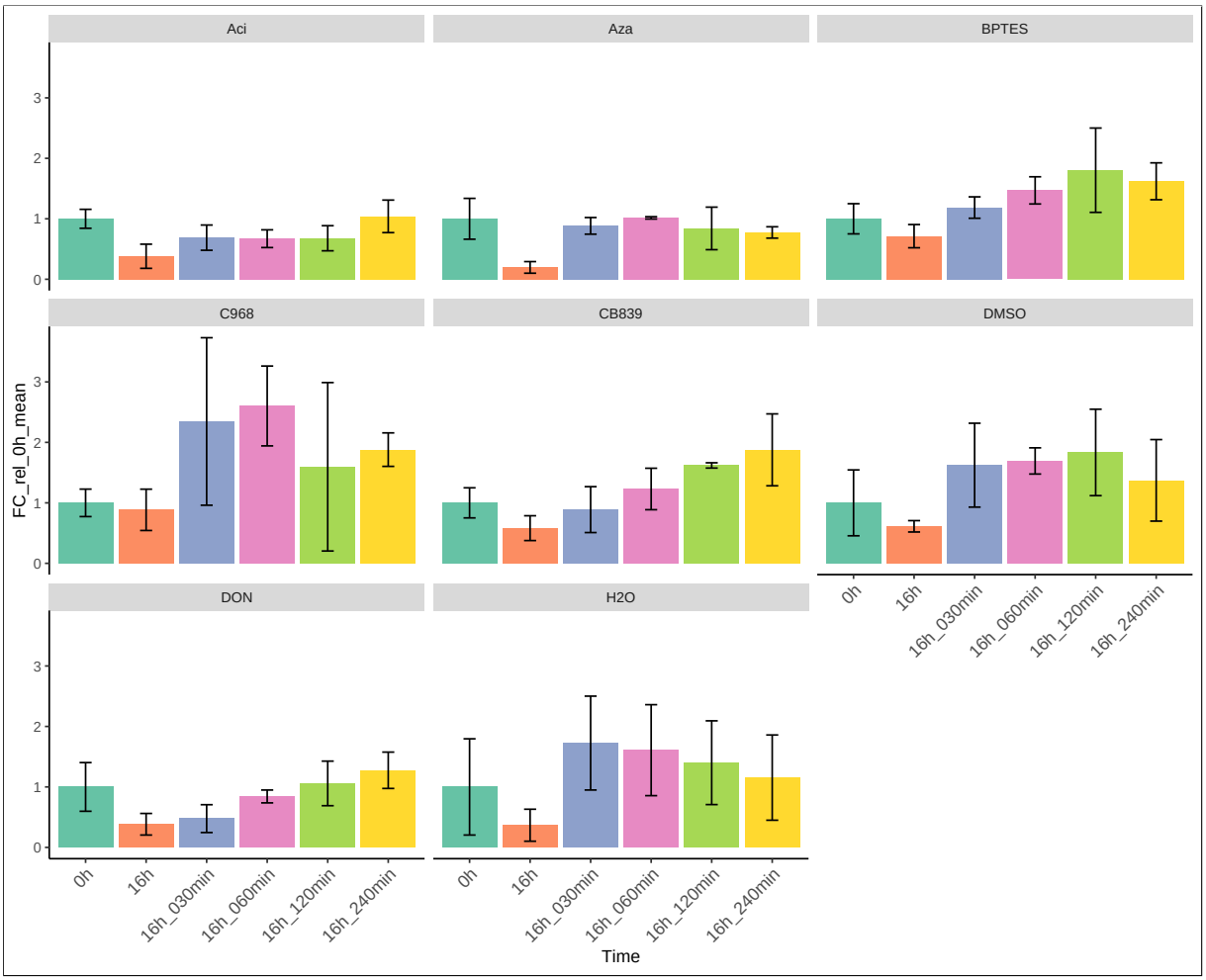

Figure 7.2: MYC protein expression upon glutamine starvation and readdition in normal FBS in RKO cells. MYC regulation after 16 h glutamine starvation and subsequent re-addition of glutamine for 30 min, 60 min, 120 min and 240 min in normal FBS medium in RKO cells. Quantification of MYC protein expression of at least three independent experiments. Each value was normalized to 0 h.).

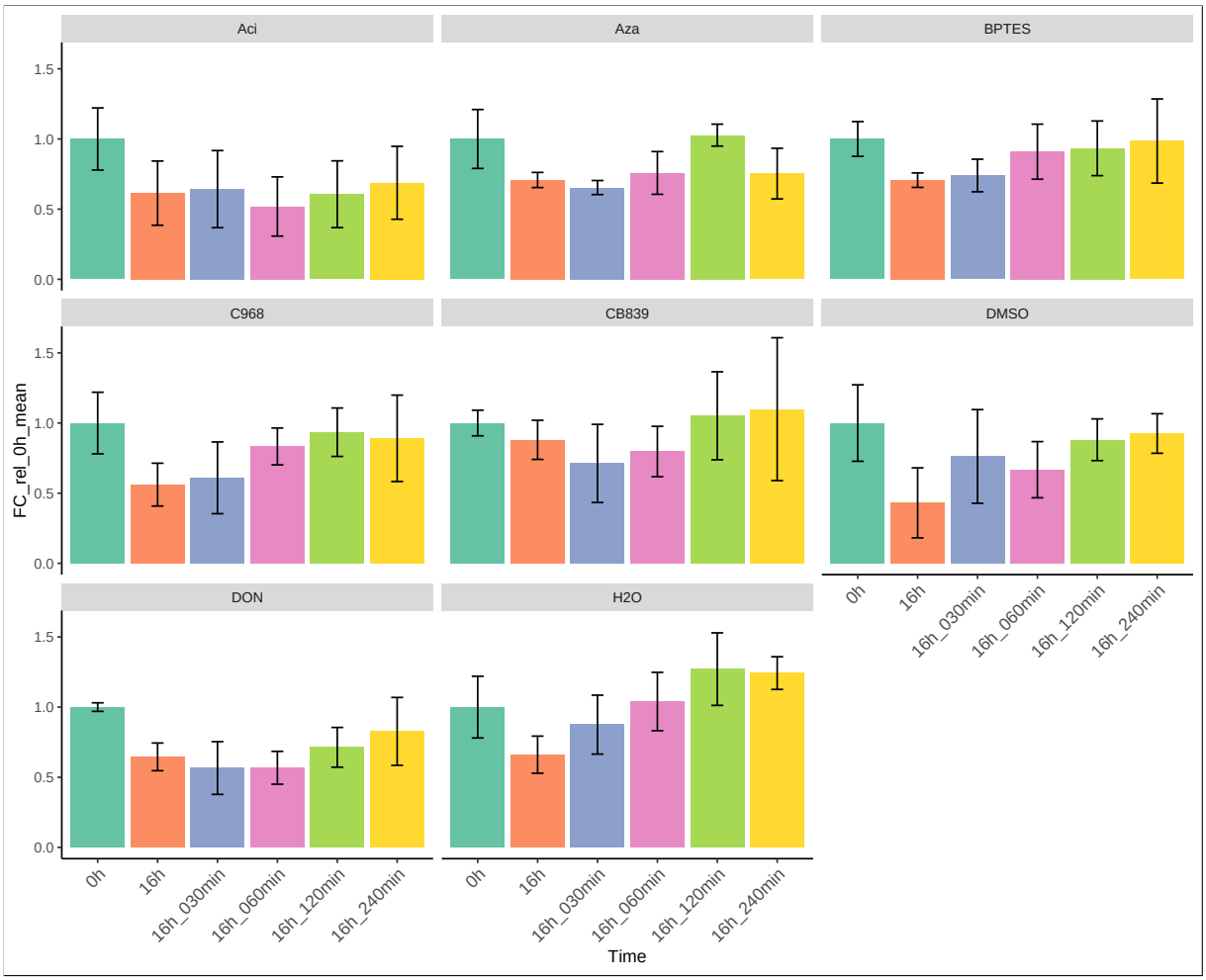

Figure 7.3: MYC protein expression upon glutamine starvation and readdition in normal FBS in HEK293 cells. MYC regulation after 16 h glutamine starvation and subsequent re-addition of glutamine for 30 min, 60 min, 120 min and 240 min in normal FBS medium in HEK293 cells. Quantification of MYC protein expression of at least three independent experiments. Each value was normalized to 0 h.).

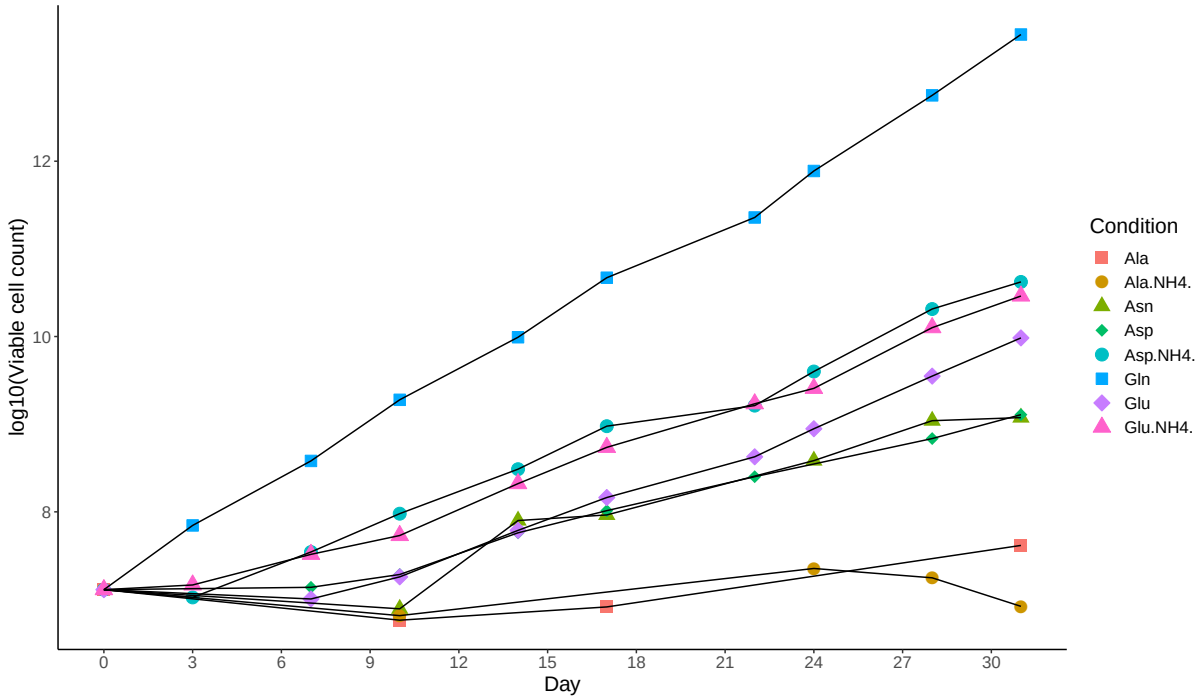

Figure 7.4: Cell Culture media compositions for cell growth assays. Cell proliferation upon the application of various amino acid substrates in dialyzed FBS medium in indicated cell lines. Day 1 till day 31 are represented graphically. Viable cell count was determined at every passage over one month. Cell count data were Log transformed to fit a non-linear regression model. Data were published in figure 3 in Bayram et al. (2022).

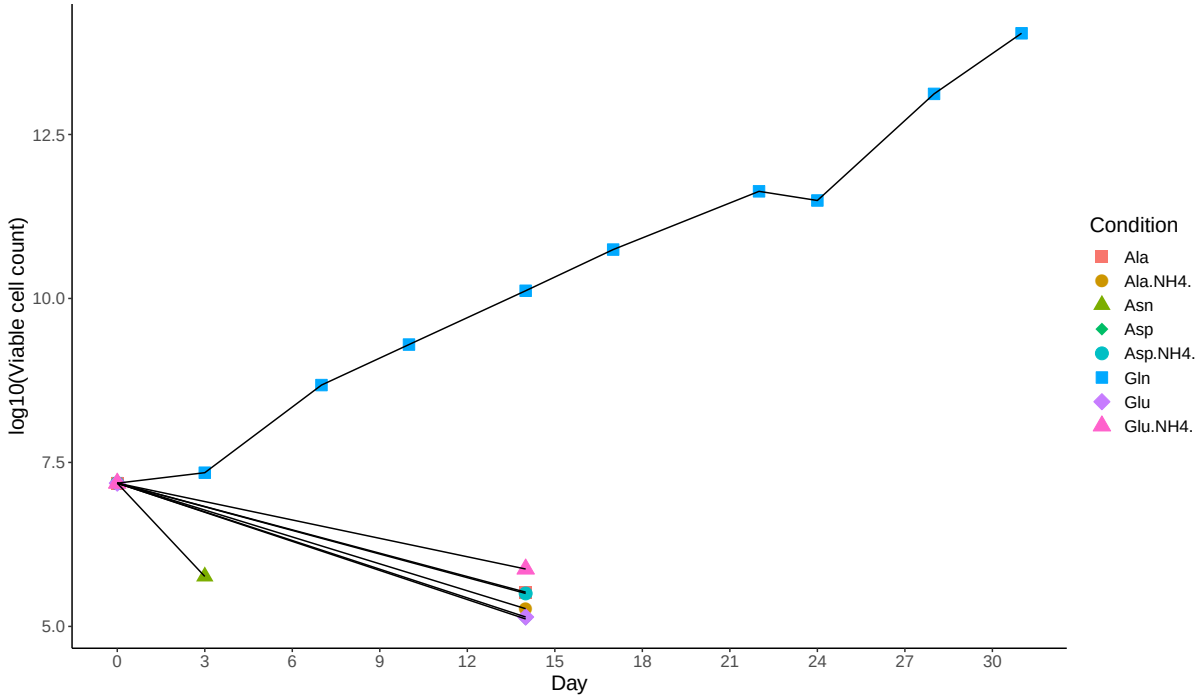

Figure 7.5: Cell Culture media compositions for cell growth assays. Cell proliferation upon the application of various amino acid substrates in dialyzed FBS medium in indicated cell lines. Day 1 till day 31 are represented graphically. Viable cell count was determined at every passage over one month. Cell count data were Log transformed to fit a non-linear regression model. Data were published in figure 3 in Bayram et al. (2022).

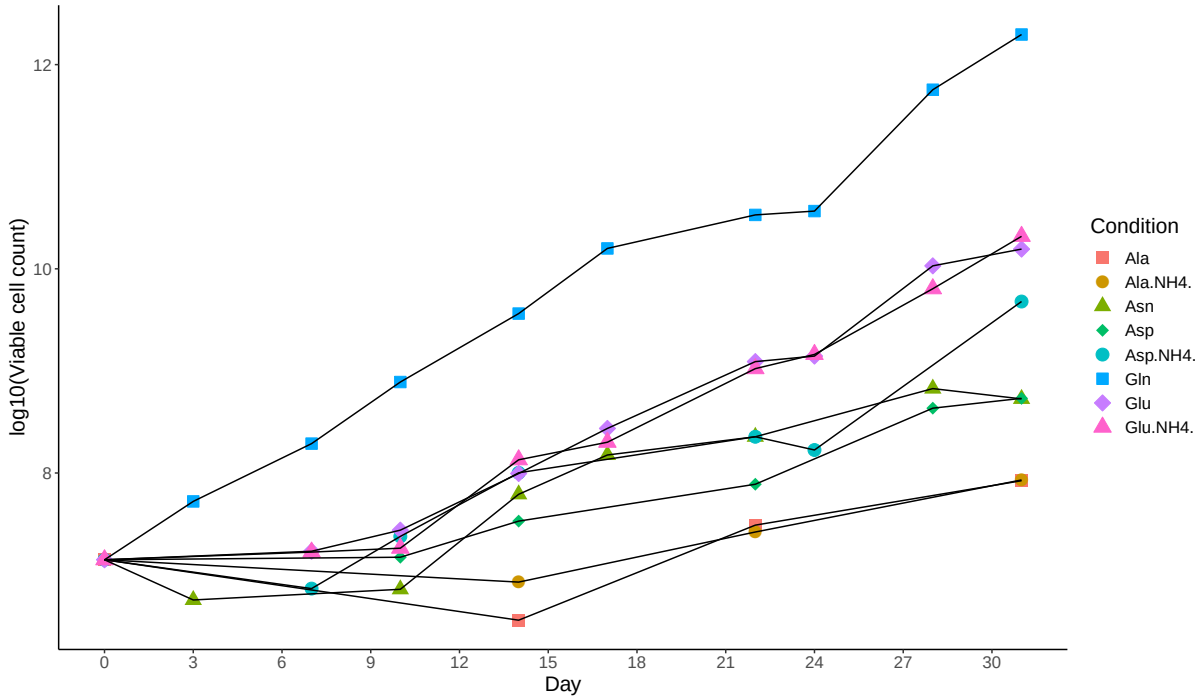

Figure 7.6: Cell Culture media compositions for cell growth assays. Cell proliferation upon the application of various amino acid substrates in dialyzed FBS medium in indicated cell lines. Day 1 till day 31 are represented graphically. Viable cell count was determined at every passage over one month. Cell count data were Log transformed to fit a non-linear regression model. Data were published in figure 3 in Bayram et al. (2022).